



### 저작자표시-비영리 2.0 대한민국

이용자는 아래의 조건을 따르는 경우에 한하여 자유롭게

- 이 저작물을 복제, 배포, 전송, 전시, 공연 및 방송할 수 있습니다.
- 이차적 저작물을 작성할 수 있습니다.

다음과 같은 조건을 따라야 합니다:



저작자표시. 귀하는 원저작자를 표시하여야 합니다.



비영리. 귀하는 이 저작물을 영리 목적으로 이용할 수 없습니다.

- 귀하는, 이 저작물의 재이용이나 배포의 경우, 이 저작물에 적용된 이용허락조건을 명확하게 나타내어야 합니다.
- 저작권자로부터 별도의 허가를 받으면 이러한 조건들은 적용되지 않습니다.

저작권법에 따른 이용자의 권리는 위의 내용에 의하여 영향을 받지 않습니다.

이것은 [이용허락규약\(Legal Code\)](#)을 이해하기 쉽게 요약한 것입니다.

[Disclaimer](#)

# **Role of Notum in Cusp and Root Patterning of Mouse Molars**

Dinuka Madhushan Adasooriya

The Graduate School

Yonsei University

Department of Applied Life Science

# **Role of Notum in Cusp and Root Patterning of Mouse Molars**

Directed by Professor Sung-Won Cho

A Doctoral Dissertation

Submitted to the Department of Applied Life Science  
and the Graduate School of Yonsei University  
in partial fulfillment of the  
requirements for the degree of  
Doctor of Philosophy in Applied Life Science

Dinuka Madhushan Adasooriya

June 2024

**This certifies that the doctoral dissertation of  
Dinuka Madhushan Adasooriya is approved.**



-----  
Thesis Supervisor: Prof. Sung-Won Cho



-----  
Thesis Committee Member: Prof. Seok Jun Moon



-----  
Thesis Committee Member: Prof. Eui-Sic Cho



-----  
Thesis Committee Member: Prof. Joo-Cheol Park



-----  
Thesis Committee Member: Prof. Jae-Young Kim

**The Graduate School**

**Yonsei University**

**June 2024**

## ACKNOWLEDGEMENTS

The time I spent at Yonsei University is filled with valuable memories and relationships I will cherish forever. I have gained a lot of experience that has helped me grow significantly professionally and personally. As I move forward in my career, I would like to acknowledge all those who have been a part of this chapter of my life.

First and foremost, I want to express my sincere gratitude to Prof. Sung-Won Cho, my PhD thesis advisor and mentor, for the kind support and guidance throughout my journey. You have taught and encouraged me to overcome the obstacles that I faced during the past few years. I consider myself extremely lucky to have had you as my mentor. I will always be grateful to you for motivating me to work towards my highest potential.

I would like to thank Prof. Seok Jun Moon, Prof. Eui-Sic Cho, Prof. Joo-Cheol Park, and Prof. Jae-Young Kim from the thesis evaluation committee for their valuable time dedicated to this work and for their insightful comments and encouragement, which considerably helped me think differently and improve.

I want to thank Prof. Eui-Sic Cho and his lab members, especially Dr. Ju-Kyung Jeong, for sharing their findings, which significantly increased the impact of this study. I also want to express my sincere gratitude towards all the past and present lab members of my lab and the Anatomy and Development Biology division for their help throughout this journey.

I thank Prof. Rasika Illeperuma, who recommended me and gave me the opportunity to enter Yonsei University and start a new chapter of my life.

I would like to thank my family, friends, and loved ones, especially my parents, who had not seen their only son for over six and half years yet cheered all the time for their love, care, and sacrifices. They were the backbone of all the success I have today. Last but not least, many thanks to everyone who supports me in becoming successful today.

This dissertation is a slightly modified version of the following paper published in “Notum regulates the cusp and root patterns in mouse molar. *Scientific reports*. (2024) 14:13633” and has been reproduced here.

## TABLE OF CONTENTS

<b>LIST OF FIGURES .....</b>	<b>iv</b>
<b>LIST OF TABLES .....</b>	<b>vi</b>
<b>LIST OF ABBREVIATIONS .....</b>	<b>vii</b>
<b>ABSTRACT .....</b>	<b>ix</b>
<b>I. INTRODUCTION .....</b>	<b>1</b>
1. Overview of mammalian tooth development.....	1
1.1. Prenatal tooth development .....	1
1.2. Tooth root development .....	5
2. Relationship between the tooth crown and root patterning .....	7
3. Wnt signaling pathway .....	8
4. Wnt signaling in tooth development .....	10
5. Notum .....	16
<b>II. MATERIALS AND METHODS .....</b>	<b>20</b>
1. Animals .....	20
2. Single-cell RNA sequencing analysis of publicly available datasets .....	22
3. Whole-mount RNA in situ hybridization .....	23
4. Section in situ hybridization .....	23

5. Micro-computed tomography and geometric morphometric analysis .....	24
6. Scanning electron microscopy .....	25
7. Whole mount immunohistochemistry .....	26
8. RNA Purification.....	27
9. RNA sequencing .....	27
10. Measurement of cusp area, root length, mesiodistal and buccolingual widths ....	28
11. Statistical analysis .....	29
<b>III. RESULTS .....</b>	<b>30</b>
1. <i>Notum</i> was expressed in primary enamel knot, secondary enamel knots, and dental papilla in developing tooth .....	30
2. <i>Notum</i> <sup>-/-</sup> mice showed abnormalities in tooth crown and root morphology .....	45
3. The size of the secondary enamel knots was notably enlarged in <i>Notum</i> <sup>-/-</sup> mice .....	57
4. <i>Notum</i> <sup>-/-</sup> mice exhibited deviations in cusp pattern and crown outline .....	68
5. The lengths of cervical tongues were diminished in <i>Notum</i> <sup>-/-</sup> mice .....	75
6. The crown outline is closely related to the root pattern .....	78
<b>IV. DISCUSSION .....</b>	<b>84</b>
<b>V. CONCLUSION .....</b>	<b>90</b>

<b>REFERENCES .....</b>	<b>92</b>
<b>ABSTRACT (in Korean) .....</b>	<b>108</b>

## LIST OF FIGURES

Figure 1. Wnt/Notum negative feedback loop .....	18
Figure 2. Schematic diagram illustrating the generation of <i>Notum</i> knockout mice .....	21
Figure 3. Single-cell RNA sequencing of developing molars at embryonic day (E)14.5 mouse embryos .....	32
Figure 4. Cell clusters and list of marker genes attributed to the cell clusters in developing mouse molars at E14.5 .....	34
Figure 5. Single-cell RNA sequencing of developing molars at E16.5 mouse embryos ..	37
Figure 6. Cell clusters and list of marker genes attributed to the cell clusters in developing mouse molars at E16.5 .....	39
Figure 7. Expression pattern of <i>Notum</i> in developing molars at E14.5 and E16.5 mouse embryos .....	42
Figure 8. <i>Notum</i> expression in developing molars in the maxilla and mandible .....	44
Figure 9. Morphological changes in crown and root of maxillary and mandibular molars in <i>Notum</i> <sup>-/-</sup> mice at postnatal day (PN) 14 .....	47
Figure 10. Variations in the crown morphology of maxillary and mandibular molars in <i>Notum</i> <sup>-/-</sup> mice at PN 14 .....	49
Figure 11. Morphological changes in tooth crown of maxillary and mandibular molars in <i>Notum</i> <sup>-/-</sup> mice at PN 35 .....	51
Figure 12. Root fusion in <i>Notum</i> <sup>-/-</sup> mice at PN 35 .....	52
Figure 13. Appearance of maxillary and mandibular molars in micro-CT sections .....	53

Figure 14. Alterations in the cusp tip area and root lengths in <i>Notum</i> <sup>-/-</sup> M1 molars .....	54
Figure 15. Variations in root fusion in <i>Notum</i> <sup>-/-</sup> maxillary and mandibular molars .....	56
Figure 16. Heatmaps displaying the alterations in the expression level of selected genes in RNA-sequencing analysis of the E14.5 and E16.5 molars of <i>Notum</i> <sup>+/+</sup> and <i>Notum</i> <sup>-/-</sup> mice .....	59
Figure 17. Expression of <i>Fgf4</i> in developing maxillary M1 and mandibular M1 .....	60
Figure 18. Geometric morphometric changes in cusp pattern and crown outline in <i>Notum</i> <sup>-/-</sup> mice maxillary molars at PN14 .....	70
Figure 19. Geometric morphometric changes in cusp pattern and crown outline in <i>Notum</i> <sup>-/-</sup> mice mandibular molars at PN14 .....	72
Figure 20. Relationship between the cusp pattern PC1 and crown outline PC1 in maxillary and mandibular molars at PN14 .....	74
Figure 21. Alteration of cervical tongue pattern in <i>Notum</i> <sup>-/-</sup> maxillary and mandibular molars .....	76
Figure 22. Changes in the cervical tongue morphology are consistent in <i>Notum</i> <sup>-/-</sup> M1 .....	77
Figure 23. Geometric morphometric changes in maxillary and mandibular crown outlines at PN 35 .....	79
Figure 24. Dimensional changes in crown and root of <i>Notum</i> <sup>-/-</sup> M1 .....	81
Figure 25. Relationship between crown outline and root pattern .....	83
Figure 26. A schematic diagram demonstrating the activity of <i>Notum</i> in the secondary enamel knot and its role in the crown and root patterning .....	91

## LIST OF TABLES

Table 1. The top 50 genes that upregulated in molars of <i>Notum</i> <sup>-/-</sup> mice compared to <i>Notum</i> <sup>+/+</sup> mice at E14.5 (fold change > 2, FPKM > 0.3) .....	61
Table 2. The genes that are downregulated in molars of <i>Notum</i> <sup>-/-</sup> mice compared to <i>Notum</i> <sup>+/+</sup> mice at E14.5 (fold change > 2, FPKM > 0.3) .....	63
Table 3. The genes that are upregulated in molars of <i>Notum</i> <sup>-/-</sup> mice compared to <i>Notum</i> <sup>+/+</sup> mice at E16.5 (fold change > 2, FPKM > 0.3) .....	64
Table 4. The top 50 genes that are downregulated in molars of <i>Notum</i> <sup>-/-</sup> mice compared to <i>Notum</i> <sup>+/+</sup> mice at E16.5 (fold change > 2, FPKM > 0.3) .....	66

## LIST OF ABBREVIATIONS

2D	Two-dimensional
3D	Three-dimensional
BCIP	5-bromo-4-chloro-3-indolyl-phosphate
BMP	Bone morphogenetic protein
CRISPR	Clustered Regularly Interspaced Short Palindromic Repeats
CNC	Cranial neural crest
CT	Computed tomography
DAB	3,3'-diaminobenzidine
DEPC	Diethyl pyrocarbonate
DFA	Discriminant function analysis
DMSO	Dimethyl sulfoxide
EDTA	Ethylenediaminetetraacetic acid
EK	Enamel knot
EMT	Epithelial-to-mesenchymal transition
ERM	Epithelial cell rests of Malassez
FGF	Fibroblast growth factor
FPKM	Fragments Per Kilobase per Million mapped fragments
GEO	Gene Expression Omnibus
HD	High definition

HERS	Hertwig's epithelial root sheath
HVG	Highly variable genes
IMPC	International Mouse Phenotyping Consortium
MVCS	Micro ventilation cage system
NBT	Nitro blue tetrazolium
NCBI	National Center for Biotechnology Information
PBS	Phosphate-buffered saline
PC	Principal component
PCR	Polymerase chain reaction
PFA	Paraformaldehyde
PN	Postnatal
QC	Quality Control
RNA	Ribonucleic acid
SEM	Scanning electron microscope
UMAP	Uniform Manifold Approximation and Projection
UMI	Unique molecular identifiers
VST	Variance stabilizing transformation
Wnt	Wingless-related integration site

## ABSTRACT

### **Role of Notum in Cusp and Root Patterning of Mouse**

#### **Molars**

Dinuka Madhushan Adasooriya

Department of Applied Life Science  
The Graduate School, Yonsei University

(Directed by Professor Sung-Won Cho)

*Notum* has been identified as a direct target of the Wnt/ $\beta$ -catenin signaling pathway and serves a crucial function as a Wnt inhibitor within the negative feedback loop. In the tooth, *Notum* expression is evident in odontoblast progenitors and early odontoblasts during root formation. Moreover, *Notum*-deficient mice exhibit severe dentin defects and irregular roots in their teeth. However, the expression pattern of *Notum* during early tooth development and its role in crown and root patterns remains elusive.

In the present study, the expression pattern of *Notum* and other tooth-specific genes was investigated with RNA in-situ hybridization and single-cell RNA sequencing analysis. The effect of *Notum* on crown and root patterning was investigated using *Notum* knockout mice by examining the phenotypic changes with microscopic and micro-CT techniques. Additionally, total RNA sequencing analysis in developing tooth germs was utilized to study the molecular changes in *Notum*-deficient mice.

*Notum* was expressed in the primary enamel knot (EK), secondary EKs, and dental papilla during tooth development. *Notum*-deficient mice exhibited enlarged secondary EKs, resulting in broader cusp tips, altered cusp patterns, and reduced concavity in crown outline. These changes in crown outline are directed to diminished cervical tongue length, which induces root fusion in the *Notum*-deficient mice. Moreover, at the molecular level, *Fgf20*, *Dkk4*, and *Fgf4*, which are the Wnt target genes expressed in the secondary enamel knots, were significantly upregulated in E16.5 *Notum*-deficient molars.

These findings support the previous concept that the tooth cusp and crown pattern considerably influence the root pattern. The size of the secondary enamel knot, regulated by the Wnt/*Notum* negative feedback loop, significantly impacts the patterns of the crown and root during tooth morphogenesis.

---

**Keywords:** Notum, Wnt signaling, enamel knot, cusp, crown, root, pattern

# **Role of Notum in Cusp and Root Patterning of Mouse Molars**

Dinuka Madhushan Adasooriya

Department of Applied Life Science  
The Graduate School, Yonsei University

(Directed by Professor Sung-Won Cho)

## **I. INTRODUCTION**

### **1. Overview of mammalian tooth development**

#### **1.1. Prenatal tooth development**

Healthy teeth play a crucial role in our lives, allowing proper mastication and being important for facial aesthetics and speech. The tooth comprises two main parts - the crown and the root. The tooth crown is the visible part of a tooth, whereas the root extends into

the jawbone and is attached to the alveolar process of the mandible and maxilla via the periodontal ligaments. Similar to the other ectodermal appendages like hair, glands, and lungs that share common morphological features, the tooth also originated from the interactions between the epithelial-mesenchymal tissues during the early stages of morphogenesis (Chai et al. 2000; Jernvall and Thesleff 2000; Pispas and Thesleff 2003).

Tooth development is initiated when localized oral ectodermal epithelial thickenings form the dental placodes around the mouse embryonic day 11 (E11). Successively, the dental epithelium proliferates and invaginates into the underlying mesenchyme, and the dental mesenchyme condenses around the epithelium, thus continuing to form the tooth bud (mouse E12.5-E13.5). Later, the epithelium extends around the mesenchyme and forms a cap (E13.5-E14.5), followed by the bell shape (E15.5-E18.5). The transition of the bud-to-cap stage in early tooth development requires signals from a transient signaling center positioned in the dental epithelium called the primary enamel knot (EK) (Jernvall et al. 1994). Primary enamel knot is a morphologically distinct structure composed of densely packed non-proliferative epithelial cells in the G1 phase, characterized by the cyclin-dependent kinase inhibitor p21 (*Cdkn1a*) expressing cells. It secretes various signaling molecules, including members of the Wnt-type MMTV integration site (*Wnt*), Sonic hedgehog (*Shh*), bone morphogenetic protein (BMP), and fibroblast growth factor (FGF) which have an effect on the surrounding epithelium and mesenchyme (Jernvall et al. 1994; Vaahtokari et al. 1996; Thesleff and Sharpe 1997; Jernvall et al. 1998).

At the end of the cap stage, the primary enamel knot undergoes apoptosis and is eventually supplanted by the secondary enamel knots at the bell stage (Jernvall et al. 1998; Coin et al. 1999). In multicuspid molars, some primary enamel knot cells are repurposed to form secondary enamel knots (Du et al. 2017). The number and positions of the secondary enamel knots correspond to the number and positions of the future tooth cusps. Therefore, the monocuspid teeth, like canines and incisors, develop only a single enamel knot, and no secondary enamel knots are formed. Nevertheless, multiple knots are seen in teeth with multi-cusps, such as molars. It is not yet fully understood how the enamel knots transit from primary to secondary enamel knots, but it is known that the proper formation of secondary enamel knots depends on the primary enamel knot. For instance, the size of the primary enamel knots can influence the positioning of the secondary enamel knots (Pispa et al. 1999; Ohazama et al. 2004).

The dental epithelial tissue responds to signals from the primary EK and elongates either transversely in molars or longitudinally in incisors. This allows it to extend into and around the underlying mesenchyme, and the formation of cervical loops (CLs) occurs on both sides of the condensed mesenchyme, which is now known as the dental papilla. The cervical loops of molars grow symmetrically around the papilla. However, the cervical loops of incisors grow unevenly along the labial-lingual axis and form a smaller, slow-growing lingual cervical loop and a larger, labial cervical loop that continues to grow during the incisor development and into adulthood (Yu and Klein 2020).

Mammals show heterogeneity and complexity in their tooth crown shapes compared to other vertebrates (Jernvall and Thesleff 2012). Therefore, the shape of the crown, which shows key morphological features such as cusp shape, cusp number, cusp arrangement, and intercuspal crests, has been used for species identifications of mammals (HersHKovitz 1962; Hunter and Jernvall 1995).

The Turing model was recently used with parameter settings for stripe vs. spot patterns that matched the upper molar vs. lower molar morphologies, respectively, and reproduced the relative location and the sequence of cusp formation in upper and lower molars (Morita et al. 2022). It was proposed that the tooth size and tooth number, as well as the cusp size and the number of cusps, can be explained in terms of a reaction-diffusion mechanism, where the key molecules, including activators and inhibitors, determine the micropatterning (size and number of cusps) macropatterning (size and number of teeth) (Cai et al. 2007). It has been suggested that *Wnt*, *Eda*, and *Fgf* pathways act as activators, whereas *Shh* and *Sostdc1* were suggested as modifiers or inhibitors of the tooth and cusps patterning (Jernvall and Thesleff 2000; Salazar-Ciudad and Jernvall 2002; Ohazama et al. 2009; Ahn et al. 2010; Salazar-Ciudad and Jernvall 2010; Cho et al. 2011; Häärä et al. 2012; Harjunmaa et al. 2012; Harjunmaa et al. 2014; Kim et al. 2019).

## 1.2. Tooth root development

Tooth root development initiates subsequent to the crown formation when the enamel tissue reaches the future cementoenamel junction, where enamel encounters the cementum and defines the boundary between the crown and root (Li et al. 2017). The apical part of the enamel organ extends, forming Hertwig's epithelial root sheath (HERS), a bilayer epithelial structure located in between the dental follicle and the dental papilla. The apical growth of the HERS directs the formation of roots, influencing the quantity, shape, and size of tooth roots (Ten Cate 1996; Li et al. 2017). Disruptions in the development of the HERS result in abnormalities in characteristics such as structure, morphology, length, and number of roots (Luder 2015). The Cranial neural crest-derived (CNC) mesenchyme condenses around and consistently interacts with the HERS. The apical papilla mesenchyme then encounters the inner layer of the HERS and differentiates into root-covering (radicular) dentin-secreting odontoblasts. The premature disruption of the HERS continuity leads to compromised root odontoblast differentiation (Kim et al. 2013). Furthermore, the HERS releases growth factors that help promote odontoblast differentiation, indicating that the HERS serves as a signaling center directing the formation of roots (Huang et al. 2009; Huang et al. 2010).

The HERS is also involved in regulating the formation of cementum. Following its active migration towards the apical area, the HERS undergoes perforation through localized cellular apoptosis or epithelial-to-mesenchymal transition (EMT), resulting in the mesh network structure formation (Huang et al. 2009; Luan et al. 2006). This enables the

interactions between epithelial cells and Cranial neural crest (CNC)-derived mesenchyme and the contact between the dental follicle and the recently formed dentin. Once dental follicle cells come into contact with dentin, they transform into cementoblasts and start secreting extracellular matrix proteins specific to the cementum, like collagen fibers (Zeichner-David 2006). Moreover, the HERS itself directly contributes to the population of root cementoblasts via the epithelial-to-mesenchymal transition (Huang et al. 2010; Xiong et al. 2013). During the root formation, the HERS does not undergo complete degeneration; in addition to going through EMT, a portion of the HERS transforms into the epithelial cell rests of Malassez (ERM), which are dormant residues that have a function in the regeneration and repairing of the cementum (Xiong et al. 2013).

In addition to its function in cell differentiation and root and cementum formation, the HERS also contributes to defining the number of roots (Ten Cate 1996). During the formation, the HERS creates tongue-shaped epithelial extensions called cervical tongues that connect horizontally to create a bridge known as the furcation, the position where the root splits and functions as the pulp cavity base (Li et al. 2017; Orban 1980; Seo et al. 2017).

## 2. Relationship between the tooth crown and root patterning.

Numerous studies have shown a relationship between tooth root patterning and the tooth crown. The root pattern is suggested to depend on the tooth type, influenced by the cusp number and the molarization (Osborn 1907; Kondo et al. 2009; Seo et al. 2017). Kondo et al. (2009) reported that the crown outline influences the positioning of roots in maxillary molars of certain insectivore species and *Tupaia*. Additionally, it was suggested that supernumerary cusps are often associated with the supernumerary roots, indicating that the formation of the roots depends on the tooth crown (Butler 1956). A study comparing tooth shapes in extant mammals indicates a direct relationship between the number of tooth roots and the main cusps on the crown of the tooth. Nonetheless, the positive correlation was only seen in maxillary teeth, where the rule of tooth root patterning might vary depending on whether it is the maxilla or mandible (Ota et al. 2009).

Seo et al. (2017) described a mechanism for the formation of cervical tongues. Dental mesenchyme grows laterally in the cuspal area, pushing the cervical loop outwards, resulting in the appearance of the cervical tongue between cusps. However, when the lateral growth is physically restricted, the formation of the cervical tongue is inhibited. Moreover, they have shown a positive correlation between the tooth cusps, cervical tongues, and the number of roots. This indicates that the cusp pattern in the crown and the lateral growth of cusps play a significant role in regulating the root pattern.

### 3. Wnt signaling pathway

Wnt signaling plays a major role in embryogenesis, tissue homeostasis, and wound repair by regulating cell proliferation, differentiation, polarization, and apoptosis. Moreover, the Wnt signaling pathway is also a key regulator during tooth and periodontal tissue development, homeostasis, and regeneration. There are 19 cysteine-rich protein ligands in the Wnt signaling pathway, and a receptor complex consists of 10 seven-pass transmembrane receptors called Frizzled (Fzd) and LDL receptor proteins 5 and 6 (LRP5 and LRP6) that mediate the signaling. Once the Wnt ligand binds to the extracellular cysteine-rich domain of Fzd, the signal is transferred to a cytoplasmic phosphoprotein named Dishevelled (Dsh/Dvl) (Birjandi and Sharpe 2021).

Wnt signaling can be divided into two: canonical and non-canonical. In canonical signaling, ligands bind to the receptors and co-receptors, form the Wnt-Fz-LRP complex, and recruit Dsh/Dvl. As this Axin complex is connected to the receptor, the Axin-mediated  $\beta$ -Catenin phosphorylation is inhibited, and  $\beta$ -Catenin is subsequently stabilized, which facilitates the translocation of  $\beta$ -catenin into the nuclei to form the TCF/LEF complex and activate the Wnt target genes. In the absence of the Wnt, a  $\beta$ -Catenin destruction complex is formed and degrades the cytoplasmic  $\beta$ -Catenin. The destruction complex is formed with Axin, Adenomatosis polyposis coli (APC), protein phosphatase 2A (PP2A), casein kinase 1 $\alpha$  (CK1 $\alpha$ ), and glycogen kinase 3 (GSK3) (Fig. 1) (Komiya and Habas 2008; Birjandi and Sharpe 2021).

Non-canonical Wnt signaling includes the Wnt-PCP and Wnt-Ca<sup>2+</sup> pathway, which signals via Fzds, RYK, ROR2, or Fzds with ROR or RYK as coreceptors. This activates downstream effectors like calcium/Calmodulin dependent protein kinase II, mobilization of Ca<sup>2+</sup>, heterotrimeric G proteins, and numerous small GTPases. Moreover, Non-canonical Wnt signaling regulates cell polarity and directional cell migration, promotes invasion, and inhibits the canonical Wnt/  $\beta$ -Catenin signaling pathway (Gordon and Nusse 2006; Birjandi and Sharpe 2021).

#### 4. Wnt signaling in tooth development

During tooth development, expression of the several components of the Wnt signaling pathway, such as Wnt ligands, receptors, transcription factors, transducers, and antagonists, are found in both the dental epithelium and mesenchyme in humans and mice (Sarkar and Sharpe 1999; Wang et al. 2014; Tamura and Nemoto 2016). *Wnt3*, *Wnt4*, *Wnt6*, *Wnt7b*, and *Wnt10b* show their expression in the epithelium, while *Wnt5a* exhibits a restricted expression in the dental mesenchyme and dental papilla. Moreover, expression patterns of *Wnt3*, *Wnt5a*, *Lrp5*, *Fzd6*,  $\beta$ -catenin, *Lef1*, and *Dkk1* are similar in humans and mice during tooth development (Wang et al. 2014). This indicates the significance of the canonical Wnt pathway in tooth formation.

The canonical Wnt/ $\beta$ -catenin signaling pathway is activated in various stages of tooth formation (Liu et al. 2008). The expression of multiple Wnt pathway genes was observed during the dental placode development. *Wnt10b* is limited to the thickenings of the dental epithelial in the oral ectoderm, whereas *Wnt4*, *Wnt6*, and *Fzd6* expression was shown all over the oral ectoderm (Dassule and McMahon 1998; Sarkar and Sharpe 1999). The *Wnt3* and *Wnt7b*, activators of the canonical Wnt signaling pathway, also show their expression in the oral epithelium but not in the future dental placodes. Concomitantly, expression of the *Wnt5a*, *Sfrp2*, and *Sfrp3* Wnt antagonists are spotted in the underlying dental mesenchyme (Sarkar and Sharpe 1999). Numerous studies have shown the Wnt/ $\beta$ -catenin pathway activity using transgenic mouse lines with Wnt reporters such as

TOPGAL, BAT-gal, *Tcf/Lef-LacZ*, or *Axin2-LacZ* in the developing dental placodes, the underlying mesenchyme, and the dental lamina (Brugmann et al. 2007; Liu et al. 2008; Lohi et al. 2010).

Expression of nuclear  $\beta$ -catenin is observed in both the epithelium and underlying mesenchyme at the early bud stage, and the restriction of canonical Wnt signaling at E12.5 could arrest tooth development (Liu et al. 2008). For instance, the overexpression of a Wnt signaling inhibitor, *Dkk1* (Liu et al. 2008), Prx-1-Cre-driven conditional deletion of  $\beta$ -catenin (Fujimori et al. 2010), or loss of *Lef1*, a downstream transcription factor of the canonical Wnt signaling pathway (van Genderen et al. 1994; Sasaki et al. 2005), results in the tooth development arrest at the bud stage. Additionally, the inhibition of *Fgf4*, which is a downstream molecule of *Lef1*/ $\beta$ -catenin, hinders odontogenic epithelial cell proliferation (Kratochwil et al. 2002). At the cap stage, *Wnt10*, along with *Shh*, *Bmp2*, and *Fgf20*, are limited to a small placodal cell cluster and form the early signaling center called the primary enamel knot (Jussila and Thesleff 2012). Wnt/ $\beta$ -catenin is suggested to be the most upstream regulator of *Fgf4* and *Fgf20* in the signaling center (Kratochwil et al. 2002; Häärä et al. 2012).

It is suggested that a negative feedback loop is formed between Wnt and Shh in the developing tooth germs. This loop is regulated via *Sostdc1* and *Lrp4*, which are Wnt co-receptors with inhibitory functions. The collaborative action of *Sostdc1* and *Lrp4* was initially revealed by the discovery that mice with *Lrp4* mutation mimic phenotypes of the

*Sostdc1* mutants, which show similar features like fused molars and extra molars and incisors (Kassai et al. 2005; Ohazama et al. 2008; Munne et al. 2009; Ahn et al. 2010). Similar phenotypes were reported in the genetically modified mice with over-expression of  $\beta$ -catenin using the K14 promoter in the epithelium and *Gas1* null mutation (Järvinen et al. 2006; Ohazama et al. 2009; Wang et al. 2009). In addition, *Shh*<sup>+/-</sup>; *Sostdc1*<sup>+/-</sup> mice show increased Wnt signaling compared to *Sostdc1*<sup>+/-</sup> mice, further supporting the existence of the negative feedback loop between Shh and Wnt via *Sostdc1* (Ahn et al. 2010; Cho et al. 2011). Moreover, Shh derived from the epithelium can directly impact the *Sostdc1* expression in the dental mesenchyme, while in vivo ablation of Shh signaling utilizing an anti-Shh antibody (5E-1) decreases the expression levels of *Sostdc1* (Cho et al. 2011; Kim et al. 2019). These reports collectively suggest that Shh, which is itself a Wnt target gene, negatively regulates Wnt/ $\beta$ -catenin signaling through its target gene *Sostdc1*, which binds to inhibitory Wnt co-receptor *Lrp4* and acts together (Ohazama et al. 2008; Hermans et al. 2021).

At the bell stage of tooth development, secondary enamel knots are localized at the tips of the prospective cusps of the molars. The secondary enamel knot patterning determines the positions and size of the tooth cusps. Furthermore, ameloblasts and odontoblasts are formed during the bell stage. Consistent with the primary enamel knot abnormalities caused by Wnt/ $\beta$ -catenin signaling dysfunction, inhibiting the pathway at the bell stage (E16) by overexpression of *Dkk1*, leads to disrupted secondary enamel knots and diminished cusp development, resulting in blunted, less prominent cusps (Liu et al. 2008).

Both primary and secondary enamel knots expressed *Wnt10a*. From the bell stage, expression of the *Wnt10a* transitions from the epithelium to the dental mesenchyme, and an elevated *Wnt10a* expression is found in the odontoblasts that differentiate later into the odontoblasts expressing DSPP (Yamashiro et al. 2007). Continuous  $\beta$ -catenin expression in the ameloblasts of mouse incisors leads to mineralization delay and reduced levels of MMP20 and KLK4, which are proteins related to amelogenesis (Fan et al. 2018). Overexpression of Wnt/ $\beta$ -catenin in *OC-Cre; Catnb<sup>+lox(ex3)</sup>* transgenic mice prompt premature odontoblasts differentiation and results in the production of vast quantities of poorly mineralized dentin and reduced expression of DSPP (Kim et al. 2011; Bae et al. 2013b). Conversely, reduced activity of the Wnt signaling in the early odontoblasts of the *OC-Cre; Wls<sup>(CO/CO)</sup>* mice leads to a decrease in dentin formation, leading to a thinner wall of dentin and broader pulp chamber (Bae et al. 2015). Moreover, the continuous expression of  $\beta$ -catenin in mesenchymal cells increases the rate of differentiation of dental pulp cells, leading to premature odontoblasts and dentin-like matrix produced within the dental pulp compartment (Chen et al. 2009). Using *Wls<sup>Shh-Cre</sup>* conditional knockout mice, it has been demonstrated that the Wnt ligand in the dental epithelium is essential for the differentiation of tooth during late tooth development (Xiong et al. 2019). MMP20 overexpressing mice exhibit increased levels of  $\beta$ -catenin and fibroblasts penetrating the enamel, resulting in soft, thin, and irregular enamel (Shin et al. 2016).

These reports partially explain the importance of Wnt signaling in tooth development. Interruptions in Wnt signaling during different stages of tooth development

account for various developmental defects that vary from tooth agenesis to odontomas (Järvinen et al. 2018; Fujii et al. 2019; Birjandi and Sharpe 2021).

Formation of the tooth roots occurs solely after the birth of mice. Wnt/ $\beta$ -catenin signaling remains consistently active in the dental epithelium (HERS) and the dental mesenchyme, such as the dental papilla cells and the dental follicle cells adjacent to HERS (Kim et al. 2011; Bae et al. 2013a). *Axin2*, a suppressor of the canonical Wnt signaling pathway, expression is found in the developing tooth roots from the postnatal day (PN) 10 near the HERS and the dental papilla (Lohi et al. 2010). Furthermore, *Wnt3a* expression is detected in the HERS and odontoblasts in PN14 mice, and it is continuously expressed in the ERM (Nemoto et al. 2016). *Wnt10a* expression is also observed in the dental epithelial and mesenchymal cells during prenatal stages and through tooth root development (Yamashiro et al. 2007; Yu et al. 2020).

During tooth root development, the Wnt/ $\beta$ -catenin signaling pathway is essential for the interaction between epithelial and mesenchymal cells. Conditional inactivation of epithelial  $\beta$ -catenin using *Shh<sup>creER</sup>* results in impaired structural integrity of the HERS and premature disruption in its bilayer structure. This inactivation further disrupts odontogenesis with decreased levels of *Osx*, *Nfic*, *Msx1*, and *Msx2* expression, eventually leading to shorter roots in the molars. These reports indicate that  $\beta$ -catenin plays a crucial role in regulating the structural integrity of HERS, which is essential for dentin formation and root development (Yang et al. 2021). Selective *Wnt10a* inactivation in the epithelial

cells of *K14-cre;Wnt10a<sup>fl/fl</sup>* mice exhibit root fusion (taurodontism) with shorter molar roots. The ablation of *Wnt10a* in *K14*-expressing cells inhibits the proliferation of the epithelial cells. This induces a compensatory increase in *Wnt4a* in the dental papilla, which leads to the elevated proliferation of dental papilla cells, ultimately disrupting the formation of the floor of the pulp chamber. In contrast, normal molars are formed in the absence of *Wnt10a* in the dental mesenchyme (Yu et al. 2020). During molar root development, loss of  $\beta$ -catenin in the cells of odontoblast lineage utilizing *Ocn-cre; Ctnnb<sup>fl/fl</sup>* inhibits the differentiation and proliferation of odontoblasts, leading to altered tooth root development. The first and second molars of the mutant mice show rootless molars with normal tooth eruption (Kim et al. 2013; Zhang et al. 2013).

*Wnt5a* and *Ror2* maintain their expression in the dental epithelium and the mesenchyme even after birth. The expression pattern turns out to be more prominent in the region of root-forming with age. Studies have shown that the *Ror2*-mediated non-canonical Wnt signaling pathway in the dental mesenchyme regulates the formation of the molar roots by activating Cell Division Cycle 42 (*Cdc42*), which is a target of the  $\text{Ca}^{2+}$  signaling pathway. This highlights the possible contribution of non-canonical Wnt signaling to tooth root development (Ma et al. 2020).

## 5. Notum

*Notum*, Palmitoleoyl-Protein Carboxylesterase is a target and an inhibitor of the Wnt/  $\beta$ -Catenin signaling pathway. Wnts are modified by *O*-linked palmitoleoylation of a conserved serine required for the binding to the Fzd receptors. Porcupine (PORCN) acyltransferase introduces the *O*- palmitoleoylation to the Wnt; in contrast, *Notum*, a serine hydrolase, removes the *O*-linked palmitoleate modification and deactivates the Wnts. (Kakugawa et al. 2015). *Notum* is a direct target of the Wnt signaling, and TCF binding sites are found in the *Notum* promoter site as in *Axin2*. This functions as a negative feedback loop, which is required for the weakening strength of the Wnt/  $\beta$ -Catenin signaling (Fig. 1) (Gerhardt et al. 2018; Suciú et al. 2018; Kleman and Leedham 2020). Moreover, Notum is the sole secreted Wnt feedback inhibitor found throughout the kingdom of Animalia (Kakugawa et al. 2015). *Notum* inhibits a number of ligands in the canonical WNT/ $\beta$ -catenin signaling pathway, like *wnt1*, *wnt3a*, and *wnt10a* (Saad et al. 2017; Brommage et al. 2019). NOTUM plays a crucial role in several *in vivo* growth and developmental processes, such as neural and head induction, formation of endocortical bone, tracheal patterning, and intestinal stem cell aging (Zhang et al. 2015; Gerhardt et al. 2018; Pentimikko et al. 2019; Choi et al. 2021).

In teeth, *Notum* was recently reported to be expressed in early odontoblasts identified near the cervical loop mesenchymal area in mouse teeth (Krivanek et al. 2020; Wen et al. 2020), and in the apical papilla region of human tooth germs (Zhao et al. 2024). *Notum* knockout mice showed a severely disrupted crown and root dentin formation in the

molars and crown dentin in the incisors, but amelogenesis was not affected (Vogel et al. 2016). Runt-related transcription factor 2 (Runx2), a transcription factor, binds to the genomic loci of *Notum* and directly controls *Notum* expression to regulate root development. Additionally, *Notum* is able to activate the expression of *Dspp*, an odontoblast marker *in-vitro*, and partially rescue the defects of the roots in *Gli1-Cre<sup>ERT2</sup>*; *Runx2<sup>fl/fl</sup>* mice (Wen et al. 2020). However, the precise expression pattern and role of *Notum* in tooth patterning remain to be elucidated.

In the present study, *Notum* expression was detected in the primary and secondary enamel knots and underlying mesenchyme. *Notum*-deficient mice showed altered cusp patterns with broader cusps, which leads to abnormal molar shapes and fusion of the molar roots. Moreover, this study demonstrated the relationship among cusps, cervical tongue, and roots in *Notum* deficient mice.

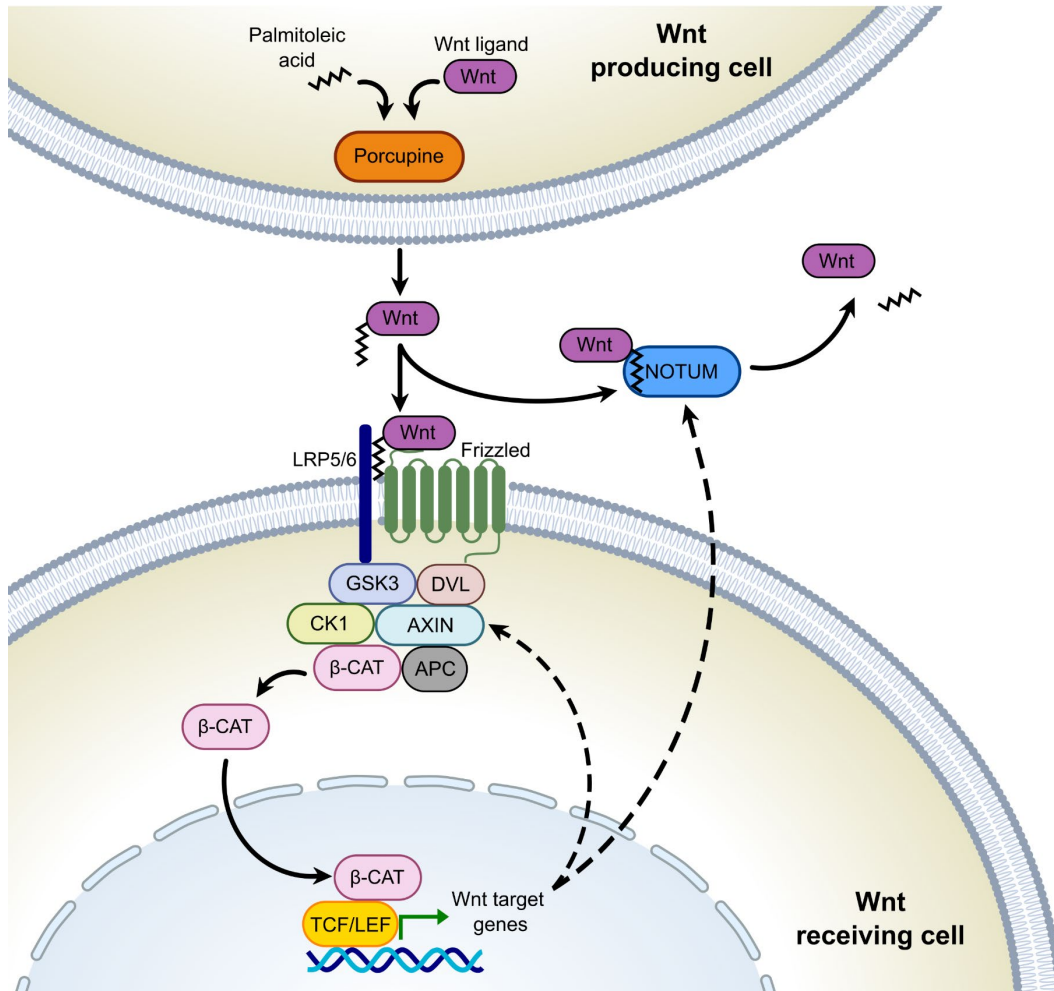


**Figure 1. Wnt/Notum negative feedback loop**

Wnt ligands secreted from the stromal cells are activated by undergoing post-translational modification, O-linked palmitoleation catalyzed by the O-acyltransferase Porcupine (PORCN). Activated Wnt ligands bind to Frizzled (FZD) receptors on the Wnt receiving cells. This inhibits the destruction complex, and  $\beta$ -catenin translocated to the nucleus, followed by the molecular complex formation with TCF/LEF and initiates the Wnt target

gene expression. The activation of the Wnt signaling pathway is regulated at multiple levels by negative feedback loops such as those mediated by AXIN2 and notum palmitoyl-protein carboxylesterase (NOTUM). NOTUM is secreted into the extracellular space and inactivates the Wnt ligands by deacetylation, removing the palmitoleic acid modification, which directly contributes to the receptor binding (Adapted from Kleeman and Leedham, 2020).

## II. MATERIALS AND METHODS

### 1. Animals

All methods, including animal experiments, were approved by the Yonsei University Health System Institutional Animal Care and Use Committee (YUHS-IACUC). All the procedures were performed in accordance with the guidelines and regulations of this committee.

The mice were housed under regular light/dark cycles (12 h light:12 h dark, LD) at a temperature of  $22\pm 1^{\circ}\text{C}$  with  $50\pm 10\%$  humidity in individually ventilated cages in a micro ventilation cage system (MVCS). Mice were provided with shaved wood aspen bedding, clean water, and a normal chow diet.

F0 *Notum* knockout mouse (*Notum*<sup>em1(IMPC)Tcp</sup>) generated on the C57BL/6N background strain were purchased from the international mouse phenotyping consortium (IMPC) ([www.mousephenotype.org](http://www.mousephenotype.org)) and mated with C57BL/6N wild type mice to get the F1 (Fig. 2). F2 and above generations of mice (*Notum*<sup>+/+</sup> and *Notum*<sup>-/-</sup>) were used for the study after euthanization utilizing CO<sub>2</sub> exposure at selected postnatal ages and embryonic days. A mix of males and females was assigned without regard to gender, and at least one subject from each gender was included in each group after screening for the genotype screening with PCR. Moreover, approximately 90% of *Notum*<sup>-/-</sup> mice show perinatal lethality.

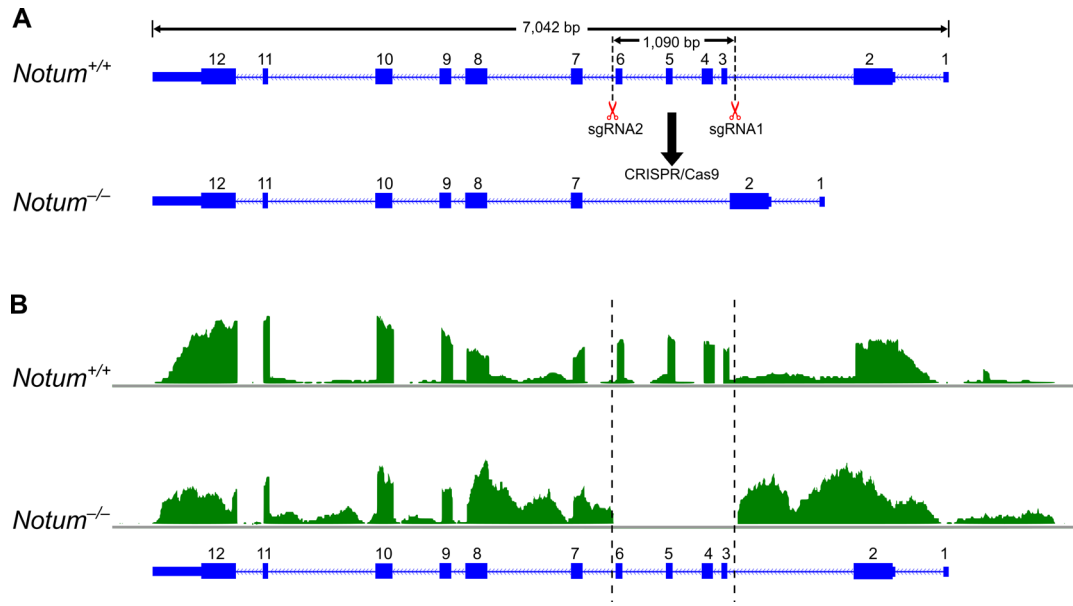


**Figure 2. Schematic diagram illustrating the generation of *Notum* knockout mice.**

**(A)** *Notum* gene deletion with CRISPR Cas9 system. **(B)** visualization of RNA-seq coverage data confirming complete deletion of *Notum* from exons 3 to 6 in the *Notum*<sup>-/-</sup> mice.

## 2. Single-cell RNA sequencing analysis of publicly available datasets

Publicly available scRNA-seq datasets of E14.5 and E16.5 mouse molars were obtained from the Gene Expression Omnibus (GEO) under the accession numbers GSE189381 (Jing et al. 2022) and GSE162413 (Hu et al. 2022). These datasets were provided as pre-processed count matrices. The single-cell RNA-seq datasets were processed, explored, and visualized using Cellenics® (currently rebranded as Tailmaker®), community instance (<https://scp.biomage.net/>) hosted by Biomage (<https://biomage.net/>).

Pre-filtered count matrices were loaded into the Cellenics®, and the barcodes were filtered sequentially using the automatic filtering settings in the four steps: cell size distribution filter, mitochondrial content filter, number of genes vs UMI filter, and doublet filter. After the filtering and quality control, a total of 30,744 cells for E14.5 and 29,307 for E16.5 were used in the final visualization and clustering. The two E14.5 datasets and the E16.5 datasets were combined independently using the "Harmony" method and normalized with the "LogNormalize" function. The top 2000 highly variable genes (HVGs) were obtained using the variance stabilizing transformation (VST) technique. Dimensionality reduction is performed to summarize and visualize the data with Principal-component analysis (PCA) using 30 Principal Components (PCs) for both E14.5 and E16.5, which account for more than 90% of the total variation within the datasets. The Louvain technique was used for generating cell clusters, which were then displayed using Uniform Manifold Approximation and Projection (UMAP) embedding at a resolution of 0.3. All cell

clusters were manually annotated using the available literature (Krivanek et al. 2020; Hu et al. 2022; Jing et al. 2022).

### 3. Whole-mount RNA in situ hybridization

Tooth germs were extracted from the mandibles and maxillae of *Notum*<sup>+/+</sup> and *Notum*<sup>-/-</sup> mice at E14.5, E16.5, E17.5, and E18.5 on cold DEPC-PBS and fixed with 4% PFA in DEPC-PBS overnight at 4°C. They were treated with proteinase K (10 µg/ml) for 45 minutes at room temperature to improve permeabilization. The hybridization was performed with *Fgf4* and *Notum* RNA probes labeled with digoxigenin (1 µg/ml) in the hybridization solution for 20 hours at 67°C. Specimens were equilibrated in color reaction buffer containing Tris, MgCl<sub>2</sub>, NaCl, Tween 20, and 4-nitro-blue-tetrazolium (NBT)/5-bromo-4chloro-3-indolyl-phosphate (BCIP) (Roche, USA). When the appropriate color was developed, samples were washed with PBS and post-fixed with 4% PFA. Images were captured using a Leica S9D microscope equipped with a Leica M170 HD digital camera.

### 4. Section in situ hybridization

Mandibles were isolated from E14.5 and E16.5 wild-type mouse embryos on the cold DEPC-PBS and fixed with 4% PFA in DEPC-PBS overnight at 4°C with rocking. Samples were washed in DEPC-PBS and decalcified with the 10% EDTA in DEPC-PBS at 4°C for four days. The decalcified samples were washed with DEPC-PBS followed by a saline wash, and then dehydrated with Saline: Ethanol 1:1 solution followed by 70%, 80%,

and 90% Ethanol with DEPC and 100% ethanol. Specimens were cleared with xylene, then infiltrated in wax, and embedded in paraffin wax. Paraffin-embedded samples were sectioned at 5  $\mu\text{m}$ , and sections were collected on glass slides. An antisense *Fgf4*, *Shh*, *Bmp4*, and *Notum* RNA probes were designed and produced by Advanced Cell Diagnostics (Newark, USA) were purchased and used. In situ hybridization was performed with the RNAscope® 2.5 High Definition (HD) assay-brown (Advanced Cell Diagnostics) according to the user manual 322452 (FFPE sample preparation and pretreatment) and 322310 (RNAscope® 2.5 HD Detection Reagent-brown user manual) provided by the manufacturer. The following RNA probes were used: (1) Mm-Fgf4 (514311, targeting NM\_010202.5, nucleotide 313–1486) (2) Mm-Shh (314361, targeting NM\_009170.3, nucleotide 307–1197) (3) Mm-Bmp4 (401301, targeting NM\_007554.2, nucleotide 586–1673), (4) Mm-Notum (428981, targeting NM\_175263.4, nucleotide 406–1623), (5) Mm-Lef1 (44186, targeting NM\_010703.4, nucleotide 1361–2354). Images were taken using an Olympus BX43 microscope equipped with an Olympus DP23 digital camera.

## **5. Micro-computed tomography and geometric morphometric analysis**

Mouse hemimaxilla and hemimandibles (*Notum*<sup>+/+</sup>, *Notum*<sup>-/-</sup> at PN14, PN35) were fixed in 4% PFA in PBS. Micro-computed tomography (micro-CT) images were taken using a micro-CT scanner (Skyscan1173, Bruker, Belgium) at 130 kV and 60  $\mu\text{A}$  alongside 0.25  $\text{g}/\text{cm}^3$  and 0.75  $\text{g}/\text{cm}^3$  Phantom rods. Micro-CT data reconstruction was done using

NRecon (Version 1.6) with consistent settings. The software 3D Slicer (Version 4.1, <http://www.slicer.org>) and OnDemand 3D (Version 1.0, Cybermed, Korea) were used to convert the Skull and teeth micro-CT images to 3D volumes. Eight and seven landmarks are placed on the cusps of the 3D-reconstructed maxillary and mandibular first molars (M1), respectively, and 64 equally spaced landmarks are placed along the crown outlines of the maxillary and mandibular M1 occlusal view 2D captures (PN14 n = 10, and PN35 n = 12 per group) (Fig. 18A, Fig. 19A) using the software Blender (Version 3.2.1, Blender Foundation, Netherlands). Principal component (PC) analysis and discriminant function (DF) analysis with leave-one-out cross-validation were performed on Procrustes shape coordinates to define the features of the shapes, using the software MorphoJ (Version 1.07a, Klingenberg lab, University of Manchester, UK).

## 6. Scanning electron microscopy

Scanning electron microscopy (SEM) was used to visualize the features of the PN35 *Notum*<sup>+/+</sup> and *Notum*<sup>-/-</sup> mandibular and maxillary molars (n = 3 per group). Mandibles and maxilla specimens were fixed in 4% PFA in PBS overnight at 4 °C. Then, they were dehydrated with ethanol series, air-dried, fixed for 2 hours in 1% OsO<sub>4</sub>, and dried with a freeze dryer (ES-2030, Hitachi, Japan). Mandibular and maxillary molars attached to the alveolar bone were mounted on metallic stubs and platinum coated to a thickness of 100 nm using an ion coater (E-1010, Hitachi) and scanned under the scanning electron microscope (S-3000N, Hitachi).

## 7. Whole mount immunohistochemistry

Maxillary and mandibular molar tooth germs were dissected from *Notum*<sup>+/+</sup> and *Notum*<sup>-/-</sup> mice at PN0 and PN7 (n = 5 per group). They were isolated in cold PBS and fixed with Methanol/DMSO (4:1) overnight at 4°C and then in Methanol/DMSO/H<sub>2</sub>O<sub>2</sub> (4:1:1) overnight at 4°C. Then the specimens were stored in 100% methanol at -20°C. The tooth germs were rehydrated in 50% Methanol in PBS, followed by PBS and then PBSMT [PBS, 5% (v/v) DMSO, 2% (w/v) non-fat skim milk, and 0.1% (v/v) Tween-20]. The primary antibody (Human/Mouse E-Cadherin Antibody, R&D Systems), which is 1:200 diluted in PBSMT, was added to the samples and incubated overnight at 4°C. The next day, the samples were washed five times with PBSMT for one hour each. The secondary antibody (Donkey anti-Goat IgG (H+L) Secondary Antibody, HRP, Invitrogen) diluted in PBSMT (1:500) was added and incubated overnight at 4°C. Then, the samples were washed five times with PBSMT for 1 hour each. The color reaction was carried out using the DAB chromogen kit (Liquid DAB+ Substrate Kit for Immunohistochemistry, GBI Labs) as described in the manufacturer's manual. Two drops of DAB chromogen were mixed with 1ml of DAB substrate buffer, and the tooth germs were incubated in an enclosed chamber at room temperature until the desired color was developed. Finally, the samples were rinsed with distilled water, post-fixed with 4% PFA, and imaged using a Leica S9D microscope equipped with a Leica M170 HD digital camera.

## 8. RNA Purification

Maxillary and mandibular molar tooth germs were isolated from *Notum*<sup>+/+</sup> and *Notum*<sup>-/-</sup> littermate mouse embryos at E14.5 and E16.5 (n = 3 per biological replicate, and 2 replicates per group) in cold DEPC-PBS, transferred to RNeasy lysis solution (Qiagen), and stored at -20°C. Tooth germs were homogenized in TRIzol® (Invitrogen) with the 0.5 mm stainless steel beads using the Bullet Blender® homogenizer (Next Advance, USA). Total RNA was phase separated with chloroform and precipitated with isopropyl alcohol. The RNA pellet was washed in 75% ethanol and eluted with RNase-free water. The concentration and quality of RNA were assessed using the RNA ScreenTape® (Agilent Technologies, Germany).

## 9. RNA sequencing

Messenger RNA (mRNA) was purified from total RNA using poly-T oligo-attached magnetic beads. Following fragmentation, random hexamer primers were used to synthesize the first strand of cDNA, which was then followed by the second strand. The library was prepared, followed by the end repair, A-tailing, adapter ligation, size selection, amplification, and purification. The library was validated with Qubit, quantified using real-time PCR, and size distribution was detected using a bioanalyzer. Quantified libraries were pooled and sequenced on the Illumina platform (Illumina NovaSeq 6000). Raw data (raw reads) of fastq format were initially processed using Novogene in-house Perl scripts where the RNA sequencing was carried out (Novogene, China). Clean data (clean reads) were

acquired by removing reads containing adapter, reads containing ploy-N, and low-quality reads from the raw data. Simultaneously, Q20, Q30, and GC content of the clean data were assessed, and all the subsequent analyses were based on clean, high-quality data. A reference genome index (mm10) was created, and paired-end clean reads were aligned to it using Hisat2 v2.0.5. The featureCounts v1.5.0-p3 was used to count the number of reads mapped to each gene. The reads per kilobase of exon per million reads mapped (FPKM) of each gene was computed using the gene length and the number of reads mapped to it.

The read counts were analyzed for differential expression in two groups (two biological replicates per condition) using the DESeq2 R package (1.20.0). The resulting P values were adjusted using the Benjamini-Hochberg method. A corrected P-value of 0.05 was set as the threshold for significantly differential expression. The raw and processed bulk RNA-Seq data used in this study have been deposited in the NCBI GEO repository under the accession number GSE255946.

## **10. Measurement of cusp area, root length, mesiodistal, and buccolingual widths**

The cusp tip area was assessed in micro-CT sections of PN14 maxillary and mandibular M1 molars of *Notum*<sup>-/-</sup> and *Notum*<sup>+/+</sup> mice (n = 10 per group). The area of the cusp tips was measured 0.1 mm beneath the cusp tip point perpendicular to the cervical plane (Fig. 14A–B). The root lengths were measured in 3D segmented PN35 maxillary and mandibular

M1 molars of *Notum*<sup>-/-</sup> and *Notum*<sup>+/+</sup> mice (n = 10 per group) (Fig. 14C – D). The mesiodistal and buccolingual widths were measured in 3D segmented PN35 maxillary M1 (n = 12) and mandibular M1 (n = 12) in *Notum*<sup>-/-</sup> and *Notum*<sup>+/+</sup> mice. Reference points were made at the most mesial and distal ends in the mesiodistal axis of the crown and the most lingual and buccal points in the buccolingual axis. Then, a three-dimensional straight line connecting two points at each axis was created, and the distance was measured using the software OnDemand 3D (Version 1.0, Cybermed, Korea).

## 11. Statistical analysis

The area of the cusp tip and the root length were plotted as bar charts with error bars representing the standard deviation (SD). The crown width, interradicular distance, and interradicular area data were presented as box and whisker plots based on 12 M1 samples per group. The Mann-Whitney U test was used for the pairwise statistical comparisons across the groups, and linear regression was applied to examine the correlation between the dimensions using the SPSS software (version 26.0; IBM Corp., USA). P value < 0.05 indicated a statistically significant difference.

### III. RESULTS

#### 1. *Notum* was expressed in primary enamel knot, secondary enamel knots, and dental papilla in developing tooth

To determine the expression pattern of *Notum* during tooth development, single-cell RNA sequencing analysis was performed in molars at E14.5 and E16.5, using two recently published single-cell RNA sequencing data sets (Hu et al. 2022; Jing et al. 2022). The uniform manifold approximation and projection (UMAP) illustration exhibits unbiased identification of 11 clusters at E14.5 and 14 clusters at E16.5 molars (Fig. 3A–B, Fig. 5A–B). The differentially expressed features (cluster markers) in each cell cluster were presented in the cluster map and heatmap (Fig. 4, Fig. 6). *Notum* expression was localized in a small subset of epithelial and dental mesenchymal cell clusters at both E14.5 and E16.5. In the cluster map (Fig. 3A–B, Fig. 5A–B) and in frontal sections of the mandibular first molars (M1) (Fig. 7A–J), *Notum* expression in epithelial cells was colocalized with other enamel knot markers, such as *Shh*, *Fgf4*, *Bmp4*, and *Lef1*. Specifically, The expression of *Notum* in epithelial cells was found in primary EK at E14.5 and secondary EKs at E16.5, resembling the expression of *Fgf4*, which is a well-known EK marker. This unique expression of *Notum* within the enamel knots suggests a crucial role of *Notum* in the complex process of cusp patterning. In spite of that, *Notum*-expressing mesenchymal cells were colocalized with *Lef1* and *Bmp4* expressing cells at E14.5 and E16.5 in the cluster map (Fig. 3A–B, Fig. 5A–B) and the mandibular M1 sections. (Fig. 7A–J). *Notum*

expression was located in a thin outer layer of the dental papilla in the sections (Fig. 7A, F). At E14.5 and 16.5, expression of *Notum* was found in both the epithelium and mesenchyme at the cuspal region. As tooth development progresses, expression of the *Notum* is maintained solely in the mesenchyme while it is diminished in the epithelium (Fig. 8A–N).

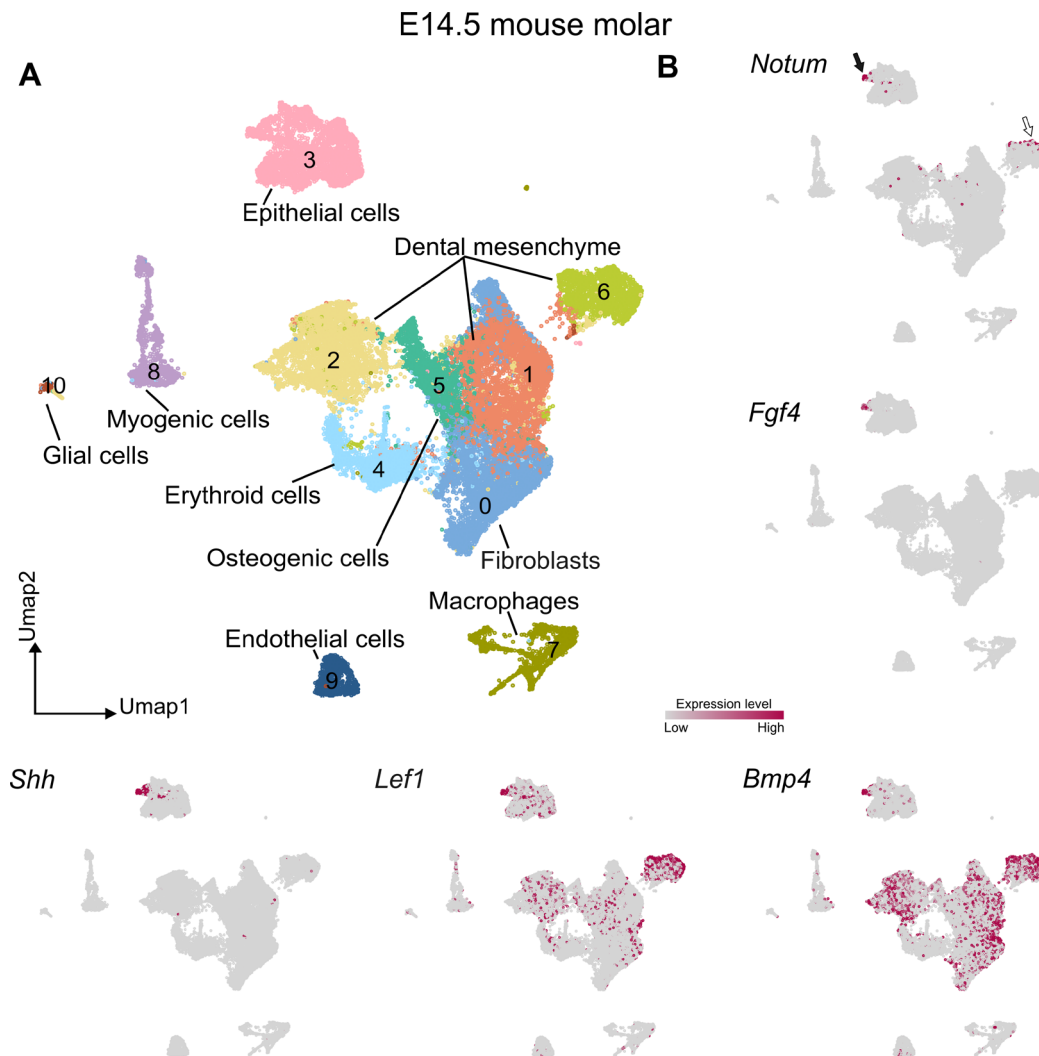
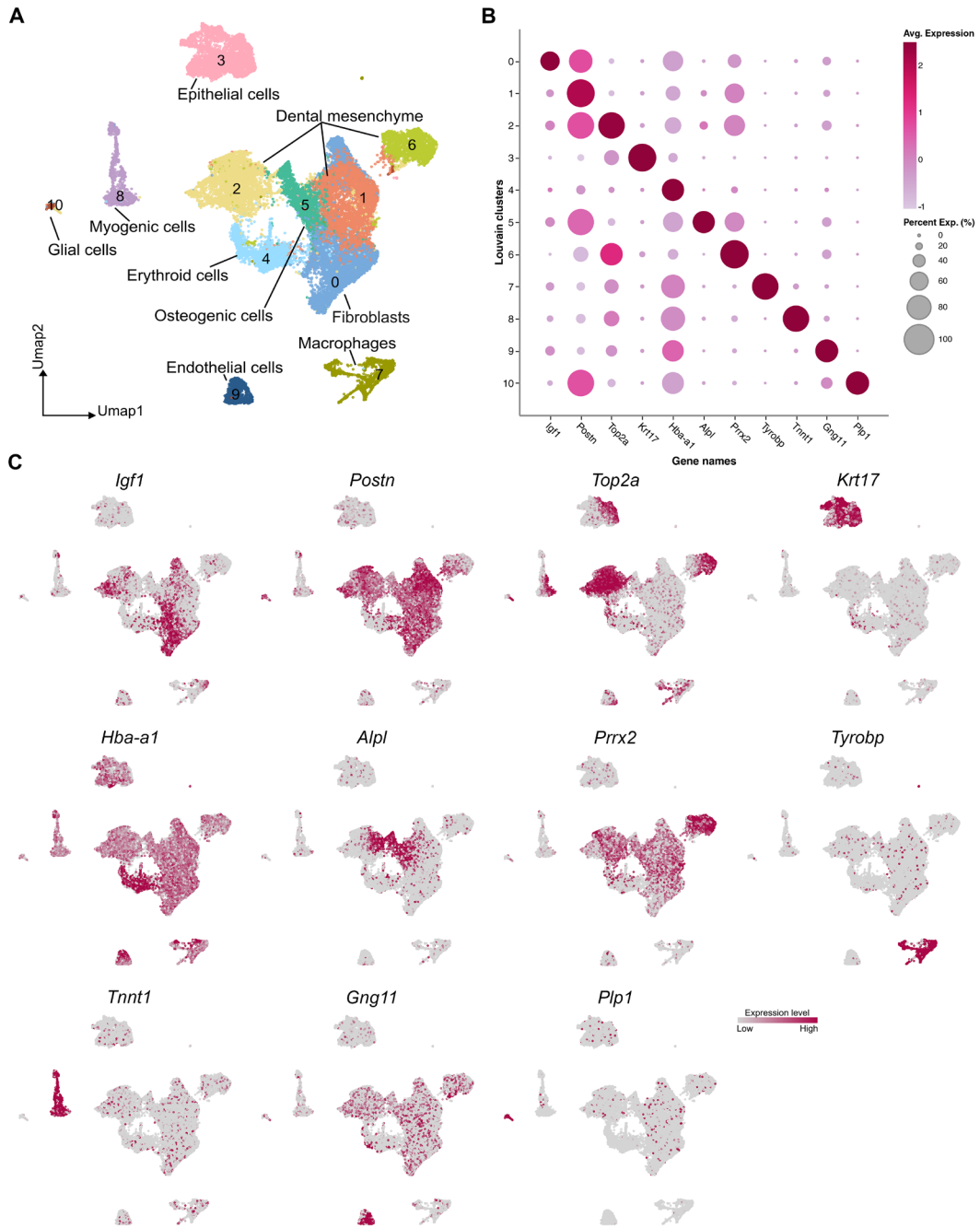


**Figure 3. Single-cell RNA sequencing of developing molars at embryonic day (E)14.5 mouse embryos.**

(A) Uniform Manifold Approximation and Projection (UMAP) visualization of cell populations identified through unbiased cluster analysis of E14.5 embryonic mouse molar tooth germs. Clusters are labeled based on the expression of canonical marker genes

colored by clusters 0–10 (Fig. 4). **(B)** UMAP visualization of cells, showing *Notum* expression with other known enamel knots (EK) markers (*Fgf4*, *Shh*, *Lef1*, and *Bmp4*). *Notum* expression is notable in both epithelial and mesenchyme cell clusters. The epithelial cells expressing *Notum* colocalize with the cells expressing *Shh*, *Fgf4*, *Bmp4*, and *Lef1* (black arrow), indicating the primary enamel knot (pEK). The mesenchymal cells expressing *Notum* (white arrow) also express *Lef1* and *Bmp4*.

E14.5 Mouse molar



D

E14.5 molar

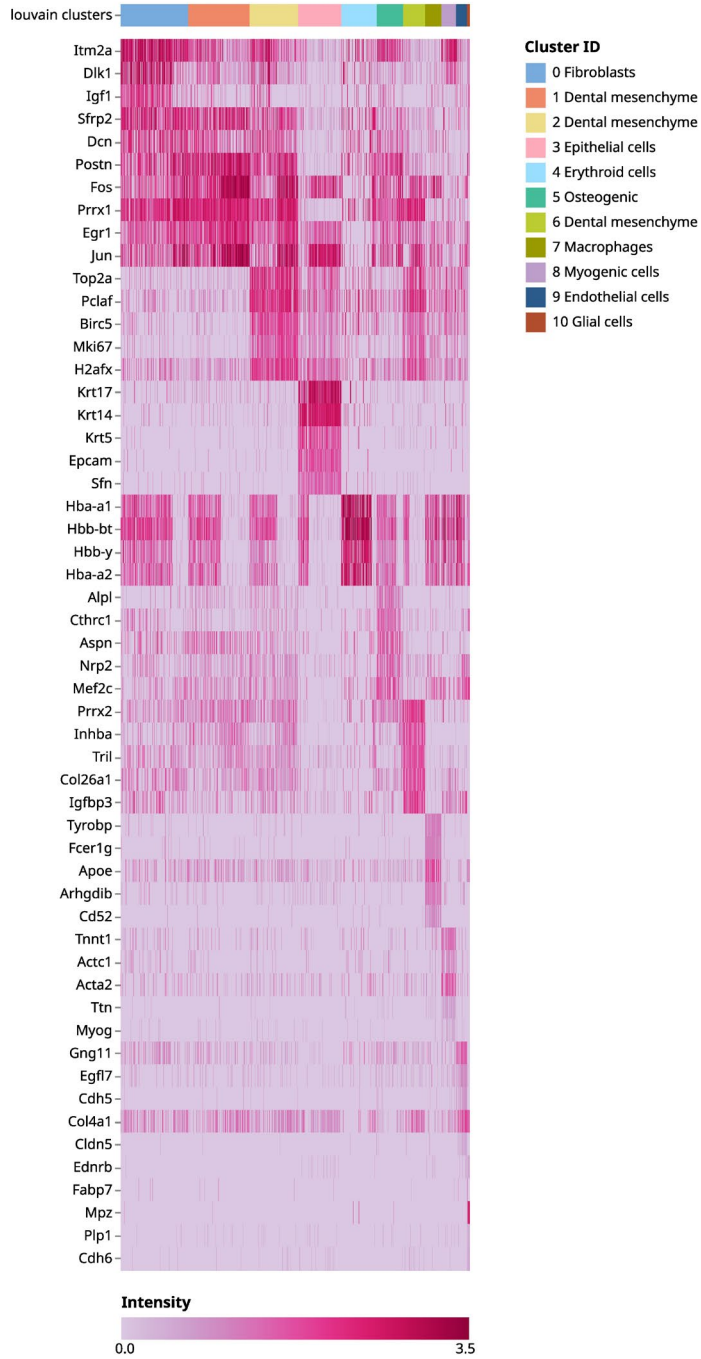


**Figure 4. Cell clusters and list of marker genes attributed to the cell clusters in developing mouse molars at E14.5.**

(A) An annotated cell cluster UMAP plot showing the cell types in the molar tooth germs at E14.5. (B) Dot plot indicating the scaled expression of differentially expressed genes (cluster markers) in the cell clusters shown in A. (C) UMAP feature plots of differentially expressed genes in dot plot B. (D) Heatmap showing the top 5 differentially expressed genes between the Louvain cell clusters in developing mouse molars at E14.5.

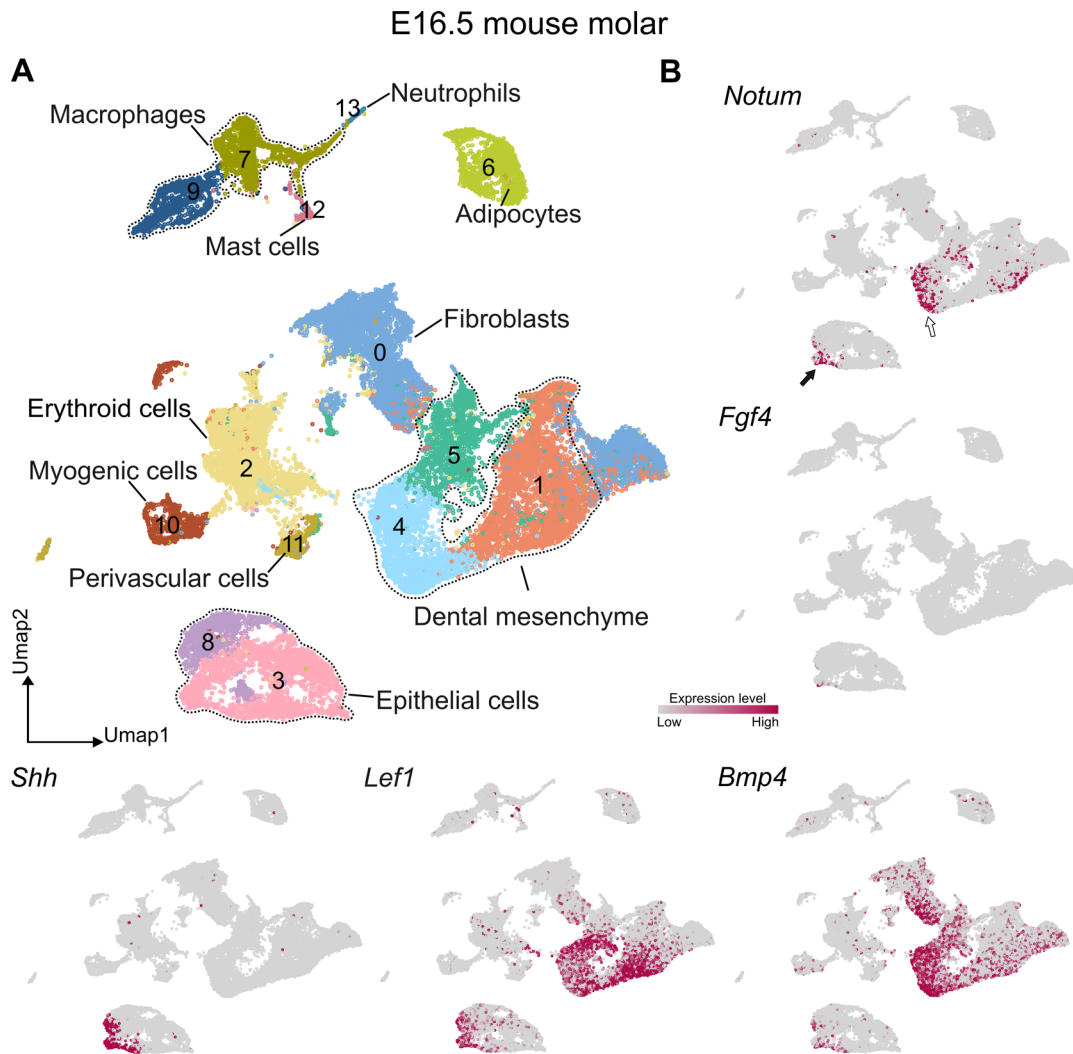
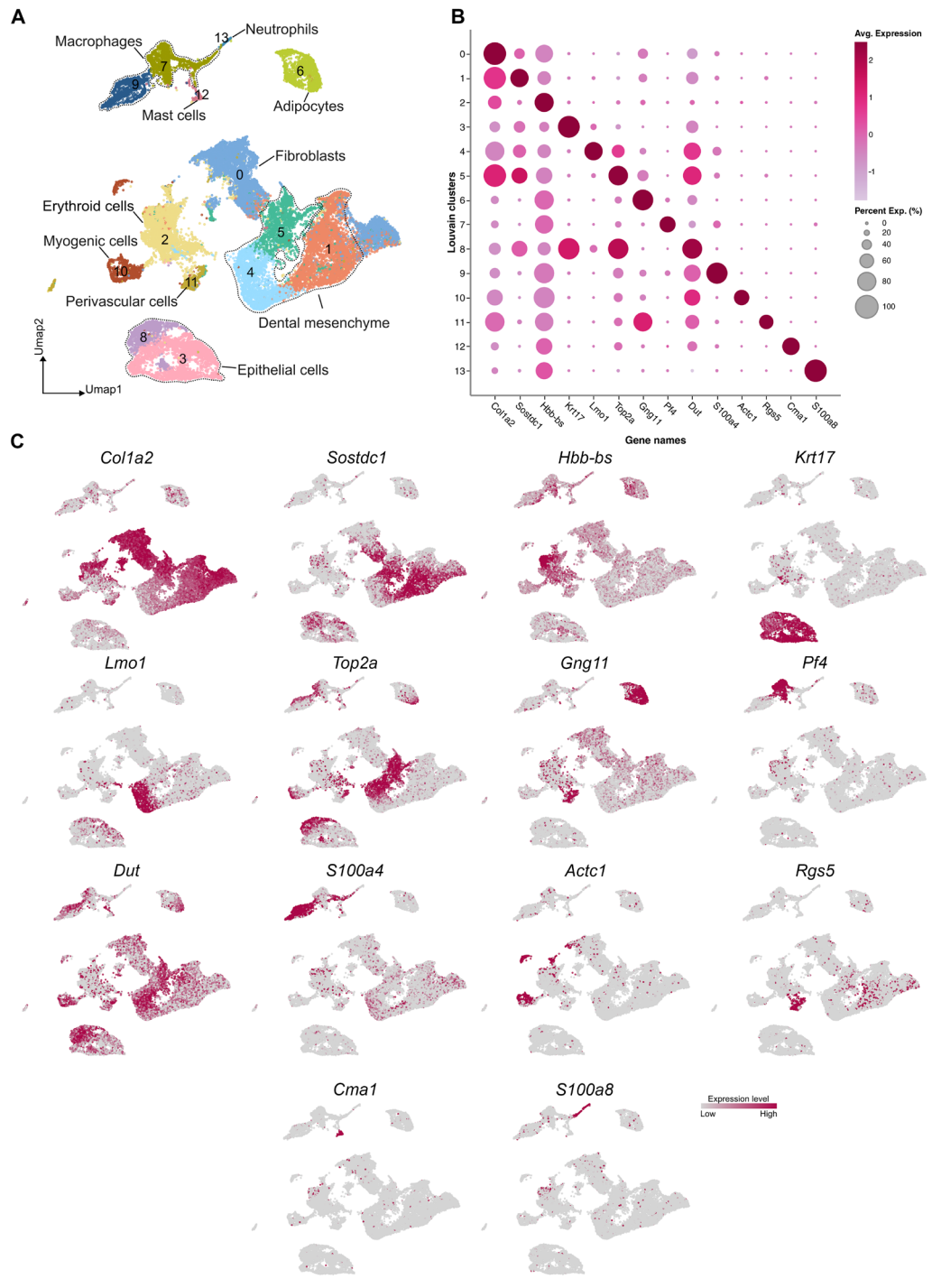


**Figure 5. Single-cell RNA sequencing of developing molars at E16.5 mouse embryos.**

(A) UMAP visualization of cell populations identified through unbiased cluster analysis of E16.5 embryonic mouse molar tooth germs. Clusters are labeled based on the expression

of canonical marker genes colored by clusters 0–13 (Fig. 6). **(B)** UMAP visualization of cells, showing *Notum* expression with other known enamel knots (EK) marker genes (*Fgf4*, *Shh*, *Lef1*, and *Bmp4*). *Notum* expression is evident in both epithelial and mesenchyme cell clusters. The epithelial cells expressing *Notum* colocalize with the cells expressing *Shh*, *Fgf4*, *Bmp4*, and *Lef1* (black arrow), indicating the secondary enamel knot (sEK). The mesenchymal cells expressing *Notum* (white arrow) also express *Lef1* and *Bmp4*.

E16.5 Mouse Molar



D

E16.5 Molar



**Figure 6. Cell clusters and list of marker genes attributed to the cell clusters in developing mouse molars at E16.5.**

(A) An annotated cell cluster UMAP plot showing the cell types in the molar tooth germs at E16.5. (B) Dot plot indicating the scaled expression of differentially expressed genes (cluster markers) in the cell clusters shown in A. (C) UMAP feature plots of differentially expressed genes in dot plot B. (D) Heatmap showing the top 5 differentially expressed genes between the Louvain cell clusters in developing mouse molars at E16.5.

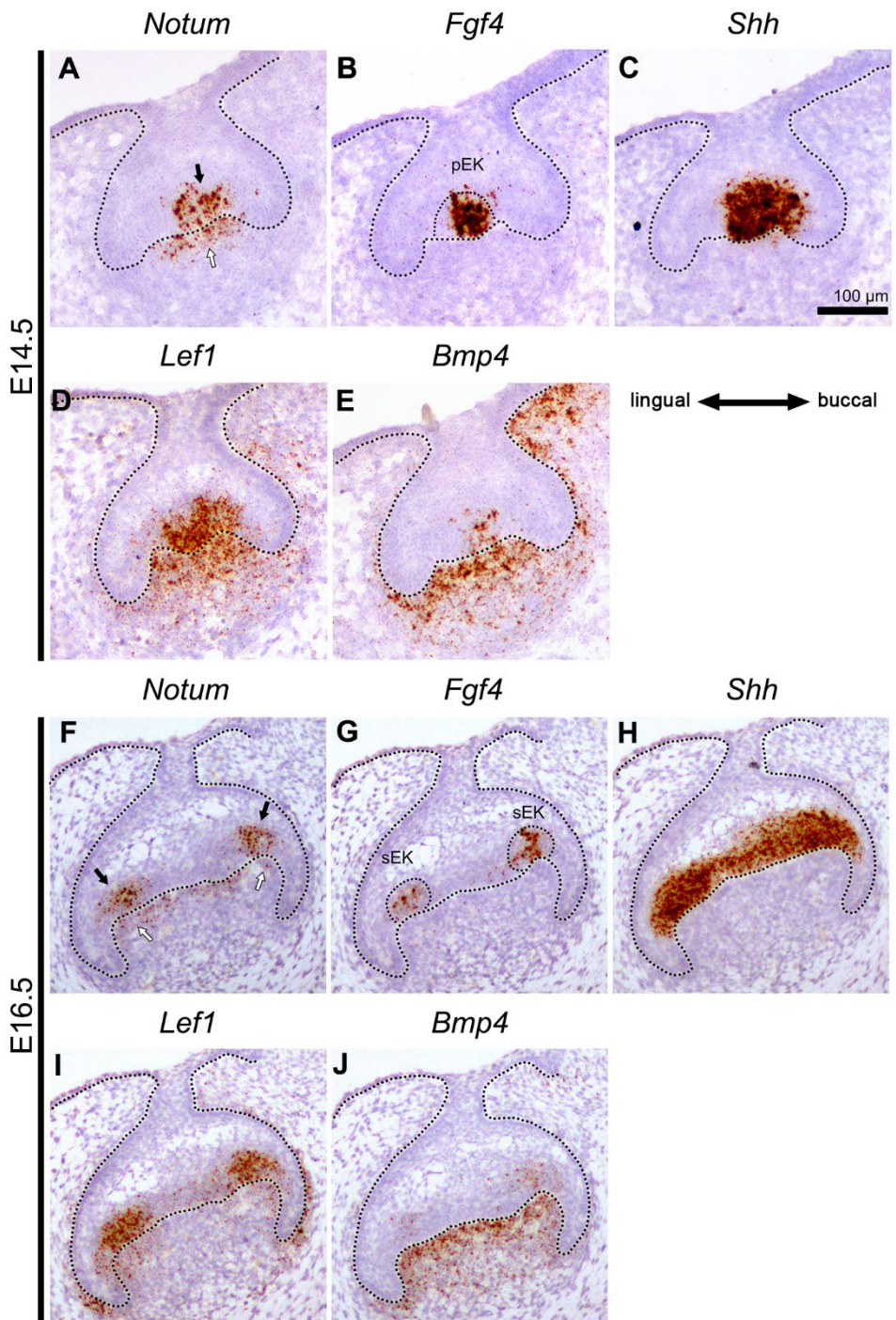


**Figure 7. Expression pattern of *Notum* in developing molars at E14.5 and E16.5 mouse embryos.**

(A–E) In the frontal sections of mandibular molars at E14.5 (cap stage), *Notum* is expressed in the primary EK (pEK) (white arrow) and in the thin outer layer of the dental papilla (black arrow). *Shh* and *Fgf4* expression is observed at the primary EK cells. *Lef1* and *Bmp4* expression is evident in the primary EK and dental papilla. (F–J) In the frontal sections of mandibular molars E16.5 (bell stage), *Notum* is expressed in the secondary EK (sEK) (white arrows) and in the thin outer layer of the dental papilla (black arrows). *Fgf4* expression is observed in the secondary EKs at E16.5. *Shh* is expressed in the inner dental epithelium at E16.5. *Lef1* and *Bmp4* are expressed in the secondary EKs and dental papilla: scale bar, 100  $\mu$ m.

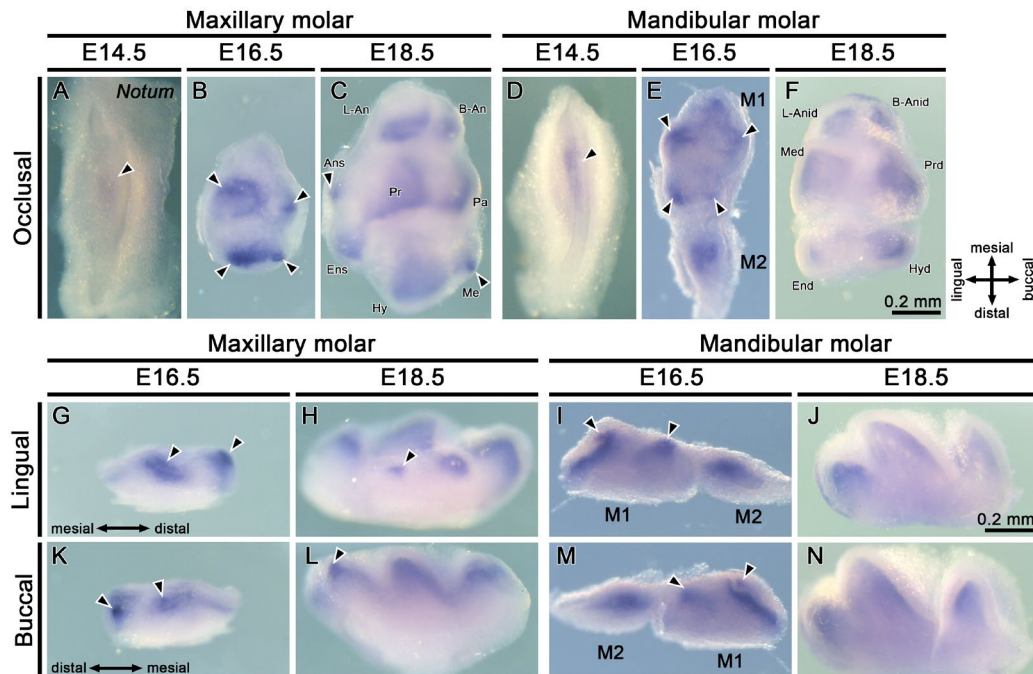


**Figure 8. *Notum* expression in developing molars in the maxilla and mandible.**

(A–F) *Notum* expression (arrowheads) in developing molars from an occlusal view. *Notum* expression is initially found in the center of the mandibular and maxillary M1 at E14.5 and later on in the cusps at E16.5 and E18.5. (G–N) Expression of *Notum* in molars from the lingual and buccal views. At E16.5, the *Notum* expression in epithelium (arrowheads) is found in the majority of M1 cusps. However, at E18.5, this *Notum* expression in the epithelium is limited to a few cusps that formed relatively late. *Notum* expression in the mesenchyme is present in the outer layer of the dental papilla at both E16.5 and E18.5.

## 2. *Notum*<sup>-/-</sup> mice showed abnormalities in tooth crown and root morphology

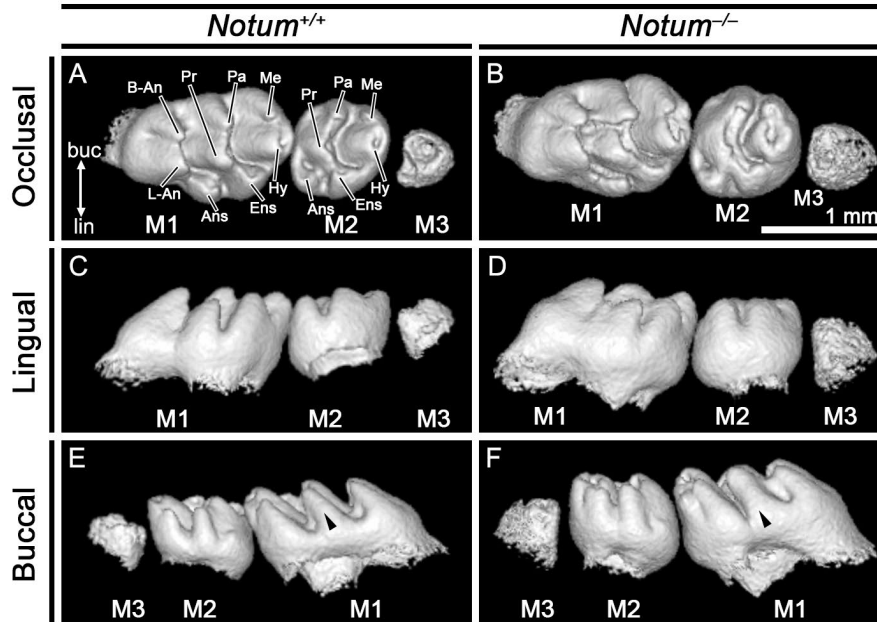
To study the role of *Notum* in tooth morphology, morphological changes in the crown and root in molars were examined at PN14 before the occlusal attrition. Notably, *Notum*<sup>-/-</sup> mice showed broader tips in the majority of the cusps of both mandibular and maxillary M1 and second molar (M2) (Fig. 9A–L, Fig. 10A–X, Fig. 14A–B). However, there were no notable changes in the cusp base dimension in *Notum*<sup>-/-</sup> mice. In *Notum*<sup>-/-</sup> mice, half of the maxillary M1s exhibited a fusion between the anterostyle and enterostyle (Fig. 10H–L), and many of the mandibular M1s displayed fusion among lingual anteroconid, buccal anteroconid, and protoconid (Fig. 10R–X). The cusp tip area was significantly increased in all other maxillary M1 cusps except the buccal anterocone, metacone, and anterostyle. In the mandible M1, all other cusps except the buccal anteroconid showed a significant increase in the cusp area (Fig. 14A–B).

*Notum*<sup>-/-</sup> mice molars showed an altered root pattern at PN35. In line with a previous study by Vogel et al. (2016), *Notum*<sup>-/-</sup> mice exhibited significantly shorter roots and severe occlusal wear in their molars compared to the *Notum*<sup>+/+</sup> mice (Fig. 11A–H). Whereas the past study described the root pattern of *Notum*<sup>-/-</sup> mice as irregular, the findings of this study indicated fusion in the roots of both the maxillary and mandibular molars of *Notum*<sup>-/-</sup> mice (Fig. 12A–H, Fig. 13A–D). No fusion between the individual molars was detected in

*Notum*<sup>-/-</sup> mice in both the maxilla and mandible. Additionally, no morphological changes were spotted between *Notum*<sup>+/-</sup> and *Notum*<sup>+/+</sup> mice molars.

Root fusion was observed in *Notum*<sup>-/-</sup> mice across all molars (n = 12). In maxillary M1, instances of fusions included partial dentin fusion (incidence = 8.33%), complete dentin fusion (16.67%), distal root pulp fusion (33.33%), mesial root pulp fusion (8.33%), and complete pulp fusion (33.33%). In mandibular M1, similar results were noted with incidences of partial dentin fusion (66.67%) and complete pulp fusion (33.33%). Interestingly, every second molar (M2) showed complete pulp fusion (Fig. 15).

PN14 Maxillary molars



PN14 Mandibular molars

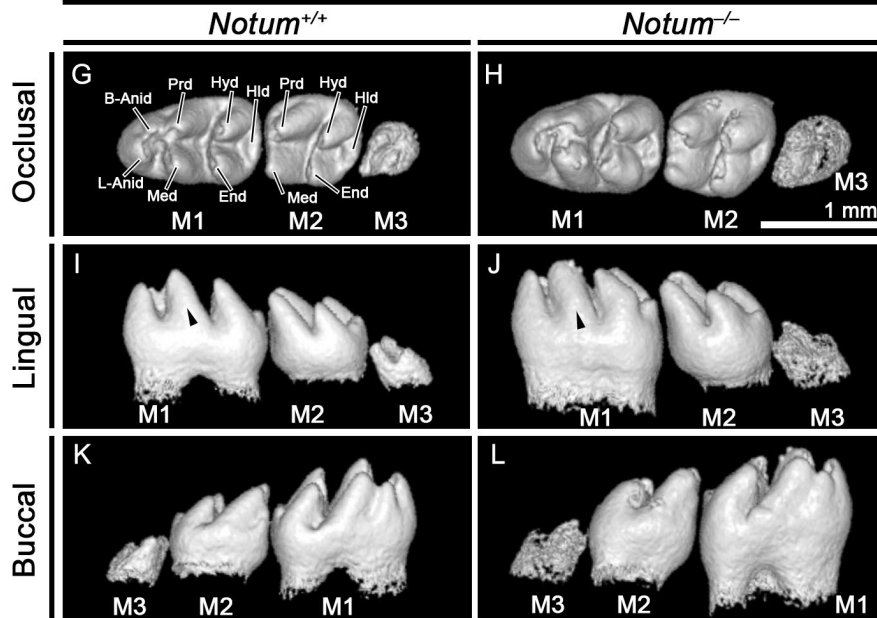


**Figure 9. Morphological changes in crown and root of maxillary and mandibular molars in *Notum*<sup>-/-</sup> mice at postnatal day (PN) 14.**

(A-L) At PN14, the first molar (M1), second molar (M2), and third molar (M3) of *Notum*<sup>-/-</sup> mice appear relatively larger compared to *Notum*<sup>+/+</sup> mice. *Notum*<sup>-/-</sup> showed broader cusp tips in molars, which is noted in both occlusal view and lateral views, especially in the paracone of maxillary M1 (arrowheads in E and F) and metaconid in mandibular M1 (arrowheads in I and J). L-An: lingual anterocone, B-An: buccal anterocone, Pa: paracone, Me: metacone, Hy: hypocone, Ens: enterostyle, Ans: anterostyle, Pr: protocone, L-Anid: lingual anteroconid, B-Anid: buccal anteroconid, Prd: protoconid, Hyd: hypoconid, Hld: hypoconulid. End: entoconid, Med: metaconid.

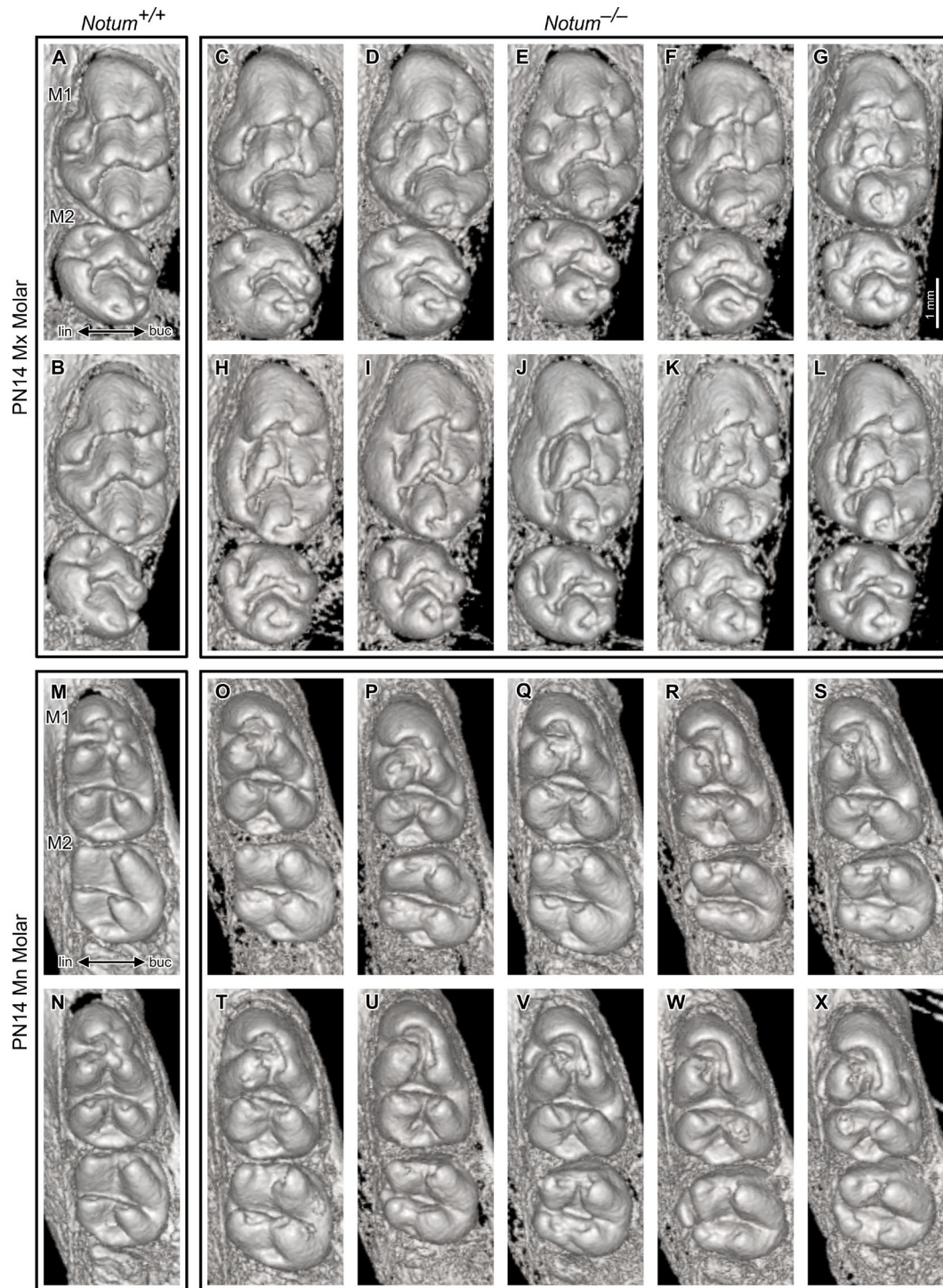


**Figure 10. Variations in the crown morphology of maxillary and mandibular molars in *Notum*<sup>-/-</sup> mice at PN 14.**

(A–B) Occlusal view showing the maxillary 3D-reconstructed molars of *Notum*<sup>+/+</sup> mice. (C–L) Occlusal view of maxillary molars in *Notum*<sup>-/-</sup> mice. *Notum*<sup>-/-</sup> M1 molars display broader cusp tips compared to the *Notum*<sup>+/+</sup> mice. (M–N) Occlusal view of mandibular molars in *Notum*<sup>+/+</sup> mice. (O–X) Occlusal view of maxillary molars in *Notum*<sup>-/-</sup> mice. *Notum*<sup>-/-</sup> mice exhibited a fusion between the anterostyle and enterostyle in maxillary M1 molars (H–L) and the fusion across the lingual anteroconid, buccal anteroconid, and protoconid in the majority of the mandibular M1s (R–X).

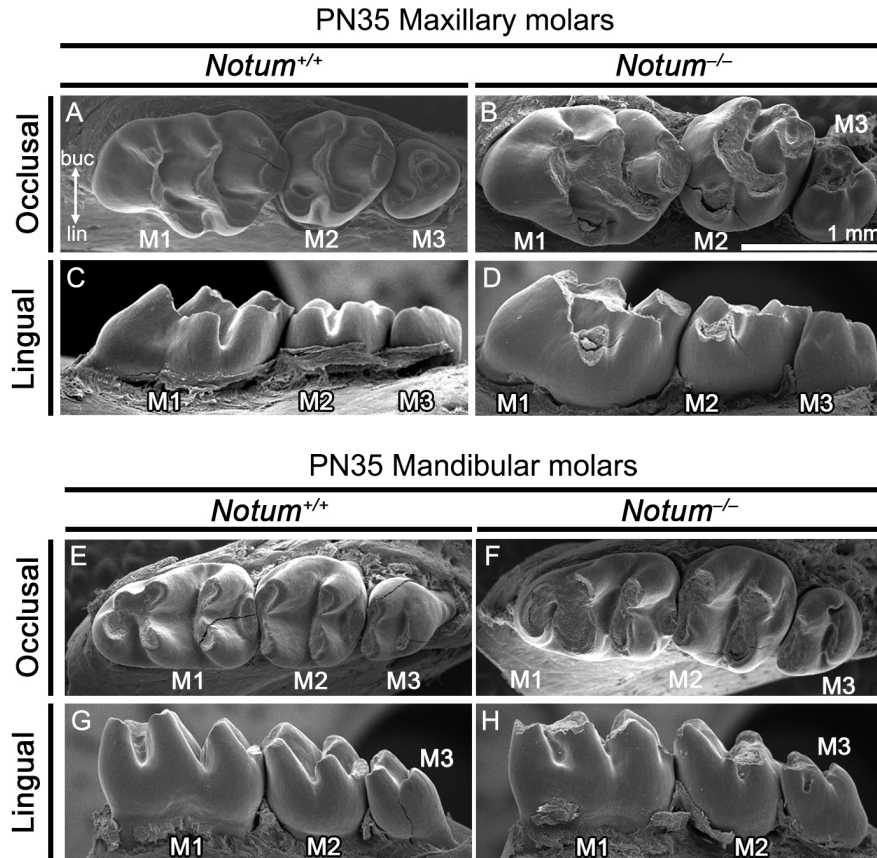


**Figure 11. Morphological changes in tooth crown of maxillary and mandibular molars in *Notum*<sup>-/-</sup> mice at PN 35.**

(A–H) Scanning electron microscopy (SEM) images showing the maxillary and molars of *Notum*<sup>+/+</sup> and *Notum*<sup>-/-</sup> mice. At PN35, the changes in the crown outline and size persist, while *Notum*<sup>-/-</sup> molars show severe attrition compared to the *Notum*<sup>+/+</sup> mice.

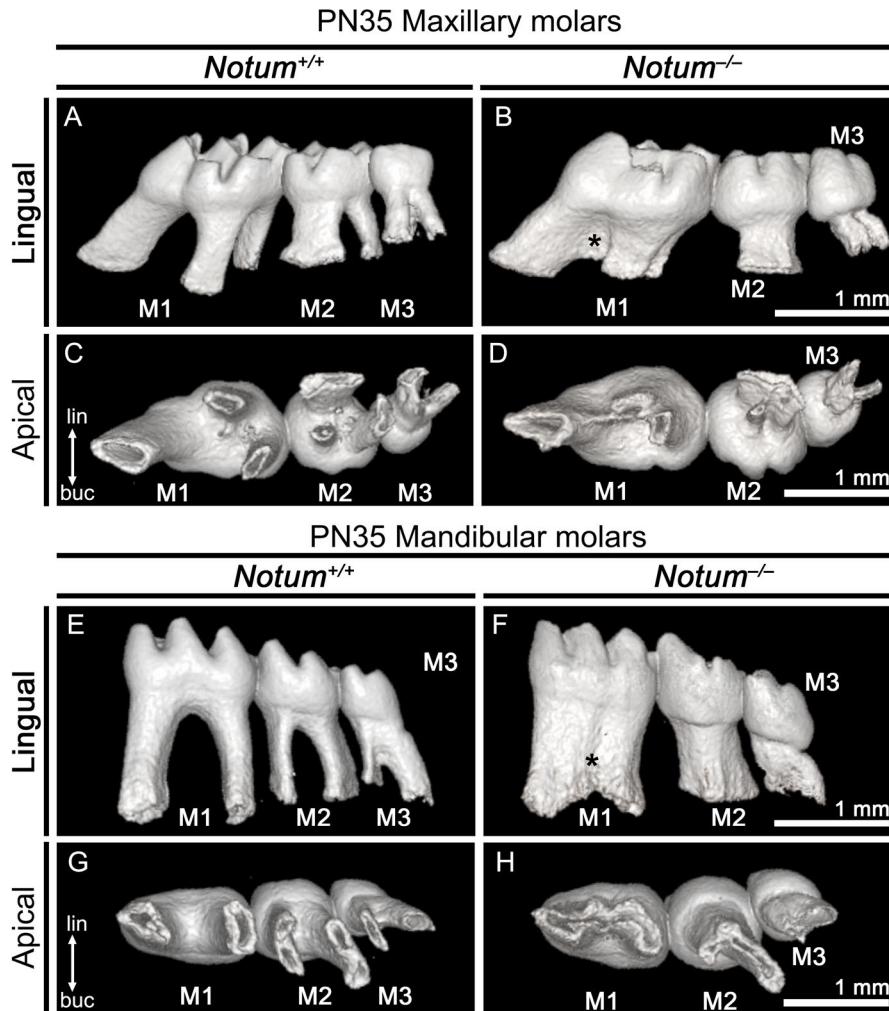


**Figure 12. Root fusion in *Notum*<sup>-/-</sup> mice at PN 35.**

(A–H) 3D-reconstructed molars show root fusion in maxillary and mandibular M1 of *Notum*<sup>-/-</sup> mice in lingual and apical views. The fusion between the molars is marked with an asterisk in the lingual view.

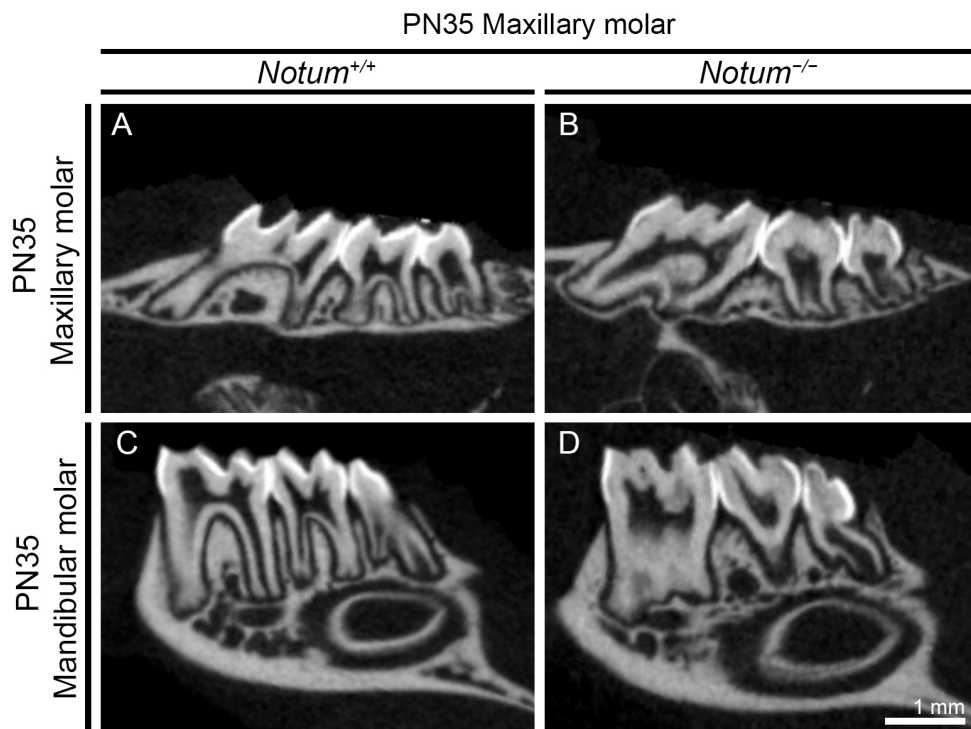


**Figure 13. Appearance of maxillary and mandibular molars in micro-CT sections.**

(A–D) The maxillary and mandibular molars of PN35 *Notum*<sup>+/+</sup> and *Notum*<sup>-/-</sup> mice. The sagittal sections exhibit the fusion of the maxillary and the mandibular M1 and M2 roots in *Notum*<sup>-/-</sup> compared to the *Notum*<sup>+/+</sup> mice. The enamel appears in a bright white color with similar intensity and thickness in both *Notum*<sup>+/+</sup> and *Notum*<sup>-/-</sup> molars. *Notum*<sup>-/-</sup> molars exhibit severe attrition, leading to the absence of enamel on the occlusal surface.

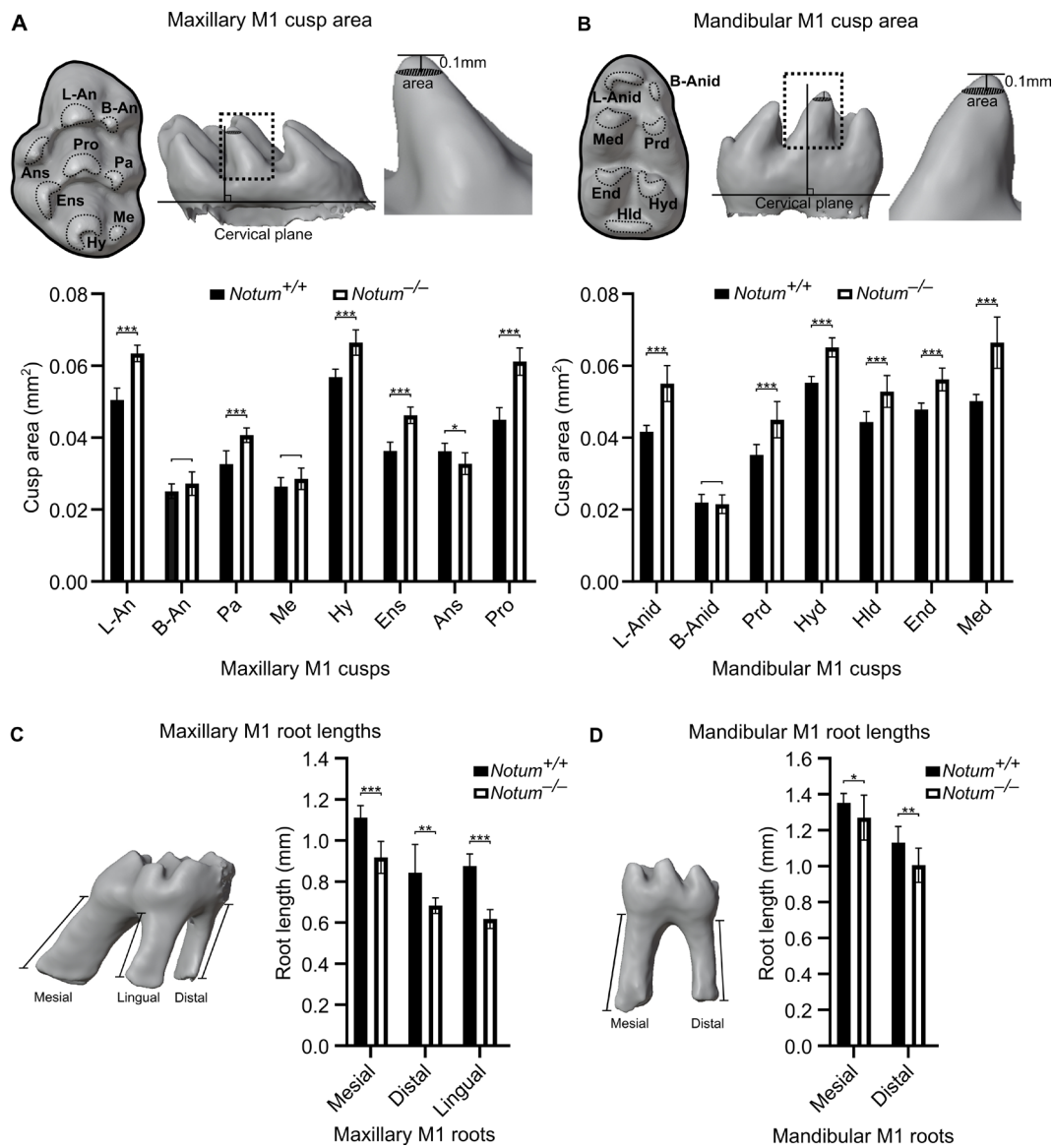


**Figure 14. Alterations in the cusp tip area and root lengths in *Notum*<sup>-/-</sup> M1 molars.**

(A–B) *Notum*<sup>-/-</sup> mice exhibit significantly larger cusp tip areas in most of the maxillary M1 cusps except the buccal anterocone, metacone, and anterostyle and in the mandibular

M1 cusps except the buccal anteroconid (n = 10 per group). **(C–D)** *Notum*<sup>-/-</sup> mice molar roots are significantly shorter in maxillary and mandibular M1 compared to the *Notum*<sup>-/-</sup> mice (n = 10 per group). L-An: lingual anterocone, B-An: buccal anterocone, Pa: paracone, Me: metacone, Hy: hypocone, Ens: enterostyle, Ans: anterostyle, Pr: protocone, L-Anid: lingual anteroconid, B-Anid: buccal anteroconid, Prd: protoconid, Hyd: hypoconid, Hld: hypoconulid. End:entoconid, Med: metaconid. (Mann Whitney U test, \*P < 0.05, \*\*P < 0.01, and \*\*\*P < 0.001.)

Root pattern	Maxillary M1						
	<i>Notum</i> <sup>+/+</sup>	<i>Notum</i> <sup>-/-</sup>					
		Partial dentin fusion	Complete dentin fusion	Distal root pulp fusion	Mesial root pulp fusion	Complete pulp fusion	
							
Number of teeth (n = 12)		1 (8.33%)	2 (16.67%)	4 (33.33%)	1 (8.33%)	4 (33.33%)	
Root pattern	Mandibular M1			Maxillary M2		Mandibular M2	
	<i>Notum</i> <sup>+/+</sup>	<i>Notum</i> <sup>-/-</sup>		<i>Notum</i> <sup>+/+</sup>	<i>Notum</i> <sup>-/-</sup>	<i>Notum</i> <sup>+/+</sup>	<i>Notum</i> <sup>-/-</sup>
		Partial dentin fusion	Complete pulp fusion		Complete pulp fusion		Complete pulp fusion
							
Number of teeth (n = 12)		8 (66.67%)	4 (33.33%)		12 (100.00%)		12 (100.00%)

**Figure 15. Variations in root fusion in *Notum*<sup>-/-</sup> maxillary and mandibular molars.**

*Notum*<sup>-/-</sup> mice exhibit root fusion across all molars, the severity of fusion ranging from partial dentin fusion to complete pulp fusion.

### 3. The size of the secondary enamel knots was notably enlarged in *Notum*<sup>-/-</sup> mice

To analyze the molecular function of *Notum* in tooth development, RNA sequencing analyses were performed on mouse molars at E14.5 and E16.5. In E14.5 and E16.5 molars, respectively, 131 and 424 genes were found to have expression level changes over two-fold (Table 1–4). The levels of *Fgf20* and *Dkk4*, which are known to be specific to EK, were notably elevated in *Notum*<sup>-/-</sup> molars at E16.5. *Fgf20* and *Dkk4* ranked as the second and sixteenth, respectively, in the list of upregulated genes (Table 1, Fig. 16). Moreover, the *Fgf4* expression level was slightly elevated in *Notum*<sup>-/-</sup> molars at both E14.5 and E16.5. *Dkk4*, *Fgf4*, and *Fgf20* are identified as the target genes of the Wnt/ $\beta$ -catenin signaling pathway. The expression levels of *Lef1*, *Axin2*, and *Bmp4*, other Wnt signaling pathway target genes expressed in both enamel knots and dental papilla, were not changed significantly in *Notum*<sup>-/-</sup> molars (Fig. 16).

To demonstrate the size and patterning of secondary EKs in *Notum*<sup>-/-</sup> mice, the expression pattern of *Fgf4*, a well-known marker for both primary and secondary EKs, was investigated with RNA in situ hybridization. At E14.5, *Notum*<sup>-/-</sup> mice displayed a primary EK in each maxillary M1, which was similar to the *Notum*<sup>+/+</sup> mice (Fig. 17A–D). At E16.5, *Notum*<sup>-/-</sup> mice showed larger secondary EKs, especially the protocone and hypocone in M1 molars, compared to the *Notum*<sup>+/+</sup> mice (Fig. 17E–F). Consequently, at E17.5 and E18.5, a considerable increase in most of the secondary EK size was detected in *Notum*<sup>-/-</sup>

mice, mainly in lingual anterocone and hypocone within M1 (Fig. 17I–J, M–N). In mandibular M1, a notable enlargement of secondary EK, particularly in protoconid and metaconid at E16.5, and lingual anteroconid, hypoconid, and entoconid at E17.5 and E18.5 was observed in *Notum*<sup>-/-</sup> mice (Fig. 17G–H, K–L, O–P). The enlargement in secondary EK size appears closely related to the concurrent increase in cusp tips dimensions of *Notum*<sup>-/-</sup> molars (Fig. 9A–L, Fig. 14 A–B). The Maxillary M1 secondary EK emergence time varies between *Notum*<sup>+/+</sup> and *Notum*<sup>-/-</sup> mice. Enterostyle was first observed at E17.5 in *Notum*<sup>+/+</sup> M1 (Fig. 17I), but was delayed until E18.5 in *Notum*<sup>-/-</sup> M1 (Fig. 17J, N). Likewise, anterostyle first appears at E18.5 in *Notum*<sup>+/+</sup> M1 but was not present until E18.5 in *Notum*<sup>-/-</sup> M1 (Fig. 17M–N).

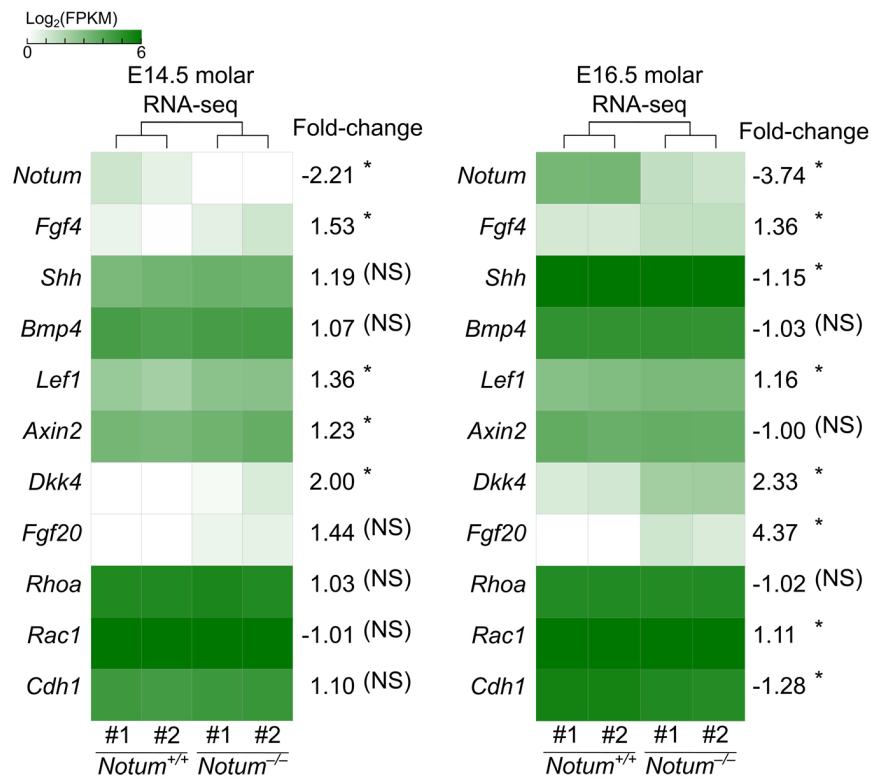


**Figure 16. Heatmaps displaying the alterations in the expression level of selected genes in RNA-sequencing analysis of the E14.5 and E16.5 molars of *Notum*<sup>+/+</sup> and *Notum*<sup>-/-</sup> mice.**

*Notum* is significantly downregulated in *Notum*<sup>-/-</sup> mice, while *Dkk4* and *Fgf20* are significantly upregulated at E16.5. *Fgf4* and *Lef1* show slight upregulation at both E14.5 and E16.5. Cell adhesion-related genes *Rac1* and *Cdh1* exhibit slight upregulation and downregulation, respectively, at E16.5. \* P < 0.05, NS: non-significant.

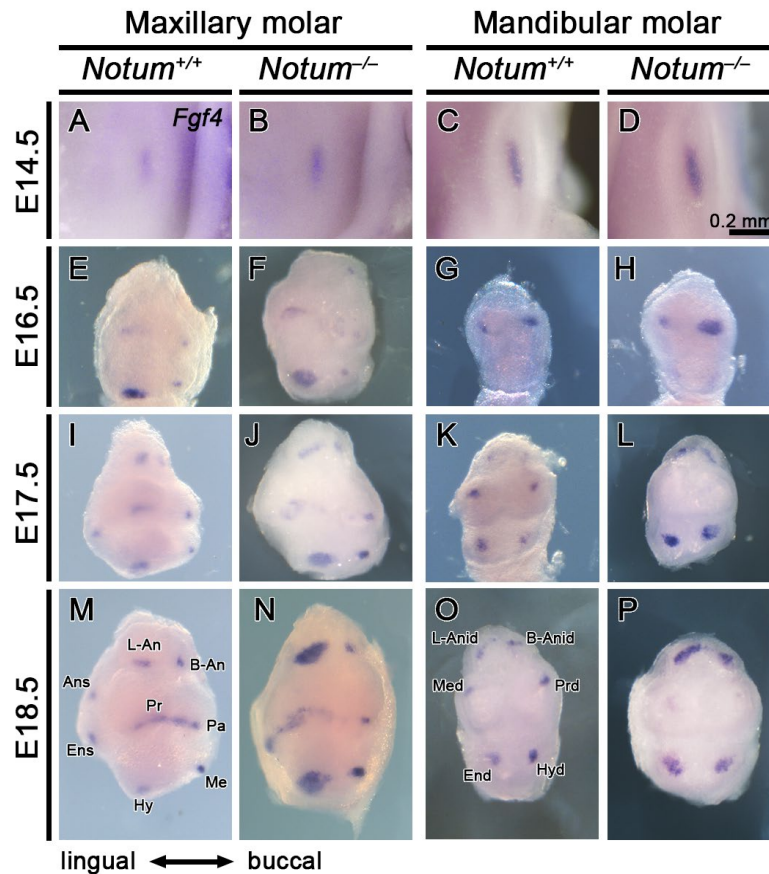


**Figure 17. Expression of *Fgf4* in developing maxillary M1 and mandibular M1.**

(A–N) *Fgf4* expression is located in the primary EK of maxillary and mandibular M1 at E14.5 and in secondary EKs at E16.5 to E18.5. At E16.5, E17.5, and E18.5, maxillary and mandibular M1s exhibit enlarged secondary EKs expressing *Fgf4* in *Notum*<sup>-/-</sup> mice compared to *Notum*<sup>+/+</sup> mice. L-An: lingual anterocone, B-An: buccal anterocone, Pa: paracone, Me: metacone, Hy: hypocone, Ens: enterostyle, Ans: anterostyle, Pr: protocone, L-Anid: lingual anteroconid, B-Anid: buccal anteroconid, Prd: protoconid, Hyd: hypoconid, Hld: hypoconulid. End: entoconid, Med: metaconid.

**Table 1.** The top 50 genes that upregulated in molars of *Notum*<sup>-/-</sup> mice compared to *Notum*<sup>+/+</sup> mice at E14.5 (fold change > 2, FPKM > 0.3)

Gene name	Gene description	P value	Fold change
<i>Krt13</i>	keratin 13	1.6731E-196	8.472408724
<i>Tpsb2</i>	trypsin beta 2	8.54034E-08	6.862759807
<i>Mmp13</i>	matrix metalloproteinase 13	2.75126E-16	6.530235624
<i>Krt4</i>	keratin 4	3.30006E-71	5.759029893
<i>Cav3</i>	caveolin 3	1.73517E-10	4.868339895
<i>Ly6d</i>	lymphocyte antigen 6 complex, locus D	2.46197E-12	4.561926433
<i>Cyp2f2</i>	cytochrome P450, family 2, subfamily f, polypeptide 2	1.12626E-10	4.296644118
<i>Cyp2t4</i>	cytochrome P450, family 2, subfamily t, polypeptide 4	4.24759E-08	4.167150112
<i>Cma1</i>	chymase 1, mast cell	1.31986E-13	3.810918215
<i>Ckm</i>	creatine kinase, muscle	8.02863E-13	3.809788332
<i>Sprr1a</i>	small proline-rich protein 1A	0.013552525	3.682952995
<i>Ngp</i>	neutrophilic granule protein	0.000257532	3.634824115
<i>Stfa2</i>	stefin A2	0.028697929	3.591219906
<i>Atp1b4</i>	ATPase, (Na <sup>+</sup> )/K <sup>+</sup> transporting, beta 4 polypeptide	2.3677E-14	3.553799041
<i>Smpx</i>	small muscle protein, X-linked	6.60277E-06	3.544493618
<i>Tnnt3</i>	troponin T3, skeletal, fast	1.28332E-18	3.533313363
<i>Hspb2</i>	heat shock protein 2	0.003232214	3.406613524
<i>Coro6</i>	coronin 6	1.63957E-05	3.288319163
<i>Mypn</i>	myopalladin	8.28225E-09	3.092999296
<i>Hdc</i>	histidine decarboxylase	3.7147E-08	3.068094229
<i>Ldb3</i>	LIM domain binding 3	8.02393E-23	2.983968723
<i>Tmem182</i>	transmembrane protein 182	0.000210177	2.900610777
<i>Sh3bgr</i>	SH3-binding domain glutamic acid-rich protein	0.002015265	2.897293432
<i>Cox6a2</i>	cytochrome c oxidase subunit 6A2	0.000210538	2.859188116
<i>Lmod3</i>	leiomodin 3 (fetal)	7.38224E-07	2.854652347
<i>S100a9</i>	S100 calcium binding protein A9 (calgranulin B)	3.0686E-05	2.822510872
<i>Dhrs7c</i>	dehydrogenase/reductase (SDR family) member 7C	0.010093723	2.798812036
<i>Cacng6</i>	calcium channel, voltage-dependent, gamma	0.00147539	2.788687603

	subunit 6		
<i>Calml3</i>	calmodulin-like 3	1.48179E-05	2.7212056
<i>Vwde</i>	von Willebrand factor D and EGF domains	7.84061E-08	2.709865461
<i>Casq2</i>	calsequestrin 2	1.26144E-18	2.683233703
<i>Acta1</i>	actin, alpha 1, skeletal muscle	2.23828E-61	2.674285926
<i>Vgll2</i>	vestigial like family member 2	8.58412E-09	2.666943116
<i>Cacng1</i>	calcium channel, voltage-dependent, gamma subunit 1	0.00394124	2.640780085
<i>Tnni2</i>	troponin I, skeletal, fast 2	4.98489E-07	2.634856831
<i>Ccl11</i>	chemokine (C-C motif) ligand 11	0.040551527	2.633279088
<i>Caana1s</i>	calcium channel, voltage-dependent, L type, alpha 1S subunit	9.80383E-08	2.596296865
<i>Myot</i>	myotilin	5.32683E-07	2.589819769
<i>Mybpc1</i>	myosin binding protein C, slow-type	3.56055E-25	2.588082671
<i>Tceal7</i>	transcription elongation factor A (SII)-like 7	2.10282E-11	2.581518632
<i>Myoz2</i>	myozenin 2	5.94744E-05	2.576291734
<i>Tigd4</i>	tigger transposable element derived 4	0.001540891	2.576152854
<i>Trim55</i>	tripartite motif-containing 55	2.29574E-09	2.569595539
<i>Mylpf</i>	myosin light chain, phosphorylatable, fast skeletal muscle	1.14324E-31	2.545394725
<i>Chrng</i>	cholinergic receptor, nicotinic, gamma polypeptide	2.66428E-10	2.519904464
<i>Myh8</i>	myosin, heavy polypeptide 8, skeletal muscle, perinatal	3.71311E-27	2.509829235
<i>Sgca</i>	sarcoglycan, alpha (dystrophin-associated glycoprotein)	0.000633746	2.495104807
<i>Tnnt2</i>	troponin T2, cardiac	1.58098E-18	2.494283998
<i>Fitm1</i>	fat storage-inducing transmembrane protein 1	0.009040807	2.490344662
<i>Cpa3</i>	carboxypeptidase A3, mast cell	2.08137E-10	2.418955725

**Table 2.** The genes that are downregulated in molars of *Notum*<sup>-/-</sup> mice compared to *Notum*<sup>+/+</sup> mice at E14.5 (fold change > 2, FPKM > 0.3)

Gene name	Gene description	P value	Fold change
<i>Sst</i>	somatostatin	0.005212	-6.50524747
<i>Prdm12</i>	PR domain containing 12	0.00707	-5.96851805
<i>Alx3</i>	aristaless-like homeobox 3	3.13E-07	-5.72628632
<i>Hand2</i>	heart and neural crest derivatives expressed 2	3.63E-14	-5.21463018
<i>Tinag</i>	tubulointerstitial nephritis antigen	0.021886	-4.95707814
<i>Sost</i>	sclerostin	0.002211	-4.86456741
<i>Alx1</i>	ALX homeobox 1	3.56E-21	-4.72369957
<i>Capn11</i>	calpain 11	2.08E-07	-4.51354410
<i>Cpne6</i>	copine VI	0.003385	-4.23600858
<i>Pax3</i>	paired box 3	1.96E-07	-3.69784715
<i>Npy1r</i>	neuropeptide Y receptor Y1	0.004502	-2.75407373
<i>Cntn2</i>	contactin 2	4.44E-06	-2.58152529
<i>Isl2</i>	insulin related protein 2 (islet 2)	0.027131	-2.41925863
<i>Notum</i>	notum palmitoleoyl-protein carboxylesterase	0.000756	-2.21190188
<i>Snrpf</i>	small nuclear ribonucleoprotein polypeptide F	5.01E-06	-2.14008280
<i>P2rx3</i>	purinergic receptor P2X, ligand-gated ion channel, 3	0.034761	-2.06319196
<i>Ntrk1</i>	neurotrophic tyrosine kinase, receptor, type 1	0.001093	-2.03138351

**Table 3.** The genes that are upregulated in molars of *Notum*<sup>-/-</sup> mice compared to *Notum*<sup>+/+</sup> mice at E16.5 (fold change > 2, FPKM > 0.3)

Gene name	Gene description	P value	Fold change
<i>Kera</i>	keratocan	7.13E-48	5.714947
<i>Fgf20</i>	fibroblast growth factor 20	2.07E-06	4.373358
<i>mt-Nd3</i>	mitochondrially encoded NADH dehydrogenase 3	2.84E-13	3.917385
<i>Ckm2</i>	creatine kinase, mitochondrial 2	1.21E-08	3.555372
<i>Agtr2</i>	angiotensin II receptor, type 2	1.81E-100	3.052717
<i>mt-Co3</i>	mitochondrially encoded cytochrome c oxidase III	4.98E-07	3.024279
<i>Ifitm6</i>	interferon induced transmembrane protein 6	0.033944	2.974692
<i>Zfp993</i>	zinc finger protein 993	0.000471	2.958191
<i>Cilp</i>	cartilage intermediate layer protein, nucleotide pyrophosphohydrolase	1.94E-11	2.925638
<i>Cpa3</i>	carboxypeptidase A3, mast cell	3.26E-16	2.608288
<i>Chst13</i>	carbohydrate (chondroitin 4) sulfotransferase 13	0.031958	2.538128
<i>Cma1</i>	chymase 1, mast cell	9.36E-19	2.460558
<i>Myh7</i>	myosin, heavy polypeptide 7, cardiac muscle, beta	1.11E-18	2.433521
<i>Wnt2</i>	wingless-type MMTV integration site family, member 2	0.010194	2.381359
<i>Msr1</i>	macrophage scavenger receptor 1	8.28E-05	2.339884
<i>Dkk4</i>	dickkopf WNT signaling pathway inhibitor 4	3.33E-05	2.332174
<i>Tbx18</i>	T-box18	8.37E-07	2.278756
<i>Ampd1</i>	adenosine monophosphate deaminase 1	2.61E-07	2.256862

<i>Peg10</i>	paternally expressed 10	4.59E-71	2.245729
<i>Abi3bp</i>	ABI gene family, member 3 (NESH) binding protein	4.70E-42	2.243991
<i>mt-Co2</i>	mitochondrially encoded cytochrome c oxidase II	6.84E-08	2.241564
<i>Ostn</i>	osteoerin	0.002977	2.214417
<i>P2ry10b</i>	purinergic receptor P2Y, G-protein coupled 10B	4.24E-05	2.208457
<i>Agtr1a</i>	angiotensin II receptor, type 1a	6.41E-05	2.202085
<i>Nrk</i>	Nik related kinase	2.57E-57	2.194555
<i>Lox</i>	lysyl oxidase	2.57E-93	2.182619
<i>Corin</i>	corin	4.78E-08	2.161709
<i>Trdn</i>	triadin	7.28E-05	2.128557
<i>Slc13a5</i>	solute carrier family 13 (sodium-dependent citrate transporter), member 5	6.74E-10	2.121354
<i>Lypd2</i>	Ly6/Plaur domain containing 2	0.035254	2.112494
<i>Sgms2</i>	sphingomyelin synthase 2	3.55E-32	2.087137
<i>Car3</i>	carbonic anhydrase 3	2.71E-16	2.075139
<i>Ogn</i>	osteo glycin	1.23E-70	2.070199
<i>Plagl1</i>	pleiomorphic adenoma gene-like 1	1.63E-109	2.065845
<i>Grem1</i>	gremlin 1, DAN family BMP antagonist	0.000162	2.060451
<i>Meox2</i>	mesenchyme homeobox 2	3.71E-09	2.055837
<i>Ttn</i>	titin	4.81E-67	2.052107
<i>Asb4</i>	ankyrin repeat and SOCS box-containing 4	2.53E-10	2.04622
<i>Sln</i>	sarcolipin	2.83E-12	2.038246
<i>Chrm2</i>	cholinergic receptor, muscarinic 2, cardiac	5.98E-06	2.031555
<i>Kcnvl</i>	potassium channel, subfamily V, member 1	2.09E-05	2.027014
<i>Gjd4</i>	gap junction protein, delta 4	0.001773	2.024189
<i>Srgn</i>	serglycin	0.000572	2.022666
<i>Prrx1</i>	paired related homeobox 1	1.30E-89	2.022269
<i>Aspn</i>	asporin	1.55E-72	2.016374

**Table 4.** The top 50 genes that are downregulated in molars of *Notum*<sup>-/-</sup> mice compared to *Notum*<sup>+/+</sup> mice at E16.5 (fold change > 2, FPKM > 0.3)

Gene name	Gene description	P value	Fold change
<i>Prdm12</i>	PR domain containing 12	5.07E-07	-236.839
<i>Hoxd1</i>	homeobox D1	2.05E-06	-192.528
<i>Skor2</i>	SKI family transcriptional corepressor 2	3.01E-06	-181.868
<i>Rph3a</i>	rabphilin 3A	2.80E-11	-145.677
<i>Slc17a6</i>	solute carrier family 17 (sodium-dependent inorganic phosphate cotransporter), member 6	3.44E-11	-143.896
<i>Mrgprx1</i>	MAS-related GPR, member X1	2.08E-05	-134.673
<i>Tyrp1</i>	tyrosinase-related protein 1	2.05E-06	-127.625
<i>Pou4f3</i>	POU domain, class 4, transcription factor 3 ]	4.55E-05	-118.419
<i>Scrt2</i>	scratch family zinc finger 2	5.19E-06	-109.476
<i>Scrt1</i>	scratch family zinc finger 1	8.39E-10	-105.039
<i>Cpne6</i>	copine VI	3.60E-20	-87.2067
<i>Scn10a</i>	sodium channel, voltage-gated, type X, alpha	4.98E-12	-78.5396
<i>Cplx1</i>	complexin 1	9.54E-35	-63.6583
<i>Ppp1r1c</i>	protein phosphatase 1, regulatory inhibitor subunit 1C	1.13E-10	-42.6793
<i>Zdhhc22</i>	zinc finger, DHHC-type containing 22	6.51E-06	-42.28
<i>Nefh</i>	neurofilament, heavy polypeptide	7.82E-59	-39.1087
<i>Nefm</i>	neurofilament, medium polypeptide	4.67E-54	-37.0878
<i>Sncg</i>	synuclein, gamma	8.34E-26	-26.0073
<i>Asic2</i>	acid-sensing (proton-gated) ion channel 2	4.44E-07	-20.0598
<i>Stmn3</i>	stathmin-like 3	1.56E-46	-19.9989
<i>Gchfr</i>	GTP cyclohydrolase I feedback regulator	0.001607	-19.0053
<i>Kenq2</i>	potassium voltage-gated channel, subfamily Q, member 2	6.42E-24	-18.9848
<i>Sncb</i>	synuclein, beta	1.70E-05	-18.5521
<i>Krt76</i>	keratin 76	0.001879	-18.493
<i>Atp2b2</i>	ATPase, Ca <sup>++</sup> transporting, plasma membrane 2	7.33E-21	-17.8797
<i>Nefl</i>	neurofilament, light polypeptide	6.64E-156	-17.6702
<i>Mt2</i>	metallothionein 2	0.00453	-16.9501

<i>Chga</i>	chromogranin A	1.77E-15	-16.2079
<i>P2rx3</i>	purinergic receptor P2X, ligand-gated ion channel, 3	5.20E-28	-15.4759
<i>Pou4f1</i>	POU domain, class 4, transcription factor 1	3.65E-13	-15.4624
<i>Ptpn5</i>	protein tyrosine phosphatase, non-receptor type 5	3.60E-08	-15.4442
<i>Lce3a</i>	late cornified envelope 3A	0.013181	-15.2098
<i>Vstm2l</i>	V-set and transmembrane domain containing 2-like	6.52E-15	-13.6106
<i>Vgf</i>	VGF nerve growth factor inducible	5.56E-10	-12.635
<i>Syp</i>	synaptophysin	1.21E-25	-12.6099
<i>Slc17a7</i>	solute carrier family 17 (sodium-dependent inorganic phosphate cotransporter), member 7	3.48E-08	-11.8672
<i>Tlx3</i>	T cell leukemia, homeobox 3	0.001867	-11.6593
<i>Atp1a3</i>	ATPase, Na <sup>+</sup> /K <sup>+</sup> transporting, alpha 3 polypeptide	2.62E-61	-11.5879
<i>Mapt</i>	microtubule-associated protein tau	1.78E-57	-11.1714
<i>Prph</i>	peripherin	9.82E-105	-11.0236
<i>Gabbr2</i>	gamma-aminobutyric acid (GABA) B receptor, 2	3.28E-17	-10.9133
<i>Isl2</i>	insulin related protein 2 (islet 2)	7.68E-09	-10.7512
<i>Tmem163</i>	transmembrane protein 163	1.37E-07	-10.6614
<i>Avil</i>	advillin	1.10E-36	-10.4753
<i>Npy1r</i>	neuropeptide Y receptor Y1	8.78E-07	-10.0518
<i>Resp18</i>	regulated endocrine-specific protein 18	0.000771	-9.09128
<i>Soga3</i>	SOGA family member 3	1.42E-08	-9.0648
<i>Lce3f</i>	late cornified envelope 3F	0.000214	-8.78343
<i>Pcsk1n</i>	proprotein convertase subtilisin/kexin type 1 inhibitor	2.95E-20	-8.70905
<i>Mpz</i>	myelin protein zero	3.67E-76	-8.50579

#### 4. *Notum*<sup>-/-</sup> mice exhibited deviations in cusp pattern and crown outline

Three-dimensional (3D) geometric morphometric analysis was performed at PN14 to compare the cusp pattern and crown outline of *Notum*<sup>-/-</sup> and *Notum*<sup>+/+</sup> M1 (Fig. 18A–E, Fig. 19A–E). Principal component (PC) analysis of maxillary M1 revealed distinct clustering of cusp patterns in *Notum*<sup>-/-</sup> mice, which showed a clear separation from *Notum*<sup>+/+</sup> mice on PC plot with PC1. Negative PC1 scores attributed to a cuspal polygon of *Notum*<sup>-/-</sup> M1 (Fig. 18B). In discriminant function (DF) analysis, *Notum*<sup>-/-</sup> M1 showed distal displacement of anterostyle and enterostyle, buccal displacement of lingual anterocone and buccal anterocone, lingual displacement of hypocone, along with mesial displacement of protocone and metacone from the mean shape (Fig. 18C). PC analysis of the maxillary M1 crown outline showed a clear separation of *Notum*<sup>-/-</sup> M1 from *Notum*<sup>+/+</sup> M1 along the PC1 of the PC plot. Negative PC1 scores analogous to the *Notum*<sup>-/-</sup> M1 crown outline. In discriminant function analysis, *Notum*<sup>-/-</sup> M1 exhibited decreased concavity in mesiolingual, mesiobuccal, and distolingual outlines (Fig. 18D–E). In the Cross-validated DF analysis of crown outline, *Notum*<sup>-/-</sup> M1 was consistently distinguished from *Notum*<sup>+/+</sup> M1. Furthermore, cusp pattern PC1 scores showed a strong direct relationship with crown outline PC1 scores ( $R^2 = 0.66$ ,  $P = 0.000014$ ) (Fig. 20A).

PC analysis of mandibular M1 cusp patterns did not show a notable separation between *Notum*<sup>-/-</sup> and *Notum*<sup>+/+</sup> M1 (Fig. 19B). The crown outline in mandibular M1 exhibited a

clear separation of *Notum*<sup>-/-</sup> M1 from *Notum*<sup>+/+</sup> M1 along the PC1 axis on the PC plot with PC1 and PC2 (Fig. 19D). Negative PC1 scores attributing to the crown outline with a buccolingually larger width in *Notum*<sup>-/-</sup> mice. In DF analysis, *Notum*<sup>-/-</sup> mandibular M1 displayed a notable change in distolingual outline (Fig. 19D–E). Cross-validated DF analysis of crown outline consistently differentiated *Notum*<sup>-/-</sup> M1 from *Notum*<sup>+/+</sup> M1. The mandibular M1 cusp pattern PC1 scores exhibited no relationship with crown outline PC1 ( $R^2 = 0.0746$ ,  $P = 0.2481$ ) (Fig. 20B).

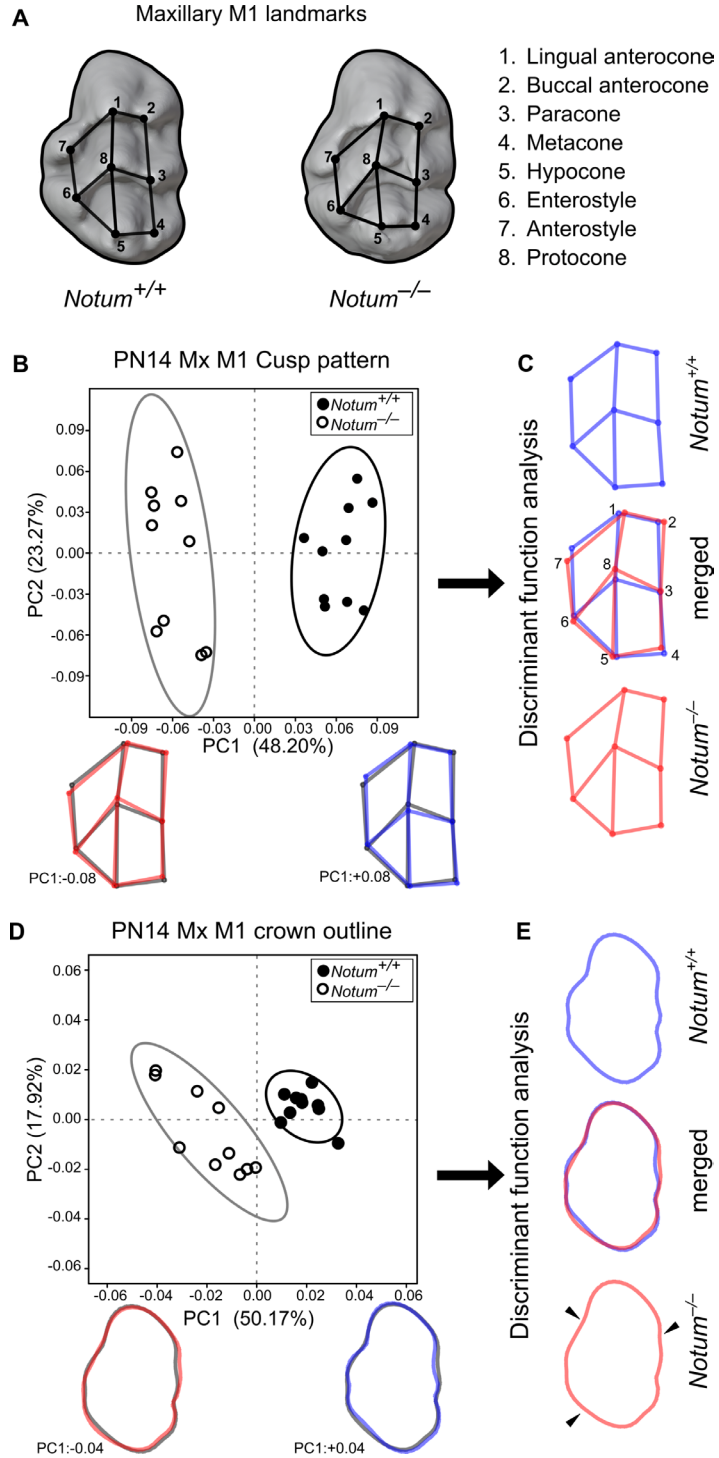
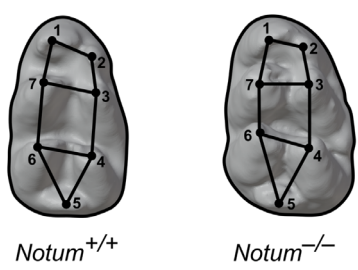


**Figure 18. Geometric morphometric changes in cusp pattern and crown outline in *Notum*<sup>-/-</sup> mice maxillary molars at PN14.**

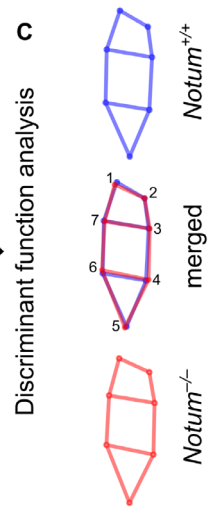
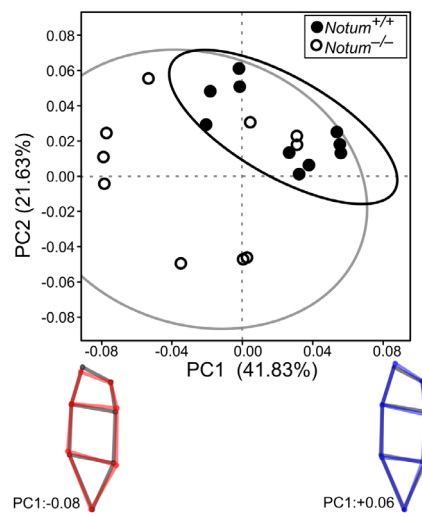
(A) Cusp landmarks and crown outlines of the maxillary molars (M1). In principal component (PC) analysis, *Notum*<sup>-/-</sup> M1 (white circles) and *Notum*<sup>+/+</sup> M1 (black circles) are plotted along the first two PCs (PC1 and PC2) scores (n = 10 per group). Blue and red wireframes or outlines correspond to the positive and negative ends of the PC1 axis, respectively. Gray wireframes or outlines indicate the Procrustes' mean of all samples along the PC1 axis. In discriminant function (DF) analysis, blue and red wireframes or outlines correspond to *Notum*<sup>+/+</sup> M1 and *Notum*<sup>-/-</sup> M1, respectively (B–C). In cross-validated DF analysis, *Notum*<sup>-/-</sup> M1s are accurately classified into *Notum*<sup>-/-</sup> M1 group with a predictive accuracy of 80%, and *Notum*<sup>+/+</sup> M1s are accurately classified into the *Notum*<sup>+/+</sup> M1 group with a predictive accuracy of 70%. (D–E) In PC analysis of crown outline in maxillary M1, *Notum*<sup>-/-</sup> M1s are clustered separately from the *Notum*<sup>+/+</sup> M1 on the PC1 axis. In cross-validated DF analysis, predictive accuracy is 100% for both *Notum*<sup>-/-</sup> M1 and *Notum*<sup>+/+</sup> M1. *Notum*<sup>-/-</sup> M1s show a significant decrease in concavity at both lingual and buccal outlines (arrowheads in E).

**A** Mandibular M1 landmarks



1. Lingual anteroconid
2. Buccal anteroconid
3. Protoconid
4. Hypoconid
5. Hypoconulid
6. Entoconid
7. Metaconid

**B** PN14 Mn M1 Cusp pattern



**D** PN14 Mn M1 crown outline

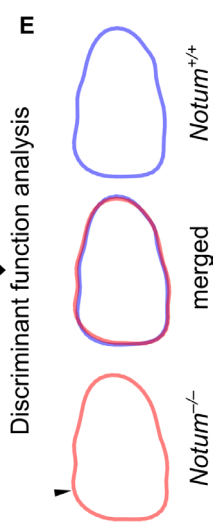
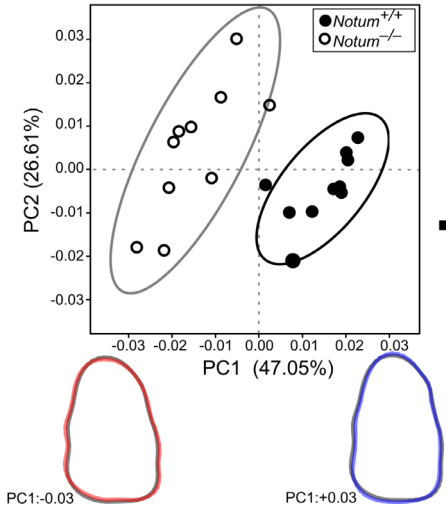


**Figure 19. Geometric morphometric changes in cusp pattern and crown outline in *Notum*<sup>-/-</sup> mice mandibular molars at PN14.**

**(A)** Landmarks of the cusps and crown outlines of the mandibular first molars (M1). **(B–C)** In PC analysis of the cusp pattern in mandibular M1, *Notum*<sup>-/-</sup> M1s are not clustered separately from *Notum*<sup>+/+</sup> M1 along the PC1 and PC2 axes. In cross-validated DF analysis, predictive accuracy is 100% for both *Notum*<sup>-/-</sup> M1 and *Notum*<sup>+/+</sup> M1. **(D–E)** In PC analysis of the crown outline of mandibular M1, *Notum*<sup>-/-</sup> M1s are clustered separately from *Notum*<sup>+/+</sup> M1s on the PC1 axis. In cross-validated DF analysis, *Notum*<sup>-/-</sup> M1s, which also shows a change in distolingual outline (arrowhead in E), are correctly classified into *Notum*<sup>-/-</sup> M1 group and *Notum*<sup>+/+</sup> M1s into *Notum*<sup>+/+</sup> M1 group with a predictive accuracy of 100% and 90%, respectively.

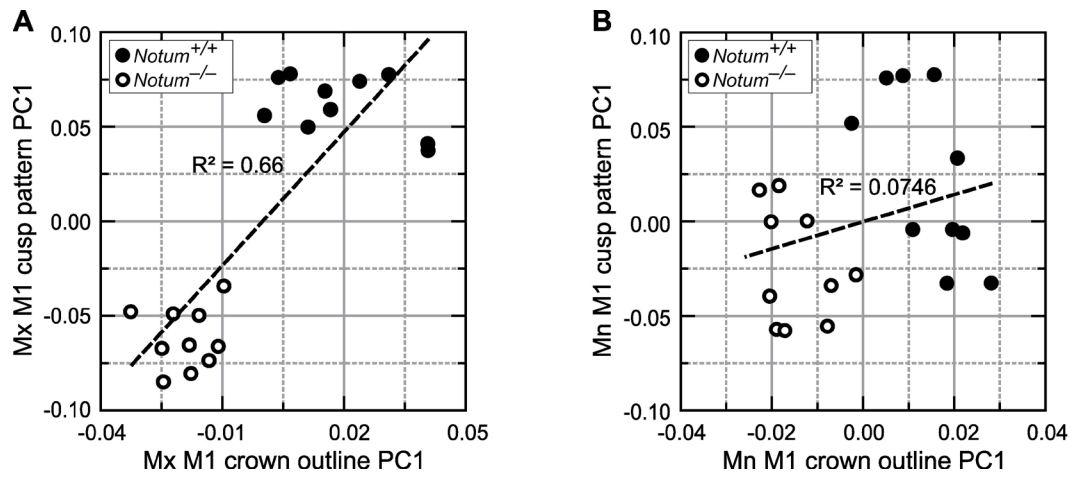


**Figure 20. Relationship between the cusp pattern PC1 and crown outline PC1 in maxillary and mandibular molars at PN14.**

**(A–B)** Linear regression analysis with the cusp pattern PC1 and crown outline PC1. There is a strong direct relationship between cusp pattern PC1 scores and crown outline PC1 scores in maxillary M1 ( $R^2 = 0.66$ ,  $p = 0.000014$ ). There is no relationship between cusp pattern PC1 scores and crown outline PC1 scores in mandibular M1 ( $R^2 = 0.0746$ ,  $P = 0.2481$ ).

## 5. The lengths of cervical tongues were diminished in *Notum*<sup>-/-</sup> mice

To inspect the early root patterning, the developmental trajectory of cervical tongues in maxillary and mandibular molars was studied with whole-mount immunohistochemistry. The cervical tongue arrangement was defined by using the localization of E-cadherin in PN0 and PN7 mice molars. In *Notum*<sup>-/-</sup> maxillary M1, two lingual cervical tongues showed considerable reduction in length, and the buccal cervical tongue showed morphological changes at PN0 and PN7 (Fig. 21A–B, E–F, Fig. 22A–J1). Similarly, *Notum*<sup>-/-</sup> mandibular M1 buccal and lingual cervical tongues displayed reduced length at PN0 (Fig. 21C–D, G–H, Fig. 22K–T1). At PN7, the distances between cervical tongues were markedly reduced in both maxillary and mandibular M1 of *Notum*<sup>+/+</sup> mice, contrasting with a notable distance in *Notum*<sup>-/-</sup> mice (Fig. 21E–H, Fig. 22A1–J1, K1–T1). This maintenance of distance may potentially obstruct the fusion of cervical tongues in *Notum*<sup>-/-</sup> molars.

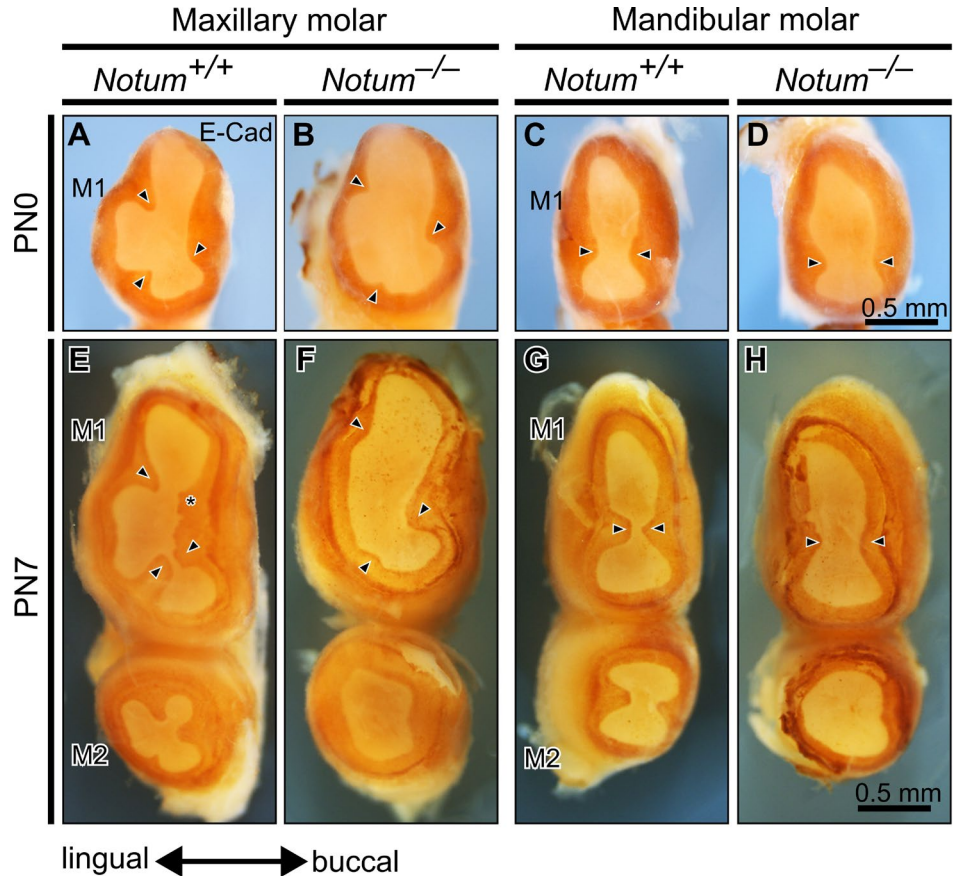


**Figure 21. Alteration of cervical tongue pattern in *Notum*<sup>-/-</sup> maxillary and mandibular molars.**

(A-H) From the apical view of maxillary and mandibular M1 at PN0 and PN7, E-cadherin localization in the epithelium depicts cervical tongue configuration. *Notum*<sup>-/-</sup> M1s display shorter cervical tongues and wider gaps between cervical tongues compared to *Notum*<sup>+/+</sup> M1.

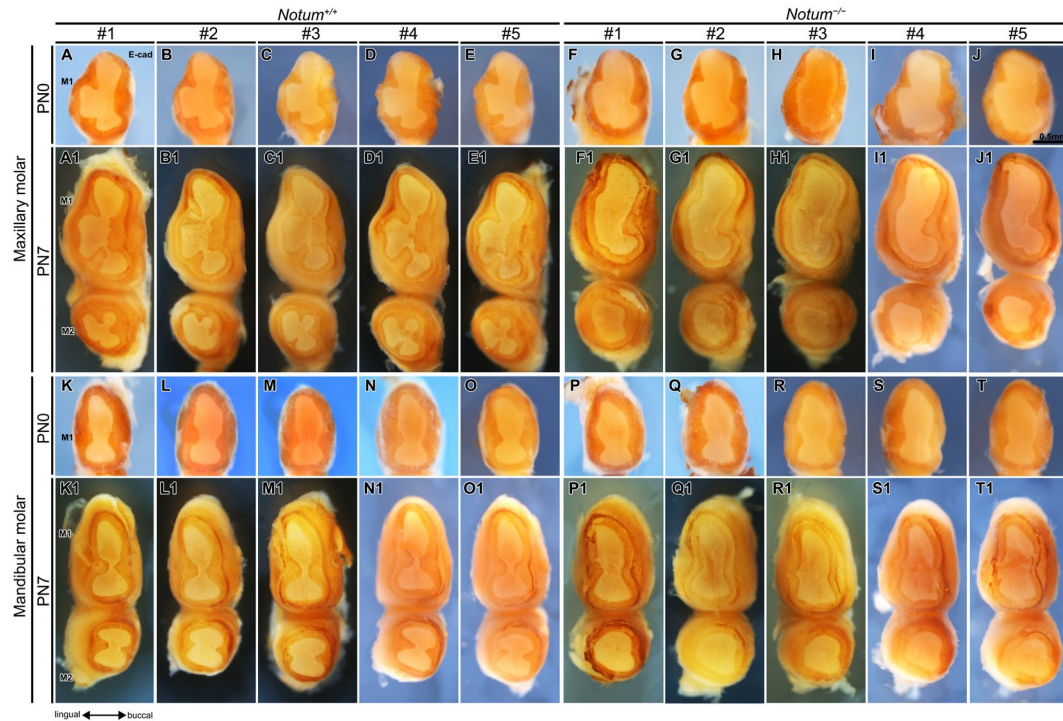


**Figure 22. Changes in the cervical tongue morphology are consistent in *Notum*<sup>-/-</sup> M1 (A-T1) Localization of the E-cadherin in the apical view of maxillary and mandibular M1 at PN0 and PN7 (n =5 per group). Compared to the *Notum*<sup>+/+</sup> M1, *Notum*<sup>-/-</sup> M1s showed consistently shorter cervical tongues and longer distances between cervical tongues across all the samples.**

## 6. The crown outline is closely related to the root pattern

To examine the relationship between the crown outline and root patterns, PC analysis of crown outlines was conducted alongside measuring the mesiodistal and buccolingual widths of the tooth crown and quantifying the extent of root fusion in M1 at PN35. A linear regression model between these parameters was established. PC analysis of the crown outline showed that *Notum*<sup>-/-</sup> M1 was separately clustered from *Notum*<sup>+/+</sup> M1 along the PC1 axis on the PC plot, mimicking the pattern observed in maxillary and mandibular M1 at PN14 (Fig. 23A–D). The maxillary and mandibular M1s of *Notum*<sup>-/-</sup> mice exhibited an increase in buccolingual width ( $p = 0.000341$ ) while showing no change in the mesiodistal width ( $p = 0.908$ ) (Fig. 24A–B, D–E). Root fusion was quantified by measuring the interradicular area between three roots in maxillary M1 and the interradicular distance between two roots in mandibular M1. *Notum*<sup>-/-</sup> M1 exhibited a significant reduction in the interradicular area ( $P = 0.000001$ ) and the interradicular distance ( $P = 0.000245$ ) compared to the *Notum*<sup>+/+</sup> M1 (Fig. 24C, F). Linear regression analysis revealed a strong relationship between the interradicular area and buccolingual width of maxillary M1 ( $R^2 = 0.5972$ ,  $P = 0.000010$ ) and a very strong relationship between the interradicular area and crown outline PC1 scores of maxillary M1 ( $R^2 = 0.8499$ ,  $P = 0.000000$ ) (Fig. 25A–B). Mandibular M1 revealed a weak relationship between interradicular distance and buccolingual width ( $R^2 = 0.3911$ ,  $P = 0.001084$ ) and a strong relationship with crown outline PC1 of mandibular M1 ( $R^2 = 0.5393$ ,  $P = 0.000044$ ) (Fig. 25C–D). These findings give concrete evidence for the close relationship between crown outline and root patterns.

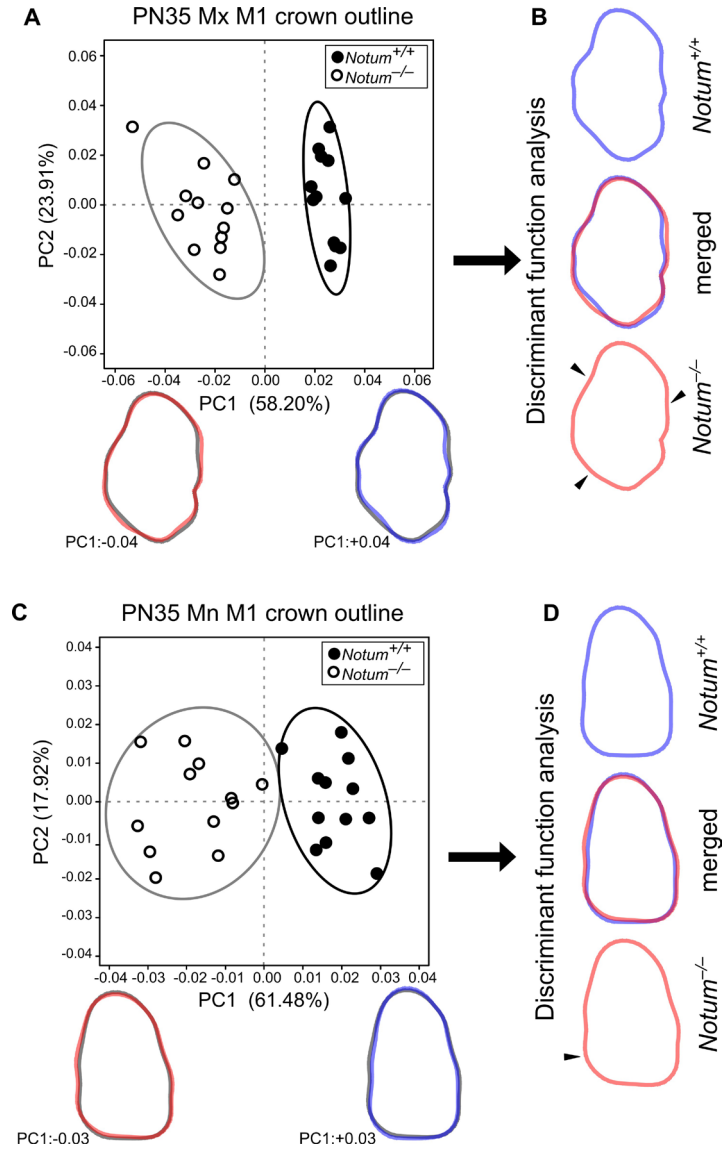


**Figure 23. Geometric morphometric changes in maxillary and mandibular crown outlines at PN 35.**

(A–D) PC analysis and DF analysis of PN35 maxillary and mandibular crown outlines.

(A, C) *Notum*<sup>-/-</sup> M1s are clustered separately from the *Notum*<sup>+/+</sup> M1 on the PC1 axis. (B,

D) Cross-validated DF analysis correctly classifies *Notum*<sup>-/-</sup> M1 into *Notum*<sup>-/-</sup> M1 group and *Notum*<sup>+/+</sup> M1 as *Notum*<sup>+/+</sup> M1 group with 100% predictive accuracy in the maxilla. In mandible. *Notum*<sup>-/-</sup> M1s are correctly classified into *Notum*<sup>-/-</sup> M1 group with 92% predictive accuracy and *Notum*<sup>+/+</sup> M1 into *Notum*<sup>+/+</sup> M1 group with 100% predictive accuracy. Morphometric changes in crown outline at PN35 mirror those at PN14 (arrowheads in B, D).

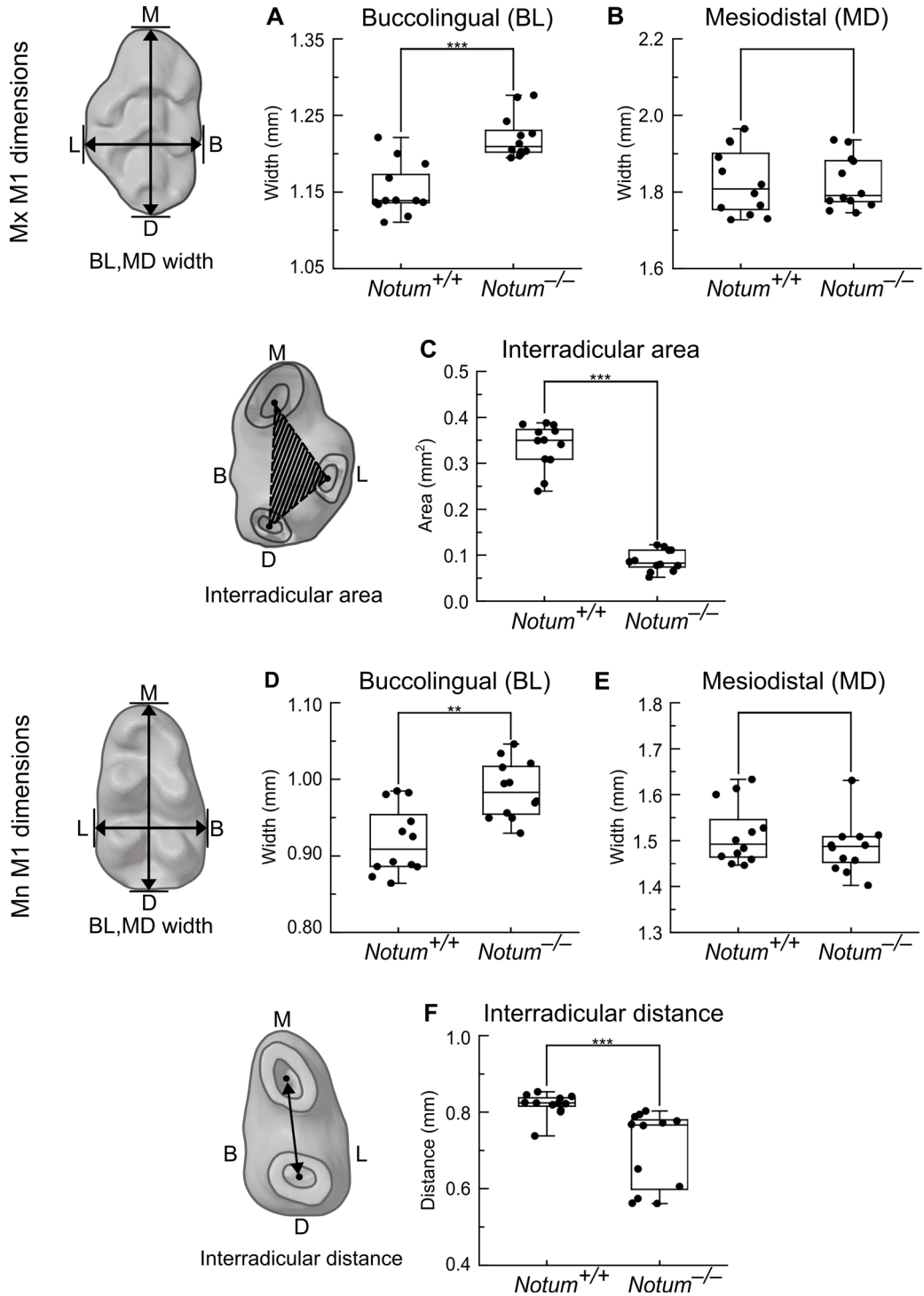


**Figure 24. Dimensional changes in crown and root of *Notum*<sup>-/-</sup> M1.**

(A-F) Box and whisker plots showing tooth dimensional measurements. *Notum*<sup>-/-</sup> mice show a significant increase in buccolingual width but no change in mesiodistal width in both the maxilla and mandible. Maxillary M1 interradicular area is significantly smaller in *Notum*<sup>-/-</sup> mice than *Notum*<sup>+/+</sup> mice, and mandibular M1 interradicular distance is shorter in *Notum*<sup>-/-</sup> mice than *Notum*<sup>+/+</sup> mice. (Mann Whitney U test, \*P < 0.05, \*\*P < 0.01 and \*\*\*P < 0.001)

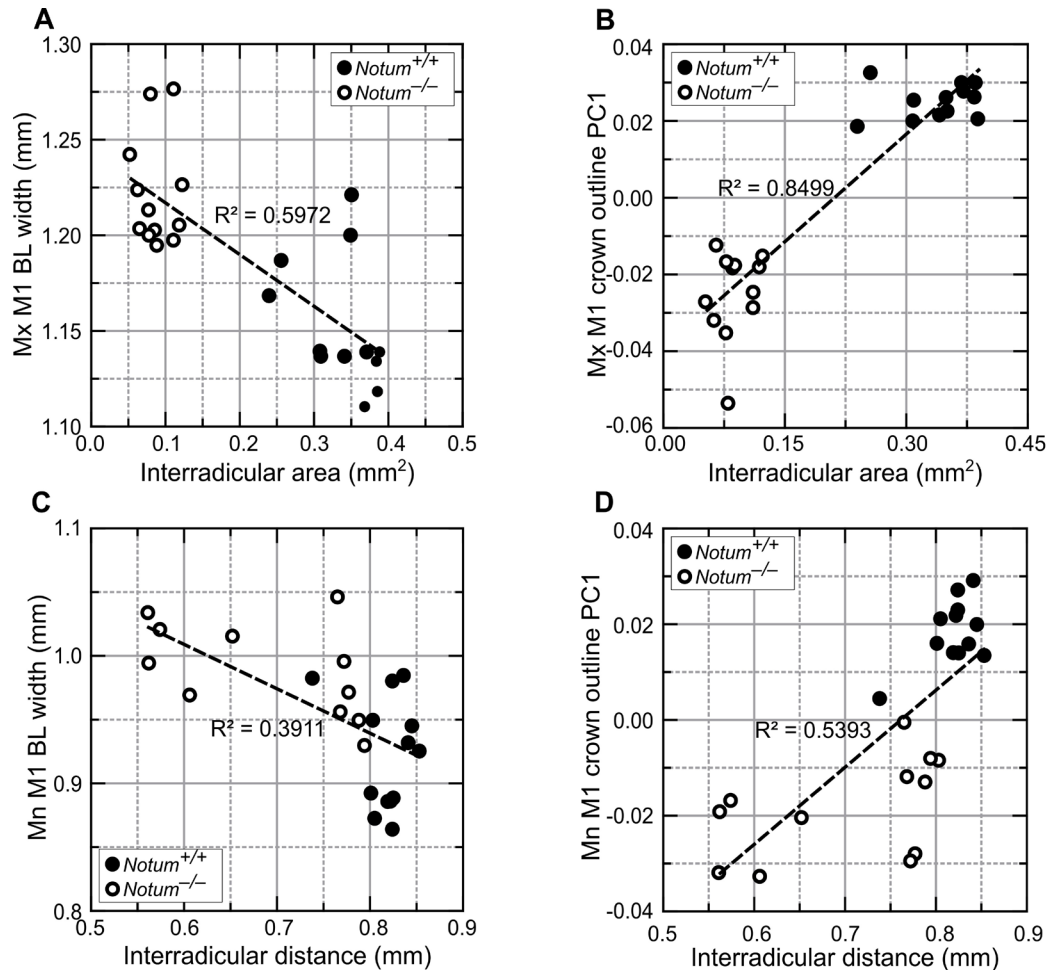


**Figure 25. Relationship between crown outline and root pattern.**

(A, C) Linear regression analyses reveal strong relationships between interradicular area dimension and buccolingual width in maxillary M1 ( $R^2 = 0.5972$ ,  $P < 0.001$  in A) but weak in mandibular M1 ( $R^2 = 0.3911$ ,  $P < 0.001$  in C). (B, D) A strong direct relationship exists between interradicular area dimension and crown outline PC1 scores in both maxillary M1 ( $R^2 = 0.8499$ ,  $P < 0.001$  in B) and mandibular M1 ( $R^2 = 0.5393$ ,  $P < 0.001$  in D).

## IV. DISCUSSION

### 1. *Notum* expression in primary EK, secondary EKs, and dental papilla

Earlier research on *Notum* in teeth mainly focused on the role of *Notum* in odontoblasts and dentin formation (Vogel et al. 2016; Krivanek et al. 2020; Wen et al. 2020). In this present study, the *Notum* expression pattern was examined during tooth development, and its role in crown and root morphogenesis was demonstrated.

During molar development, *Notum* expression within the dental papilla appeared as a thin outer layer of the dental papilla. Given the crucial roles that *Lef1* and *Bmp4* play in odontoblast differentiation, the co-expression of *Notum* with mesenchymal *Lef1* and *Bmp4* implies a potential connection between *Notum* and odontoblast differentiation (Narayanan et al. 2001; Nakatomi et al. 2013). This finding holds up with earlier studies that defined the *Notum* expression pattern in early odontoblasts during postnatal root formation (Krivanek et al. 2020; Wen et al. 2020). In dental epithelium, *Notum* expression was found exclusively within the primary and secondary EKs. Specific expression of *Notum* in primary and secondary EKs suggests an influence of *Notum* in formations of cusp pattern and crown morphogenesis, given the recognized importance of enamel knots as regulators shaping the tooth crown by modulating the cusp patterns (Jernvall et al. 1994; Jernvall and Thesleff 2000).

## 2. Cusp tip expansion due to enlarged secondary EKs in *Notum*-deficient mice

The primary EK is a transient signaling center playing an important role in the bud-to-cap transition of early tooth development (Jernvall et al. 1994). The secondary EK number and positions correspond to those of the future tooth cusps (Pispa et al. 1999). EK size is suggested to be controlled by a sophisticated negative feedback loop within intricate signaling networks for the patterning of EKs. Within this feedback loop, Wnts play a crucial role as the primary activator (Zhang et al. 2009), largely documented in the formation of the tooth and cusp pattern (Jernvall and Thesleff 2000; Salazar-Ciudad and Jernvall 2002; Ohazama et al. 2009; Ahn et al. 2010; Salazar-Ciudad and Jernvall 2010; Cho et al. 2011; Häärä et al. 2012; Harjunmaa et al. 2012; Harjunmaa et al. 2014; Seo et al. 2018; Kim et al. 2019). Since *Dkk4* functions as both a downstream target and an inhibitor of Wnt/ $\beta$ -catenin signaling (Zhang et al. 2009), its expression is found particularly in EKs, and a Wnt/*Dkk4* negative feedback loop has been suggested (Järvinen et al. 2018). However, no morphological changes have been observed in the teeth of *Dkk4*-deficient mice (Ahtiainen et al. 2016; Järvinen et al. 2018), leaving the role of *Dkk4* in EK patterning unclear.

Comparable to *Dkk4*, *Notum* is also a direct target gene of the Wnt/ $\beta$ -catenin signaling pathway and serves an important function as a Wnt inhibitor in a negative feedback loop, which is essential for the development of wings in *Drosophila* and the brain development of *Xenopus* (Gerlitz and Basler 2002; Kakugawa et al. 2015; Zhang et al. 2015). *Notum* plays an exclusive role in inhibiting Wnt family members, and *Notum* is the

only secreted Wnt feedback inhibitor found across the kingdom Animalia (Kakugawa et al. 2015). Moreover, *Notum* plays a critical role in the dorsal-ventral patterning of the trachea. Loss of *Notum* in tracheal mesenchyme results in mispatterning of the tracheal cartilage and trachealis muscle, leading to tracheal stenosis, highlighting the function of *Notum* in Pattern formation (Gerhardt et al. 2018).

In this current study, the *Notum* expression was uncovered in primary and secondary EKs along with the outer layer of the dental papilla. *Notum*-deficient mice showed a considerable increase in secondary EK size in M1 of both maxilla and mandible. The loss of *Notum* leads to a significant increase in the expression levels of target genes of the Wnt signaling pathway, including *Fgf20*, *Dkk4*, and *Fgf4*, in secondary EKs (Kratochwil et al. 2002; Järvinen et al. 2006; Järvinen et al. 2018). Interestingly, these three marker genes of the EK exhibited a significant elevation, whereas no considerable change was detected in the expression level of the target genes of the Wnt signaling pathway in the mesenchyme. Taken together, these results indicate that an activation in Wnt/ $\beta$ -catenin signaling, caused by the suppression of the inhibitors within the Wnt/*Notum* negative feedback loop, results in the expansion of secondary EKs. Previous research on *Eda*-null mice or *c<sup>IkBa</sup> $\Delta$ N* mice has shown that the number and size of cusps are determined by the size of primary EK, with a smaller primary EK leading to a decrease in cusp number and size (Pispa et al. 1999; Harjunmaa et al. 2014). However, the influence of the secondary EK size on the dimensions of the cusps and tooth remains unknown. In the current study, the enlargement of secondary EKs was found to result in broader cusp tips without changing

the cusp base dimensions in all molars of *Notum*-deficient mice. A probable mechanism through which the secondary EK size impacts the dimensions of the cusp tip involves Fgf signaling, which is well-known for its function in the remodeling of cellular geometry. A linear expression pattern of *Fgf4* in gerbil molars induces long, flat lophs in place of cusps. Modification in Fgf signaling in gerbil tooth germs alters the epithelial morphology and invagination and transformation from lophs to cusps. (Li et al. 2018). Consistent with a regulatory module that was previously identified comprising *Fgf4*, *Fgf20*, *RhoA*, *Rac1*, and *Cdh1*, *Notum*-deficient mice exhibited elevated levels of *Fgf4* and *Fgf20* expression. However, no significant change in the levels of *Rac1*, *Cdh1*, and *RhoA* was observed, probably due to the expression of these genes not only in the EKs but also in numerous other cells. These findings collectively imply that Notum controls cusp tip dimensions by controlling the size of the secondary EK. Further research using conditional *Notum*-deficient mice is required to determine whether the regulation of secondary EK size is attributable to the epithelial Notum, the mesenchymal Notum, or both.

### **3. Relationship between cusp pattern and crown outline pattern**

Previous research has mostly investigated the effect of alterations in *Shh*, *Sostdc1*, *Spry1*, *Spry2*, *Spry4*, *Rsk2*, *Eda*, *Edar*, and *Fgf3* on cusp number or tooth number in mice and humans (Kassai et al. 2005; Charles et al. 2011; Häärä et al. 2012; Harjunmaa et al. 2014; Marangoni et al. 2015; Kim et al. 2019). Molars with alterations in the cusp configuration without changes in the number of cusps have been overlooked. In the current work, the maxillary M1 of *Notum*-deficient mice showed changes in cusp arrangement but

no detectable change in total cusp number. The displacement of several cusps in maxillary M1 of *Notum*-deficient mice had a direct influence on the crown outline. As a result, *Notum*-deficient mice exhibited a decreased concavity in mesiolingual, mesiobuccal, and distolingual crown outlines in their maxillary M1. The crown outline pattern displayed a strong and direct relationship with the cusp pattern in maxillary M1. Although significant changes were observed in the crown outline in mandibular M1 of *Notum*-deficient mice, no close relationship between the cusp pattern and the crown outline pattern was observed as *Notum*-deficient mandibular M1 showed distinct scattering compared to wild-type mandibular M1 in the PC analysis of cusp pattern.

#### **4. Connection between crown outline and root patterns**

Numerous sources suggested a close relationship between the root and crown morphogenesis in mammalian teeth, given that root development typically follows the crown development (Butler 1956; Kondo et al. 2009; Ota et al. 2009). Anomalies in crown morphology are frequently associated with abnormalities in root morphology. For example, human patients with mutations in the *CACNAIS* or *WNT10A* and *Wnt10a*-deficient mice exhibit round-shaped molar crowns with root fusion and taurodontism (Yang et al. 2015; Laugel-Haushalter et al. 2018; Yu et al. 2020; Kantaputra et al. 2023). The cusp pattern and arrangement of the crown outline have been recognized as crucial factors in the shaping of the cervical tongues, which successively determine the root pattern (Seo et al. 2017). In line with the findings of earlier studies, this study has demonstrated that the cervical tongue became considerably shorter in the regions where the concavity in the crown outline of

maxillary M1 was reduced in *Notum*-deficient mice. The joining between the short cervical tongues was delayed or failed, leading to a partial or complete root fusion. In addition, the linear regression model once more confirmed the presence of a strong and direct relationship between the crown outline pattern and root pattern in both maxillary and mandibular M1.

## V. CONCLUSION

In conclusion, *Notum* expression was detected in primary enamel knots, secondary enamel knots, and dental papillae cells during tooth development. The loss of *Notum* resulted in enlarged secondary EKs, which contributed to broader cusp tips, indicating that the secondary EK size is regulated through the Wnt/Notum negative feedback loop. The displacement of cusps in *Notum*-deficient mice led to alterations in crown outline patterns, resulting in shorter cervical tongues. This, in turn, led to an incomplete fusion between cervical tongues, causing an incomplete division of molar roots in *Notum*-deficient mice (Fig. 26). These findings emphasize the pivotal role of *Notum* in determining the both crown and root pattern by regulating the secondary EK size in the Wnt/Notum negative feedback loop.

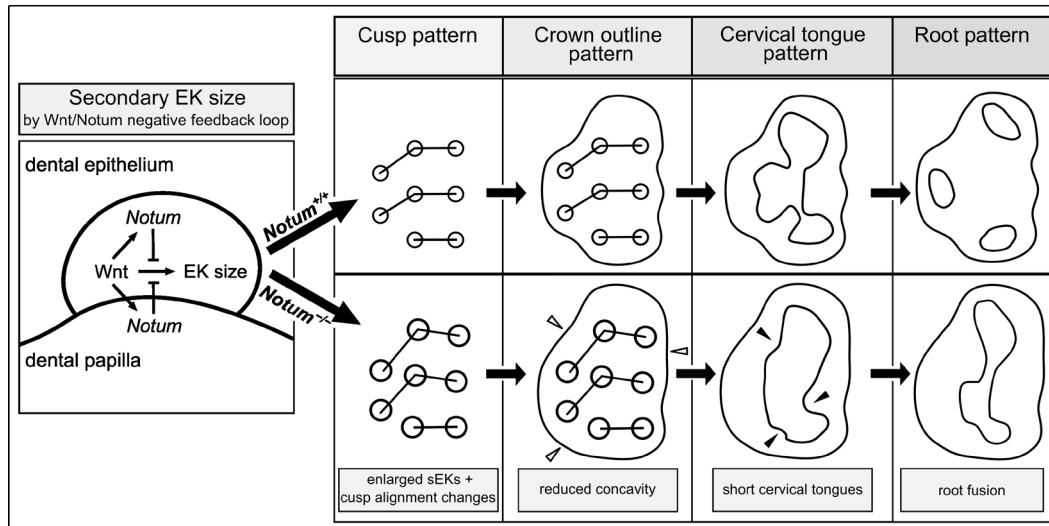


**Figure 26. A schematic diagram demonstrating the activity of *Notum* in the secondary enamel knot and its role in the crown and root patterning.**

*Notum* in the secondary enamel knot (EK) and dental papilla regulates the size of secondary EK by inhibiting *Wnt* signaling. The absence of *Notum* results in enlarged secondary EKs, leading to broader cusp tips. The displacement of the cusps alters the crown outline patterns, resulting in shorter cervical tongues. In turn, an incomplete fusion between cervical tongues occurs, causing incomplete division of molar roots in *Notum*-deficient mice.

## REFERENCES

- Ahn Y, Sanderson BW, Klein OD, Krumlauf R. 2010. Inhibition of Wnt signaling by Wise (Sostdc1) and negative feedback from Shh controls tooth number and patterning. *Development*. 137(19):3221–31.
- Ahtiainen L, Uski I, Thesleff I, Mikkola ML. 2016. Early epithelial signaling center governs tooth budding morphogenesis. *J Cell Biol*. 214(6):753–67.
- Bae C-H, Kim T-H, Chu J-Y, Cho E-S. 2013a. New population of odontoblasts responsible for tooth root formation. *Gene Expr Patterns*. 13(5–6):197–202.
- Bae CH, Kim TH, Ko SO, Lee JC, Yang X, Cho ES. 2015. Wntless regulates dentin apposition and root elongation in the mandibular molar. *J Dent Res*. 94(3):439–45.
- Bae CH, Lee JY, Kim TH, Baek JA, Lee JC, Yang X, Taketo MM, Jiang R, Cho ES. 2013b. Excessive Wnt/ $\beta$ -catenin signaling disturbs tooth-root formation. *J Periodontal Res*. 48(4):405–10.
- Birjandi AA, Sharpe P. 2021. Wnt Signalling in Regenerative Dentistry. *Frontiers in Dental Medicine*. 2:725468.
- Brommage R, Liu J, Vogel P, Mseeh F, Thompson AY, Potter DG, Shadoan MK, Hansen GM, Jeter-Jones S, Cui J, et al. 2019. NOTUM inhibition increases endocortical bone formation and bone strength. *Bone Res*. 7(1):2.

Brugmann SA, Goodnough LH, Gregorieff A, Leucht P, ten Berge D, Fuerer C, Clevers H, Nusse R, Helms JA. 2007. Wnt signaling mediates regional specification in the vertebrate face. *Development*. 134(18):3283–3295.

Butler PM. 1956. The Ontogeny of Molar Pattern. *Biological Reviews*. 31(1):30–69.

Cai J, Cho S-W, Kim J-Y, Lee M-J, Cha Y-G, Jung H-S. 2007. Patterning the size and number of tooth and its cusps. *Dev Biol*. 304(2):499–507.

Ten Cate AR. 1996. The role of epithelium in the development, structure and function of the tissues of tooth support. *Oral Dis*. 2(1):55–62.

Chai Y, Jiang X, Ito Y, Bringas P, Han J, Rowitch DH, Soriano P, McMahon AP, Sucov HM. 2000. Fate of the mammalian cranial neural crest during tooth and mandibular morphogenesis. *Development*. 127(8):1671–1679.

Charles C, Hovorakova M, Ahn Y, Lyons DB, Marangoni P, Churava S, Biehs B, Jheon A, Lesot H, Balooch G, et al. 2011. Regulation of tooth number by fine-tuning levels of receptor-tyrosine kinase signaling. *Development*. 138(18):4063–73.

Chen J, Lan Y, Baek J-A, Gao Y, Jiang R. 2009. Wnt/beta-catenin signaling plays an essential role in activation of odontogenic mesenchyme during early tooth development. *Dev Biol*. 334(1):174–85.

Cho S-W, Kwak S, Woolley TE, Lee M-J, Kim E-J, Baker RE, Kim H-J, Shin J-S, Tickle C, Maini PK, et al. 2011. Interactions between Shh, Sostdc1 and Wnt signaling and a new feedback loop for spatial patterning of the teeth. *Development*. 138(9):1807–1816.

Choi RB, Bullock WA, Hoggatt AM, Horan DJ, Pemberton EZ, Hong JM, Zhang X, He X, Robling AG. 2021. Notum Deletion From Late-Stage Skeletal Cells Increases Cortical Bone Formation and Potentiates Skeletal Effects of Sclerostin Inhibition. *Journal of Bone and Mineral Research*. 36(12):2413–2425.

Coin R, Lesot H, Vonesch JL, Haikel Y, Ruch J V. 1999. Aspects of cell proliferation kinetics of the inner dental epithelium during mouse molar and incisor morphogenesis: a reappraisal of the role of the enamel knot area. *Int J Dev Biol*. 43(3):261–7.

Dassule HR, McMahon AP. 1998. Analysis of epithelial-mesenchymal interactions in the initial morphogenesis of the mammalian tooth. *Dev Biol*. 202(2):215–27.

Du Wei, Hu JK-H, Du Wen, Klein OD. 2017. Lineage tracing of epithelial cells in developing teeth reveals two strategies for building signaling centers. *J Biol Chem*. 292(36):15062–15069.

Fan L, Deng S, Sui X, Liu M, Cheng S, Wang Y, Gao Y, Chu C-H, Zhang Q. 2018. Constitutive activation of  $\beta$ -catenin in ameloblasts leads to incisor enamel hypomineralization. *J Mol Histol*. 49(5):499–507.

Fujii S, Nagata K, Matsumoto S, Kohashi K, Kikuchi A, Oda Y, Kiyoshima T, Wada N. 2019. Wnt/ $\beta$ -catenin signaling, which is activated in odontomas, reduces *Sema3A* expression to regulate odontogenic epithelial cell proliferation and tooth germ development. *Sci Rep.* 9(1):4257.

Fujimori S, Novak H, Weissenböck M, Jussila M, Gonçalves A, Zeller R, Galloway J, Thesleff I, Hartmann C. 2010. Wnt/ $\beta$ -catenin signaling in the dental mesenchyme regulates incisor development by regulating *Bmp4*. *Dev Biol.* 348(1):97–106.

van Genderen C, Okamura RM, Fariñas I, Quo RG, Parslow TG, Bruhn L, Grosschedl R. 1994. Development of several organs that require inductive epithelial-mesenchymal interactions is impaired in *LEF-1*-deficient mice. *Genes Dev.* 8(22):2691–703.

Gerhardt B, Leesman L, Burra K, Snowball J, Rosenzweig R, Guzman N, Ambalavanan M, Sinner D. 2018. Notum attenuates Wnt/ $\beta$ -catenin signaling to promote tracheal cartilage patterning. *Dev Biol.* 436(1):14–27.

Gerlitz O, Basler K. 2002. Wingful, an extracellular feedback inhibitor of Wingless. *Genes Dev.* 16(9):1055–9.

Gordon MD, Nusse R. 2006. Wnt Signaling: Multiple Pathways, Multiple Receptors, and Multiple Transcription Factors. *Journal of Biological Chemistry.* 281(32):22429–22433.

Häärä O, Harjunmaa E, Lindfors PH, Huh S-H, Fliniaux I, Åberg T, Jernvall J, Ornitz DM, Mikkola ML, Thesleff I. 2012. Ectodysplasin regulates activator-inhibitor balance in murine tooth development through Fgf20 signaling. *Development*. 139(17):3189–99.

Harjunmaa E, Kallonen A, Voutilainen M, Hämäläinen K, Mikkola ML, Jernvall J. 2012. On the difficulty of increasing dental complexity. *Nature*. 483(7389):324–7.

Harjunmaa E, Seidel K, Häkkinen T, Renvoisé E, Corfe IJ, Kallonen A, Zhang Z-Q, Evans AR, Mikkola ML, Salazar-Ciudad I, et al. 2014. Replaying evolutionary transitions from the dental fossil record. *Nature*. 512(7512):44–8.

Hermans F, Hemeryck L, Lambrichts I, Bronckaers A, Vankelecom H. 2021. Intertwined Signaling Pathways Governing Tooth Development: A Give-and-Take Between Canonical Wnt and Shh. *Front Cell Dev Biol*. 9:758203.

Herskovitz P. 1962. Evolution of neotropical cricetine rodents (Muridae) with special reference to the phyllotine group. [Chicago]: Chicago Natural History Museum.

Hu Hong, Duan Y, Wang K, Fu H, Liao Y, Wang T, Zhang Z, Kang F, Zhang B, Zhang H, et al. 2022. Dental niche cells directly contribute to tooth reconstitution and morphogenesis. *Cell Rep*. 41(10):111737.

Huang X, Bringas P, Slavkin HC, Chai Y. 2009. Fate of HERS during tooth root development. *Dev Biol*. 334(1):22–30.

Huang X, Xu X, Bringas P, Hung YP, Chai Y. 2010. Smad4-Shh-Nfic signaling cascade-mediated epithelial-mesenchymal interaction is crucial in regulating tooth root development. *Journal of Bone and Mineral Research*. 25(5):1167–1178.

Hunter JP, Jernvall J. 1995. The hypocone as a key innovation in mammalian evolution. *Proceedings of the National Academy of Sciences*. 92(23):10718–10722.

Järvinen E, Salazar-Ciudad I, Birchmeier W, Taketo MM, Jernvall J, Thesleff I. 2006. Continuous tooth generation in mouse is induced by activated epithelial Wnt/ $\beta$ -catenin signaling. *Proceedings of the National Academy of Sciences*. 103(49):18627–18632.

Järvinen E, Shimomura-Kuroki J, Balic A, Jussila M, Thesleff I. 2018. Mesenchymal Wnt/ $\beta$ -catenin signaling limits tooth number. *Development*. 145(4).

Jernvall J, Åberg T, Kettunen P, Keränen S, Thesleff I. 1998. The life history of an embryonic signaling center: BMP-4 induces p21 and is associated with apoptosis in the mouse tooth enamel knot. *Development*. 125(2):161–169.

Jernvall J, Kettunen P, Karavanova I, Martin LB, Thesleff I. 1994. Evidence for the role of the enamel knot as a control center in mammalian tooth cusp formation: non-dividing cells express growth stimulating Fgf-4 gene. *Int J Dev Biol*. 38(3):463–9.

Jernvall J, Thesleff I. 2000. Reiterative signaling and patterning during mammalian tooth morphogenesis. *Mech Dev*. 92(1):19–29.

Jernvall J, Thesleff I. 2012. Tooth shape formation and tooth renewal: evolving with the same signals. *Development*. 139(19):3487–3497.

Jing J, Feng J, Yuan Y, Guo T, Lei J, Pei F, Ho T-V, Chai Y. 2022. Spatiotemporal single-cell regulatory atlas reveals neural crest lineage diversification and cellular function during tooth morphogenesis. *Nat Commun*. 13(1):4803.

Jussila M, Thesleff I. 2012. Signaling networks regulating tooth organogenesis and regeneration, and the specification of dental mesenchymal and epithelial cell lineages. *Cold Spring Harb Perspect Biol*. 4(4):a008425.

Kakugawa S, Langton PF, Zebisch M, Howell S, Chang T-H, Liu Y, Feizi T, Bineva G, O'Reilly N, Snijders AP, et al. 2015. Notum deacylates Wnt proteins to suppress signalling activity. *Nature*. 519(7542):187–192.

Kantaputra P, Leelaadisorn N, Hatsadaloi A, Quarto N, Intachai W, Tongsimma S, Kawasaki K, Ohazama A, Ngamphiw C, Wiriyakijja P. 2023. A Mutation in CACNA1S Is Associated with Multiple Supernumerary Cusps and Root Maldevelopment. *Diagnostics (Basel)*. 13(5):895.

Kassai Y, Munne P, Hotta Y, Penttilä E, Kavanagh K, Ohbayashi N, Takada S, Thesleff I, Jernvall J, Itoh N. 2005. Regulation of Mammalian Tooth Cusp Patterning by Ectodin. *Science (1979)*. 309(5743):2067–2070.

- Kim J, Ahn Y, Adasooriya D, Woo EJ, Kim HJ, Hu KS, Krumlauf R, Cho SW. 2019. Shh Plays an Inhibitory Role in Cusp Patterning by Regulation of *Sostdc1*. *J Dent Res*. 98(1):98–106.
- Kim TH, Bae CH, Lee JC, Ko SO, Yang X, Jiang R, Cho ES. 2013.  $\beta$ -catenin is Required in Odontoblasts for Tooth Root Formation. *J Dent Res*. 92(3):215–221.
- Kim T-H, Lee J-Y, Baek J-A, Lee J-C, Yang X, Taketo MM, Jiang R, Cho E-S. 2011. Constitutive stabilization of  $\beta$ -catenin in the dental mesenchyme leads to excessive dentin and cementum formation. *Biochem Biophys Res Commun*. 412(4):549–55.
- Kleeman SO, Leedham SJ. 2020. Not All Wnt Activation Is Equal: Ligand-Dependent versus Ligand-Independent Wnt Activation in Colorectal Cancer. *Cancers (Basel)*. 12(11):1–16.
- Komiya Y, Habas R. 2008. Wnt signal transduction pathways. *Organogenesis*. 4(2):68–75.
- Kondo S, Ota MS, Kozawa Y. 2009. Overview: The Mechanisms Controlling Root Morphogenesis in Mammalian Molars: —Morphological Relevance of the Tooth Root and Crown, Developmental Mechanisms, and Phylogenetic Aspect of the Tooth Roots—. *J Oral Biosci*. 51(4):188–192.
- Kratochwil K, Galceran J, Tontsch S, Roth W, Grosschedl R. 2002. FGF4, a direct target of LEF1 and Wnt signaling, can rescue the arrest of tooth organogenesis in *Lef1(-/-)* mice. *Genes Dev*. 16(24):3173–85.

Krivanek J, Soldatov RA, Kastriti ME, Chontorotzea T, Herdina AN, Petersen J, Szarowska B, Landova M, Matejova VK, Holla LI, et al. 2020. Dental cell type atlas reveals stem and differentiated cell types in mouse and human teeth. *Nat Commun.* 11(1):4816.

Laugel-Haushalter V, Morkmued S, Stoetzel C, Geoffroy V, Muller J, Boland A, Deleuze J-F, Chennen K, Pitiphat W, Dollfus H, et al. 2018. Genetic Evidence Supporting the Role of the Calcium Channel, CACNA1S, in Tooth Cusp and Root Patterning. *Front Physiol.* 9:1329.

Li J, Parada C, Chai Y. 2017. Cellular and molecular mechanisms of tooth root development. *Development.* 144(3):374–384.

Li L, Tang Q, Kwon H-JE, Wu Z, Kim E-J, Jung H-S. 2018. An Explanation for How FGFs Predict Species-Specific Tooth Cusp Patterns. *J Dent Res.* 97(7):828–834.

Liu F, Chu EY, Watt B, Zhang Y, Gallant NM, Andl T, Yang SH, Lu M-M, Piccolo S, Schmidt-Ullrich R, et al. 2008. Wnt/beta-catenin signaling directs multiple stages of tooth morphogenesis. *Dev Biol.* 313(1):210–24.

Lohi M, Tucker AS, Sharpe PT. 2010. Expression of Axin2 indicates a role for canonical Wnt signaling in development of the crown and root during pre- and postnatal tooth development. *Developmental Dynamics.* 239(1):160–167.

Luan X, Ito Y, Diekwisch TGH. 2006. Evolution and development of Hertwig's epithelial root sheath. *Developmental Dynamics.* 235(5):1167–1180.

Ma Y, Jing J, Feng J, Yuan Y, Wen Q, Han X, He J, Chen S, Ho T-V, Chai Y. 2020. Ror2-mediated non-canonical Wnt signaling regulates Cdc42 and cell proliferation during tooth root development. *Development*. 148(2).

Marangoni P, Charles C, Tafforeau P, Laugel-Haushalter V, Joo A, Bloch-Zupan A, Klein OD, Viriot L. 2015. Phenotypic and evolutionary implications of modulating the ERK-MAPK cascade using the dentition as a model. *Sci Rep*. 5:11658.

Morita W, Morimoto N, Otsu K, Miura T. 2022. Stripe and spot selection in cusp patterning of mammalian molar formation. *Sci Rep*. 12(1):9149.

Munne PM, Tummers M, Järvinen E, Thesleff I, Jernvall J. 2009. Tinkering with the inductive mesenchyme: *Sostdc1* uncovers the role of dental mesenchyme in limiting tooth induction. *Development*. 136(3):393–402.

Nakatomi M, Hovorakova M, Gritli-Linde A, Blair HJ, MacArthur K, Peterka M, Lesot H, Peterkova R, Ruiz-Perez VL, Goodship JA, et al. 2013. *Evc* regulates a symmetrical response to *Shh* signaling in molar development. *J Dent Res*. 92(3):222–8.

Narayanan K, Srinivas R, Ramachandran A, Hao J, Quinn B, George A. 2001. Differentiation of embryonic mesenchymal cells to odontoblast-like cells by overexpression of dentin matrix protein 1. *Proc Natl Acad Sci U S A*. 98(8):4516–21.

Nemoto E, Sakisaka Y, Tsuchiya M, Tamura M, Nakamura T, Kanaya S, Shimonishi M, Shimauchi H. 2016. *Wnt3a* signaling induces murine dental follicle cells to differentiate

into cementoblastic/osteoblastic cells via an osterix-dependent pathway. *J Periodontal Res.* 51(2):164–74.

Ohazama A, Courtney J-M, Tucker AS, Naito A, Tanaka S, Inoue J-I, Sharpe PT. 2004. Traf6 is essential for murine tooth cusp morphogenesis. *Dev Dyn.* 229(1):131–5.

Ohazama A, Haycraft CJ, Seppala M, Blackburn J, Ghafoor S, Cobourne M, Martinelli DC, Fan C-M, Peterkova R, Lesot H, et al. 2009. Primary cilia regulate Shh activity in the control of molar tooth number. *Development.* 136(6):897–903.

Ohazama A, Johnson EB, Ota MS, Choi HY, Porntaveetus T, Oommen S, Itoh N, Eto K, Gritli-Linde A, Herz J, et al. 2008. Lrp4 modulates extracellular integration of cell signaling pathways in development. *PLoS One.* 3(12):e4092.

Orban BJ. 1980. Orban's Oral histology and embryology . St. Louis: Mosby .

Osborn HF. 1907. Evolution of Mammalian Molar Teeth. Macmillan.

Ota MS, Nakahara T, Kanri Y, Kozawa Y, Ohazama A, Aoba T, Kondo T, Iseki S. 2009. Patterning of Molar Tooth Roots in Mammals. *J Oral Biosci.* 51(4):193–198.

Pentimikko N, Iqbal S, Mana M, Andersson S, Cognetta AB, Suci RM, Roper J, Luopajarvi K, Markelin E, Gopalakrishnan S, et al. 2019. Notum produced by Paneth cells attenuates regeneration of aged intestinal epithelium. *Nature.* 571(7765):398–402.

Pispa J, Jung HS, Jernvall J, Kettunen P, Mustonen T, Tabata MJ, Kere J, Thesleff I. 1999. Cusp patterning defect in Tabby mouse teeth and its partial rescue by FGF. *Dev Biol.* 216(2):521–34.

Pispa J, Thesleff I. 2003. Mechanisms of ectodermal organogenesis. *Dev Biol.* 262(2):195–205.

Saad K, Otto A, Theis S, Kennerley N, Munsterberg A, Luke G, Patel K. 2017. Detailed expression profile of all six Glypicans and their modifying enzyme Notum during chick embryogenesis and their role in dorsal-ventral patterning of the neural tube. *Gene.* 609:38–51.

Salazar-Ciudad I, Jernvall J. 2002. A gene network model accounting for development and evolution of mammalian teeth. *Proc Natl Acad Sci U S A.* 99(12):8116–20.

Salazar-Ciudad I, Jernvall J. 2010. A computational model of teeth and the developmental origins of morphological variation. *Nature.* 464(7288):583–6.

Sarkar L, Sharpe PT. 1999. Expression of Wnt signalling pathway genes during tooth development. *Mech Dev.* 85(1–2):197–200.

Sasaki T, Ito Y, Xu X, Han J, Bringas P, Maeda T, Slavkin HC, Grosschedl R, Chai Y. 2005. LEF1 is a critical epithelial survival factor during tooth morphogenesis. *Dev Biol.* 278(1):130–43.

Seo H, Amano T, Seki R, Sagai T, Kim J, Cho SW, Shiroishi T. 2018. Upstream Enhancer Elements of Shh Regulate Oral and Dental Patterning. *J Dent Res.* 97(9):1055–1063.

Seo H, Kim J, Hwang JJ, Jeong H-G, Han S-S, Park W, Ryu K, Seomun H, Kim J-Y, Cho E-S, et al. 2017. Regulation of root patterns in mammalian teeth. *Sci Rep.* 7(1):12714.

Shin M, Suzuki M, Guan X, Smith CE, Bartlett JD. 2016. Murine matrix metalloproteinase-20 overexpression stimulates cell invasion into the enamel layer via enhanced Wnt signaling. *Sci Rep.* 6:29492.

Suciu RM, Cognetta AB, Potter ZE, Cravatt BF. 2018. Selective Irreversible Inhibitors of the Wnt-Deacylating Enzyme NOTUM Developed by Activity-Based Protein Profiling. *ACS Med Chem Lett.* 9(6):563–568.

Tamura M, Nemoto E. 2016. Role of the Wnt signaling molecules in the tooth. *Jpn Dent Sci Rev.* 52(4):75–83.

Thesleff I, Sharpe P. 1997. Signalling networks regulating dental development. *Mech Dev.* 67(2):111–23.

Vahtokari A, Aberg T, Jernvall J, Keränen S, Thesleff I. 1996. The enamel knot as a signaling center in the developing mouse tooth. *Mech Dev.* 54(1):39–43.

Vogel P, Read RW, Hansen GM, Powell DR, Kantaputra PN, Zambrowicz B, Brommage R. 2016. Dentin Dysplasia in Notum Knockout Mice. *Vet Pathol.* 53(4):853–62.

Wang B, Li H, Liu Y, Lin X, Lin Y, Wang Y, Hu X, Zhang Y. 2014. Expression patterns of WNT/ $\beta$ -CATENIN signaling molecules during human tooth development. *J Mol Histol.* 45(5):487–96.

Wang X-P, O’Connell DJ, Lund JJ, Saadi I, Kuraguchi M, Turbe-Doan A, Cavallesco R, Kim H, Park PJ, Harada H, et al. 2009. Apc inhibition of Wnt signaling regulates supernumerary tooth formation during embryogenesis and throughout adulthood. *Development.* 136(11):1939–1949.

Wen Q, Jing J, Han X, Feng J, Yuan Y, Ma Y, Chen S, Ho T-V, Chai Y. 2020. Runx2 Regulates Mouse Tooth Root Development Via Activation of WNT Inhibitor NOTUM. *J Bone Miner Res.* 35(11):2252–2264.

Xiong J, Gronthos S, Bartold PM. 2013. Role of the epithelial cell rests of Malassez in the development, maintenance and regeneration of periodontal ligament tissues. *Periodontol 2000.* 63(1):217–33.

Xiong Y, Fang Y, Qian Y, Liu Y, Yang X, Huang H, Huang H, Li Y, Zhang X, Zhang Z, et al. 2019. Wnt Production in Dental Epithelium Is Crucial for Tooth Differentiation. *J Dent Res.* 98(5):580–588.

Yamashiro T, Zheng L, Shitaku Y, Saito M, Tsubakimoto T, Takada K, Takano-Yamamoto T, Thesleff I. 2007. Wnt10a regulates dentin sialophosphoprotein mRNA expression and

possibly links odontoblast differentiation and tooth morphogenesis. *Differentiation*. 75(5):452–62.

Yang J, Wang S-K, Choi M, Reid BM, Hu Y, Lee Y-L, Herzog CR, Kim-Berman H, Lee M, Benke PJ, et al. 2015. Taurodontism, variations in tooth number, and misshapened crowns in Wnt10a null mice and human kindreds. *Mol Genet Genomic Med*. 3(1):40–58.

Yang S, Choi H, Kim T-H, Jeong J-K, Liu Y, Harada H, Cho E-S. 2021. Cell dynamics in Hertwig's epithelial root sheath are regulated by  $\beta$ -catenin activity during tooth root development. *J Cell Physiol*. 236(7):5387–5398.

Yu M, Liu Y, Wang Y, Wong SW, Wu J, Liu H, Feng H, Han D. 2020. Epithelial Wnt10a Is Essential for Tooth Root Furcation Morphogenesis. *J Dent Res*. 99(3):311–319.

Yu T, Klein OD. 2020. Molecular and cellular mechanisms of tooth development, homeostasis and repair. *Development*. 147(2).

Zeichner-David M. 2006. Regeneration of periodontal tissues: cementogenesis revisited. *Periodontol 2000*. 41(1):196–217.

Zhang R, Yang G, Wu X, Xie J, Yang X, Li T. 2013. Disruption of Wnt/ $\beta$ -catenin signaling in odontoblasts and cementoblasts arrests tooth root development in postnatal mouse teeth. *Int J Biol Sci*. 9(3):228–36.

Zhang X, Cheong S-M, Amado NG, Reis AH, MacDonald BT, Zebisch M, Jones EY, Abreu JG, He X. 2015. Notum is required for neural and head induction via Wnt deacylation, oxidation, and inactivation. *Dev Cell*. 32(6):719–30.

Zhang Y, Tomann P, Andl T, Gallant NM, Huelsken J, Jerchow B, Birchmeier W, Paus R, Piccolo S, Mikkola ML, et al. 2009. Reciprocal requirements for EDA/EDAR/NF-kappaB and Wnt/beta-catenin signaling pathways in hair follicle induction. *Dev Cell*. 17(1):49–61.

Zhao Q, Ren H, Wang N, Yuan X, Zhao Y, Wen Q. 2024. NOTUM plays a bidirectionally modulatory role in the odontoblastic differentiation of human stem cells from the apical papilla through the WNT/ $\beta$ -catenin signaling pathway. *Arch Oral Biol*. 160:105896.

## ABSTRACT (in Korean)

### 마우스 어금니 교두와 뿌리 패턴형성 과정에서 Notum 의 역할

디누카 마두산 아다수리아

(지도교수: 조성원)

연세대학교 대학원

응용생명과학과

*Notum* 은 Wnt/ $\beta$ -catenin 신호전달 경로의 직접적인 표적이면서 동시에 Wnt 억제체로서의 역할도 하므로, Wnt/Notum 음성되먹임 기전이 알려져있다. 지금까지 치아 영역에서는, 치아뿌리형성 중 상아질모세포 전구체와 초기 상아질모세포에서 *Notum* 이 발현된다는 것과 *Notum*-결손 시 상아질에 결함이 생기고 치아뿌리의 형태가 변형된다는 사실이 보고되었다. 하지만, 치아발생 초기 치아머리에서 *Notum* 의 발현 패턴과 치아머리 형태형성 과정 중 Notum 역할은 여전히 불분명하다.

본 연구에서는 RNA in situ hybridization 와 단일 세포 RNA-sequencing 분석을 통해 치아발생 초기단계에서 *Notum* 의 발현 패턴을 조사하였고, *Notum* 유전자 결손 마우스의 치아를 전자현미경 및 마이크로-CT 기법으로 관찰함으로써, 교

두와 치아머리, 치아뿌리 패턴형성 과정에서 Notum 의 역할을 확인하였다. 또한, 발생중인 치배에서 추출한 RNA-sequencing 분석을 통해 *Notum* 결손으로 야기되는 분자적 변화를 조사하였다.

결과로서, 치아발생동안 *Notum* 은 1 차 법랑질결절, 2 차 법랑질결절 및 치아유두에서 강하게 발현되었다. *Notum*-결손 마우스의 어금니에서 2 차 법랑질결절이 커지고, 교두 끝이 뭉툭해지고, 교두의 배열이 달라지며, 치아머리 윤곽의 굴곡이 감소한 것을 확인했다. 이러한 치아머리 윤곽의 변화에 이어 치아목 부분에서 혀 모양 상피의 길이가 짧아지고, 치아뿌리들이 융합되었다. 이처럼 발생단계에 따른 순차적인 변화는 교두의 패턴이 치아머리와 치아뿌리 패턴을 조절한다는 이전의 개념과 일치한다. 또한, *Notum*-결손 마우스의 어금니에서, 2 차 법랑질결절에서 발현되면서 Wnt 표적 유전자이기도 한 *Fgf20*, *Dkk4* 와 *Fgf4* 유전자의 발현량이 유의하게 증가된 것을 분자 수준에서 확인하였다.

이상의 결과를 바탕으로, Wnt/Notum 음성 되먹임 기전이 2 차 법랑질결절의 크기를 조절함으로써 치아머리와 치아뿌리의 패턴형성을 조절한다는 것을 제안한다.

---

**핵심되는 말:** Notum, Wnt 신호전달, 법랑질결절, 교두, 치아머리, 치아뿌리, 패턴